125
39

SHOCK WAVE END WALL BOUNDARY LAYER INTERACTION IN A TRANSONIC COMPRESSOR ROTOR

by

Douglas Cameron Rabe

Dissertation submitted to the Faculty of the
Virginia Polytechnic Institute and State University
in partial fulfillment of the requirements for the degree of

DOCTOR OF PHILOSOPHY

in

Mechanical Engineering

APPROVED:

W. F. O'Brien Jr., Chairman

H. L. Moses

F. J. Pierce

H. L. Wood

F. R. Ostdiek
AFWAL/POTX, WPAFB OHIO

A. J. Wennerstrom
AFWAL/POTX, WPAFB OHIO

May, 1987

Blacksburg, Virginia

SHOCK WAVE END WALL BOUNDARY LAYER INTERACTION IN A TRANSONIC COMPRESSOR ROTOR

by

Douglas Cameron Rabe

Committee Chairman: Walter F. O'Brien Jr.
Mechanical Engineering

(ABSTRACT)

The passage shock wave end wall boundary layer interaction in a transonic compressor was investigated with a laser transit anemometer. A two stage transonic compressor designed without inlet guide vanes was used in this flow field investigation. Measurements of the flow velocity were made within the first stage rotor passage of this transonic compressor. Laser measurements were made in two blade passages at six axial locations from 10% of the axial blade chord in front of the leading edge to 30% of the axial blade chord into the blade passage. At three of these axial locations, laser traverses were taken at different radial immersions to investigate the flow behavior near the tip end wall. Twenty-six different locations were traversed circumferentially. The measurements reveal that the end wall boundary layer in this region is separated from the core flow by what appears to be a shear layer where the passage shock wave and all ordered flow seem to end abruptly.

ACKNOWLEDGEMENTS

The test program described within this report was conducted by the Technology Branch of the Turbine Engine Division in the Aero Propulsion Laboratory of the Air Force Wright Aeronautical Laboratories, Wright-Patterson Air Force Base, Ohio.

The author wishes to acknowledge the contributions and support of all of those co-workers at the Compressor Research Facility whose participation made the testing and subsequent data analysis possible. I am especially grateful to Dr F. R. Ostdiek for the continual support and guidance he has given me during my doctoral program and, in particular, for finding time in the Compressor Research Facility test schedule to conduct this research. I am also indebted to all of the members of the Compressor Test Group who have supported me during the compressor test, data analysis and, most recently, during the documentation phases of this research. I would especially like to thank Jack Downey and Jeff Braun for their invaluable assistance during the compressor test and to Norman Poti for his support and encouragement throughout this research program.

The author is deeply indebted to his major professor, Dr W. F. O'Brien, for his technical guidance and support throughout this doctoral program. Our friendship, resulting from this program, will always be special to me.

The author wishes to acknowledge the other members of his committee, Dr H. L. Moses, Dr F. J. Pierce, Dr H. L. Wood and Dr A. J.

Wennerstrom for their guidance and support of the research reported in this dissertation. The efforts of each member of my committee made this research possible. I am particularly grateful to Dr A. J. Wennerstrom for his technical direction and guidance during the compressor test and data analysis. His contribution to this research was invaluable.

The author wishes to acknowledge the employees of the General Electric Company who developed the compressor test vehicle. In particular the author is grateful to Mr T. Sullivan for his support and technical discussion during this research.

The collective contribution of time and effort by many individuals made the preparation of this dissertation possible. Im am especially indebted to Michelle Behringer, Beverly Rhodes and Kristine Webb who typed the many drafts and final manuscript. I am grateful to Mark Reitz for his efforts in preparing the compressor data summary table and to Jeff Brewer for preparing the drawn figures.

Finally, no words can appropriately describe the hardships endured by my wife and children during this project. Successful completion of this doctoral program would not have been possible without their understanding and patience during the many long days and missed weekends that were necessary for the completion of this dissertation.

I wish to dedicate this dissertation to the memory of my mother, who taught me to achieve; to my wife, , for her love and support; and to my children, for their understanding.

TABLE OF CONTENTS

LIST OF ILLUSTRATIONS

LIST OF TABLES

NOMENCLATURE

AL	Axial length between measurement locations
ALPHA	Relative velocity angle
BACK	Final value of background
BETA	Absolute flow angle
C	Absolute flow velocity
CBU	Velocity calibration bias uncertainty
C(I)	Population (number of events) in the Ith bin
CRF	Compressor Research Facility
cp	Specific heat of air at constant pressure
DT	Time width of a Correlex bin
d	Beam diameter at focal point
dn	Spacing on the viewing screen for n fringes
$\vec{E},\vec{F}$	Vector fluxes in the mean flow equation
e	Specific energy
HIGH	Maximum value of I used to calculate the final background
HW	Hot wire
I	Index representing the number of a given correlogram bin
IPEAK	Correlogram bin containing the maximum number of events
i	Grid index along x direction
j	Grid index along y direction
k	Heat transfer coefficient
L	Distance from the focal point to the viewing screen
L/D	Length-to-diameter ratio
LDA	Laser doppler anemometer

LOW	Minimum value of I used to calculate the final background
LTA	Laser transit anemometer
l_{eff}	Effective length or depth of field of LTA probe volume
N	Total number of transit events used to calculate the velocity
NOB	Number of bins included in the calculation of background
N1	Number of PAC timing pulses for one blade passage
N2	Number of Stations within a blade passage
N3	Number of passages to the second measurement passage using the two-blade mode
n	Numerical calculation step index
n_f	Number of fringes
OPB	Once per blade
OPR	Once per revolution
P	Static pressure
PA	Number of passages from OPR to the first measurement passage using the two-blade mode
PAC	Phase address card
PBACK	Preliminary (or first) calculation of correlogram background
PBC	N1 cycles between OPB and first measurement station
PD	N1 cycle for one station
PDU	Particle velocity dynamics uncertainty
PE	N1 cycles between stations
PSL	Polystyrene latex
Po	Stagnation (Total) pressure
$\dot{q}_x$	Heat flux in x direction

$\dot{q}_y$	Heat flux in y direction
SBU	System velocity bias uncertainty
SPU	System velocity precision uncertainty
SS	Spot separation distance at focal point
V	Velocity
STSU	Velocity station-to-station uncertainty
SU	Velocity statistical uncertainty
SW	Measurement length along the line of measurements (station width)
T	Static temperature
TPU	Velocity temporal uncertainty
TSU	Total system velocity measurement uncertainty
TTB	Most probable transit time bin, used to calculate the velocity
To	Stagnation (total) temperature
t	Time
t_{95}	Value of the two-tailed Student's "t" distribution
U	Compressor wheel speed
$\vec{U}$	Dependent variable flux vector
u	Axial velocity components
V	Velocity
v	Tangential velocity component
y	y step in the circumferential direction
Xw	Maximum deceleration distance perpendicular to the shock wave
x	x step in the axial direction
Z	Axial distance from free jet exit

α_r	Spot rotation angle with respect to the LTA system
β	Angle between the optical axis and the jet axis
β_{min}	Minimum angle between the optical axis and jet axis
γ	Ratio of specific heats
δ	Streamtube contraction distribution
Δt	Time step determined by the Courant - Frederick Levy stability criteria
$\dot{\phi}$	Shock wave angle with respect to compressor axis
$\Delta\phi$	Resolution of measured shock wave angle
Δx	Finite step in x direction
Δy	Finite step in y direction
λ	Wave length of light
μ	Molecular viscosity coefficient
ρ	Density
τ	Turbulence level in percent
τ_{xy}	Shear stress
σ_{xx}	Normal stress in the axial direction
σ_{yy}	Normal stress in the circumferential direction

I INTRODUCTION

Continued advances in transonic axial flow compressor designs require an increased understanding of the actual flow field behavior. With the advances in laser anemometry, detailed nonintrusive measurements can now be made within complex compressor flow fields. Improved understanding of the physics of the compression process results from such measurements. Analytical models may also be improved to the level where they can approximate the complete compressor flow field behavior through a comparison with these detailed compressor flow field measurements. This capability will enable designers to improve transonic compressor designs.

From a design standpoint, compressor performance improvement initially means a reduction of losses which will result in increased efficiency. Also involved are important considerations of operating range and flow stability. Three categories of losses in a transonic compressor without part-span shrouds are identified in reference 1. First, there are losses due to the blade profile and wake; second, end wall boundary layer and clearance losses are identified; and third, there are shock losses. Shock losses are defined to include only the losses due to shock waves in the primary flow field. Losses resulting from the intersection of a shock wave with blade and end wall boundary layers would be included in the blade profile and end wall losses, respectively. According to Hansen and Herzig in Chapter 15 of reference 2, future improvement of compressor efficiencies will depend

significantly upon understanding the behavior of the blade end losses. Simon and Grahl (3)* reinforce this point by stating that the correct qualitative calculation of the end wall boundary layer losses on the hub and tip annuli is essential to the quality of the design of turbomachines. By a continuing application of experimental techniques to provide the detailed understanding of these losses, computational design models can be advanced and verified.

The characterization of the passage shock wave boundary layer interaction reported here helps to improve the understanding of shock losses and tip end wall boundary layer development in transonic flow compressors. Laser transit anemometer (LTA) measurements are presented to show the features of this flow behavior. Extensive studies of the LTA measurement accuracy and capability are included as Appendix A to support the measurement data. Appendix B describes the mechanical configuration of the experimental setup, and Appendix C contains the complete set of laser anemometer measurement data from the transonic compressor. From this flow field investigation, the discovery of a shear layer separating the well ordered core flow from the end wall boundary layer in a transonic compressor is reported.

---

* numbers in parentheses refer to references in Section IX

II BACKGROUND

Many experimental studies on axial flow compressors have been performed to investigate the flow behavior within a rotor passage. These studies have incorporated gas fluorescence techniques (4), hot wire probes (5-8), holographic techniques (9-11), and laser doppler (12-19) and laser transit (20-24) anemometer measurements. Generally, these studies have been directed at an understanding of the overall compressor flow field. Most investigators (9-13, 15-18, and 22-24) have either enhanced measurement techniques and/or used the measurement techniques to investigate the details of the complete compressor flow field. Some of the other studies (4, 14, 20 and 21) have been mainly directed at comparing the detailed flow field measurements with computational results.

Four related papers (5-7 and 15) report studies of the detailed flow field behavior near the tip of a low speed compressor rotor. The present study investigates this region in a state-of-the-art low aspect ratio transonic compressor. This region of the flow is important because it can contribute significantly to the overall losses of the rotor. Using the prediction guidelines of reference 1, the efficiency loss associated with the tip end wall flow can be estimated. For an entrance boundary layer displacement thickness of about 8.6 mm, the compressor studied in this work would have an estimated 3% efficiency loss due to the tip end wall boundary layer losses. The total blockage

due to blade and end wall boundary layers was calculated by Denton (25) to be 10% for the NASA 33 transonic compressor rotor investigated by Chima and Strazisar (19). Thus, the blade and end wall boundary regions of the flow field can contribute significantly to the total losses and flow blockage in a compressor.

The flow behavior near the tip end wall of a transonic compressor rotor is thought to have three major sources of losses. First, losses are generated by the boundary layer development in this region. There are additional losses resulting from the leakage flow across the tip of the rotor blade. Finally, shock waves generated within the passage can interact with the end wall flow, introducing additional losses through boundary layer growth or separation. The end wall boundary layer development along with tip leakage effects are covered in references 3 and 26-29 for low speed compressors.

Generally, the losses due to shock waves interacting with the tip end wall boundary layer are not well reported. For instance, only the shock wave boundary layer interaction on the blade surface is considered in the review of loss and deviation prediction methods reported in reference 26. This report suggests that the shock wave boundary layer interaction on the blade surface can be calculated through an empirical treatment. This interaction has been shown in a transonic compressor rotor experiment using gas fluorescence (4). Schafer (30) demonstrated that laser anemometry could measure the shock wave boundary layer interaction on a stationary airfoil.

The objective of the present work was to provide the first data on the passage shock wave interaction with the tip end wall boundary layer region of a transonic compressor rotor. In all cases where a shock wave originates or reflects from a solid surface, shock wave boundary layer interaction occurs. There are two possibilities for the passage shock wave boundary layer interaction on the end wall. First, if the passage shock wave bends normal to the end wall, then it will interact with the end wall without a reflected shock wave. With a normal shock wave at the end wall, the flow passing through the shock wave near the wall can decelerate without turning into or away from the annulus wall. If, on the other hand, the shock wave is not perpendicular to the wall surface, the shock wave would have to reflect from the wall or boundary layer to satisfy the boundary condition of no flow through the solid surface. The classical representation of this flow field is presented by Liepmann and Roshko (31) and Shapiro (32). With an oblique interaction there could be a complicated series of shock waves and expansion waves as shown by reference 32. Ultimately this series of waves would result in at least one reflected shock wave and a rapid thickening of the boundary layer. In either event the presence of the boundary layer can spread the pressure jump produced by the shock wave on the wall over a considerable region (31). According to reference 31, this can be as much as 50 boundary layer thicknesses. This behavior would introduce additional concerns for the interpretation of high response static wall pressure measurements over the tip region of a transonic compressor rotor.

No references were found in the literature that provide a detailed understanding of the tip end wall flow field within a transonic compressor rotor. However, the investigations by Lakshminarayana, et al. (5-7 and 15), and Hunter and Cumpsty (8) have provided significant experimental detail of this region for subsonic compressor rotors. Hah (29) has provided similar analytical definition of this same flow region in a subsonic compressor rotor. From the work of reference 5, it is seen that the tip end wall boundary layer extends inward to about 90% of the radius in the first 25% of the blade chord in the experiments reported. The tip leakage flow was found to originate near the quarter chord region with peak values occurring near 50% chord. Reference 29 predicts the origin of the leakage flow location to be at about 45% of the chord. The flow calculations of Hah (29) showed no evidence of the end wall boundary layer at 95% of the radius. For the present investigation the compressor design codes (33) predicted that radial flow effects would be minimal at 90% of the radius. Because of the inconclusive reference data, and to insure that the complete end wall boundary layer region was investigated, transonic compressor flow field measurements were planned from 90% of the blade radius outward to the end wall surface.

III EXPERIMENTAL CONFIGURATION

A. Overall Configuration

The experimental configuration of the transonic compressor and laser measurement system is detailed schematically in Figure 1. Two views of the actual setup in the test chamber of the Compressor Research Facility (CRF) are shown in Figures 2 and 3. Since the inlet ducting and bellmouth are removed in Figure 3, the first stage rotor of the compressor is completely visible. The LTA used in the experimentation was manufactured by Spectron Development Laboratories. A detailed description of the system is presented in Appendix A, Sections 1 - 3. Except for the laser system, the hardware used in the setup is covered in more detail in Appendix B.

As indicated in Figures 2 and 3, the laser was mounted at 20 degrees to the horizon to use an existing penetration in the compressor case for an optical window mount. The laser was placed inside a wooden box which was lined with soundproofing to reduce the possibility of damage to the laser head from the high noise environment of the test chamber. In both figures, one side of the box has been removed to show the laser head installation.

The optical axis of the laser system was perpendicular to the axis of the compressor as implied in Figure 1. Traversing of the complete laser system was provided by the table shown in Figures 2 and

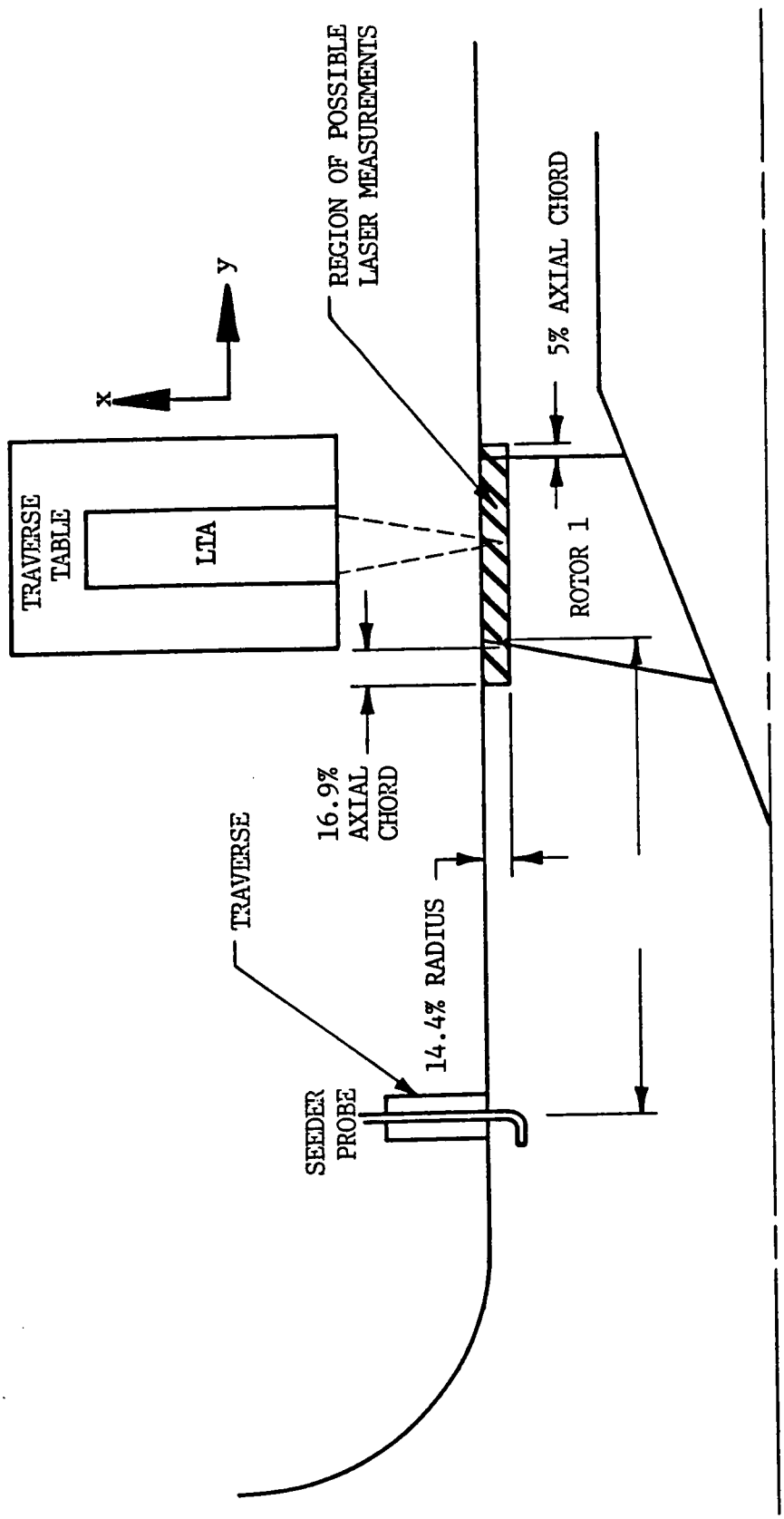

FIGURE 1 SCHEMATIC OF LTA COMPRESSOR TEST

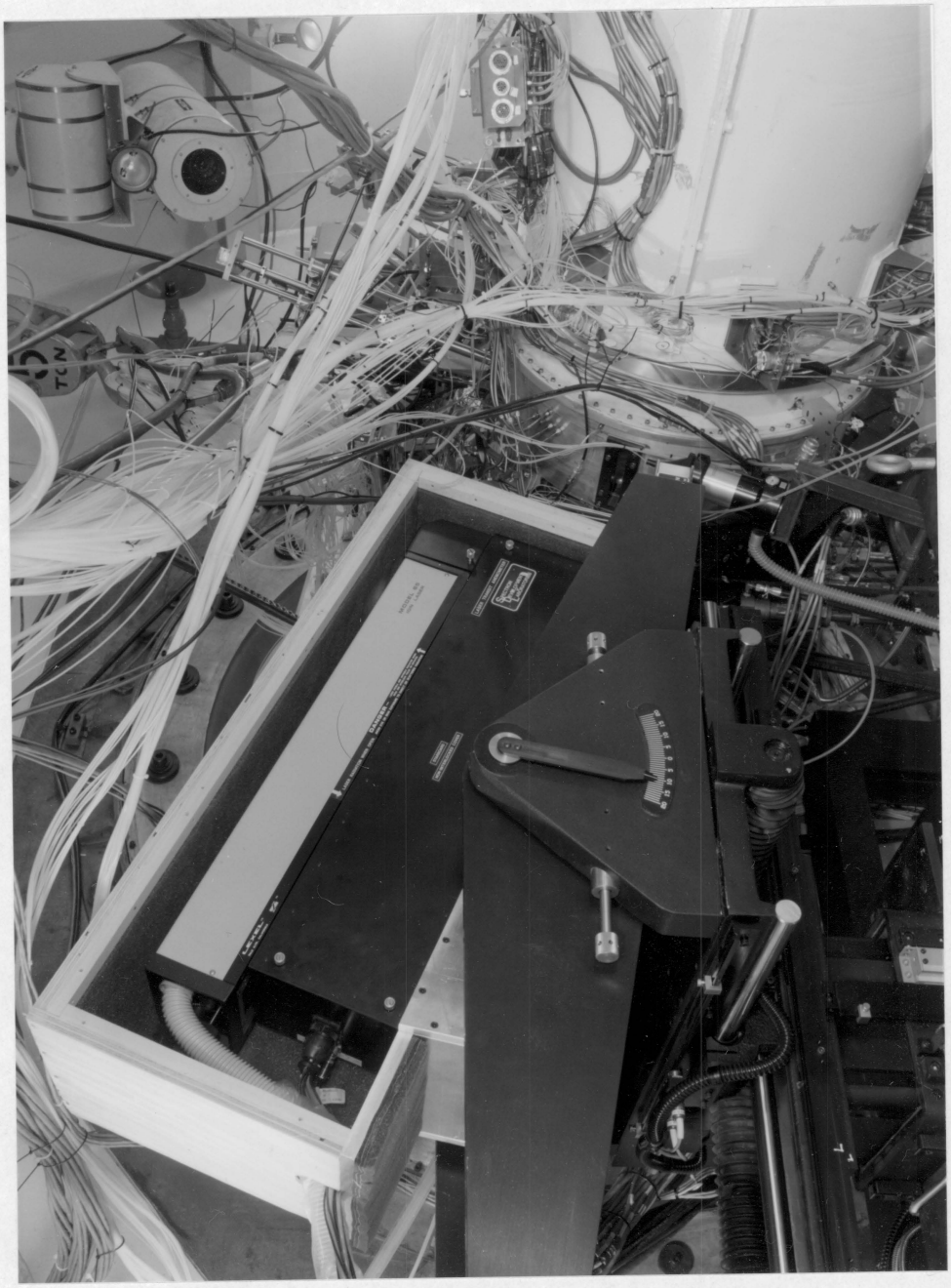

FIGURE 2 TRANSONIC COMPRESSOR MEASUREMENT SETUP

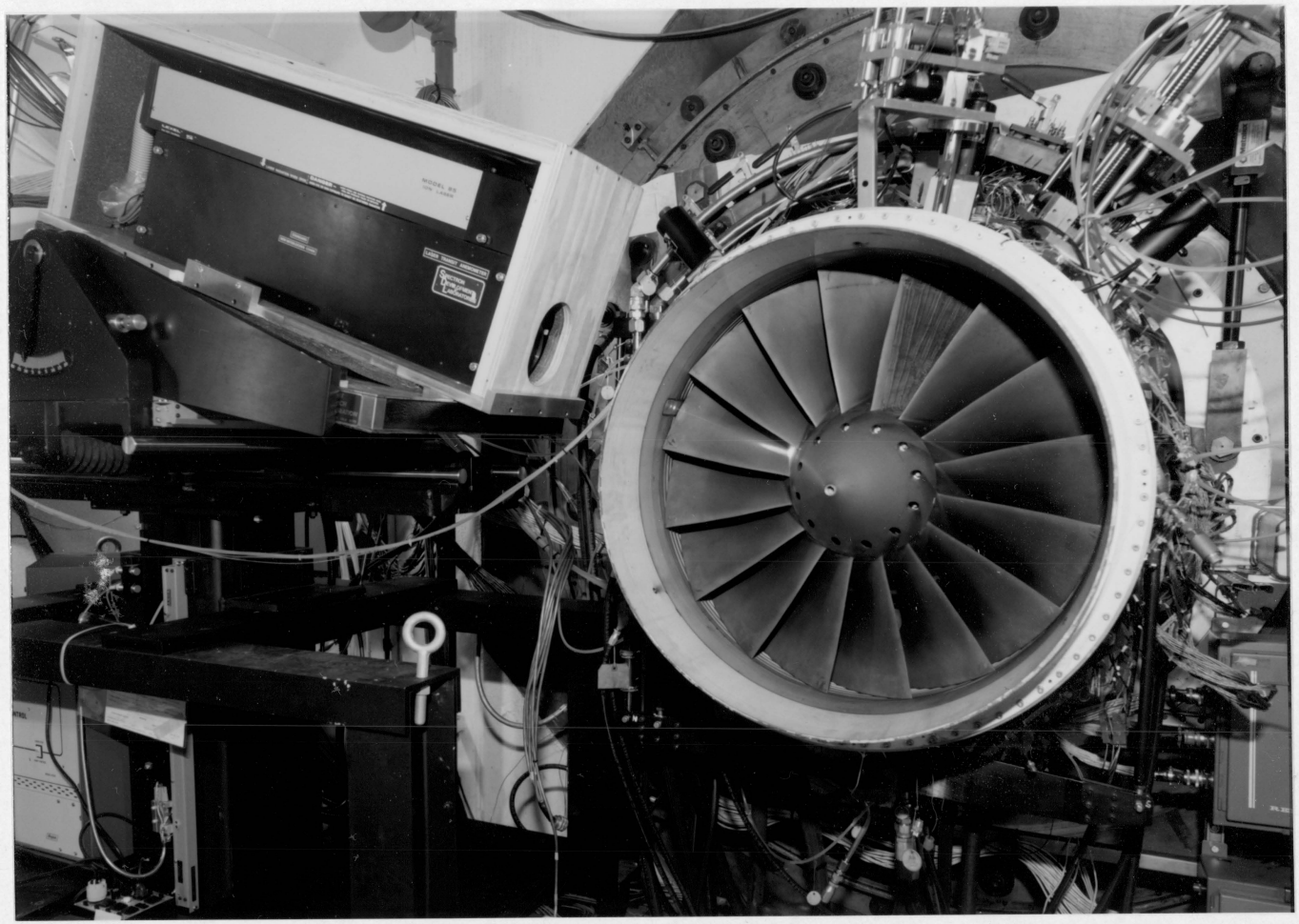

FIGURE 3 TRANSONIC COMPRESSOR
MEASUREMENT SETUP WITH INLET DUCTING REMOVED

3. With remote control, the laser system could be moved in two orthogonal horizontal directions and in the vertical direction. One horizontal movement direction was along the compressor axis, which permitted measurements at different chord locations. With a combination of the vertical and the second horizontal movement, the measurement point could be moved along the radius of the compressor. Further description of the laser traversing, including the accuracy of the movement of the measurement point, is presented in Section 1 of Appendix B. Axial locations are referenced to the blade leading edge and are reported as a percentage of the axial chord at the blade tip. In the figures this is referred to as % chord. The radial locations are referenced to the blade tip radius and are reported as a percentage of this value.

Artificial seed was introduced into the air flow to improve the rate of laser measurements. The injection probe is shown schematically in Figure 1. Through translation and rotation, the seed could be introduced at different radial and circumferential locations within the air flow. Polystyrene latex (PSL) spheres of 0.48 micron diameter were used during the experiment. The seed injection system is described more fully in Appendix B, Section 6.

The optical access to the compressor flow was provided by the window shown in Figures 2 and 3. With the configuration of the laser system and the size and mounting of this window, the measurement point could be positioned to 85.6% of the radius. This point could be moved

along the compressor axis from 16.9% of the axial chord in front of the blade leading edge to 5% of the axial chord behind the blade trailing edge. The region of possible laser measurements with the optical configuration used in the experiment is shown schematically in Figure 1. By changing the output lens of the laser system, the coverage of possible measurement locations could be extended radially all the way to the hub at the blade leading edge. For these measurements of the tip flow region, it was more advantageous to only use the shorter focal length lens to obtain a shorter probe volume dimension along the optical axis. More details of the laser optics and compressor window are presented in Section 2 of Appendix A and Section 3 of Appendix B, respectively.

B. Compressor Configuration

The transonic compressor used in the investigation was developed by the General Electric Company under contract to the Air Force. A detailed schematic of the flow path of the compressor is shown in Figure 4. This two stage compressor incorporates low aspect ratio blading as described by Wennerstrom (34). It is configured without inlet guide vanes. The flow field measurements were performed in the first stage rotor which has 16 blades. The blade aspect ratio of this stage is 1.00, based on the average span divided by the root axial chord. The inlet hub-to-tip ratio of the first stage is 0.29, and the tip clearance near the peak efficiency speed was measured to be 0.196% of the radius of the compressor. Figure 5 shows a close-up view of the

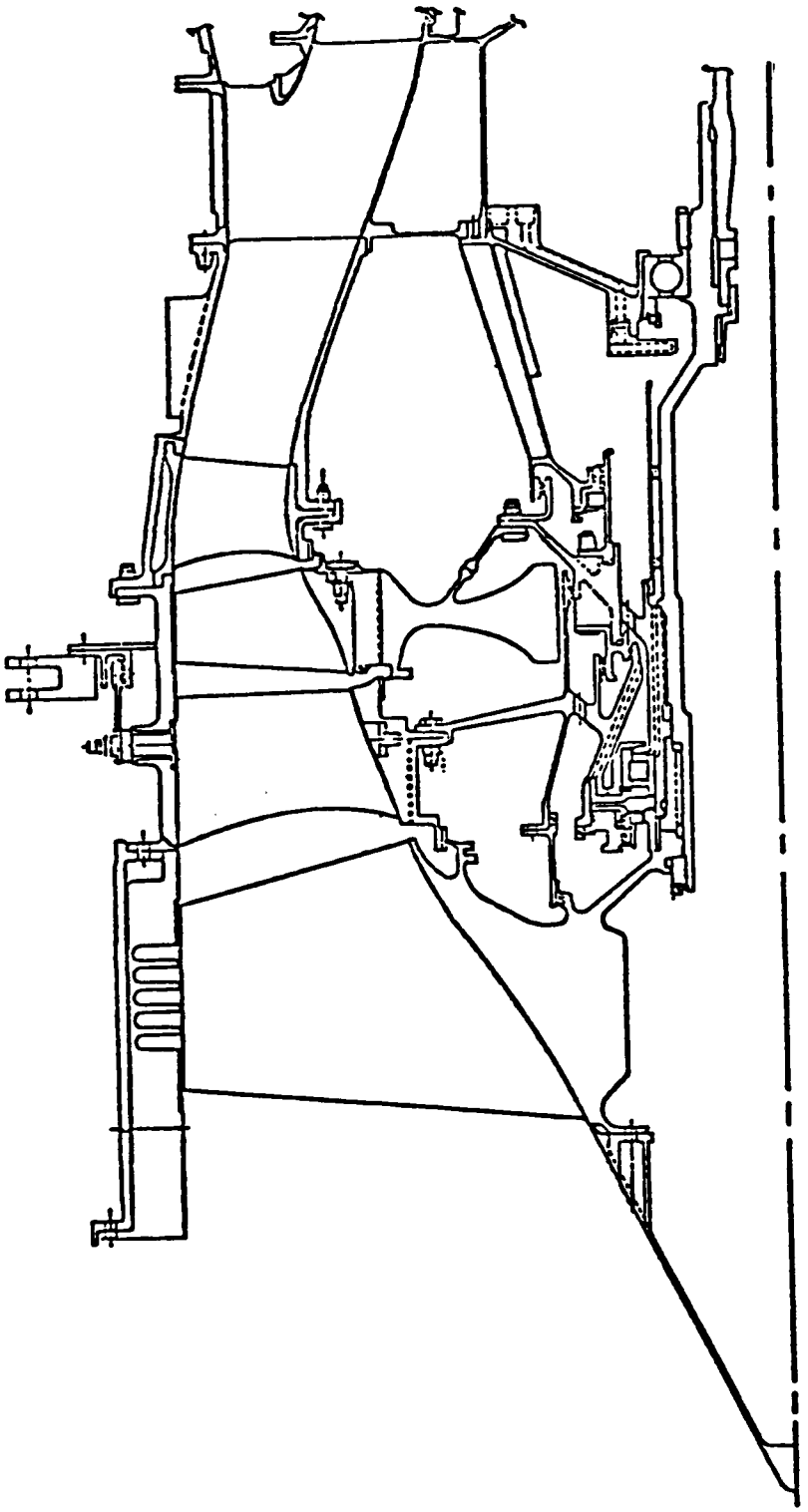

FIGURE 4 Two Stage Transonic Compressor Schematic

FIGURE 5 CLOSE-UP VIEW OF THE FIRST STAGE ROTOR

first stage rotor. In both Figures 4 and 5 the circumferential groove tip treatment is visible. This tip treatment was installed to improve the stall margin performance of the compressor. More details of the actual blade tip region are shown in the description of the laser window in Figures 52 and 53 of Appendix B. The blade profile at 91.7% of the radius is shown in Figure 6. This figure represents the flow field from the point of view of the LTA optical system. An outline of the optical window is provided in this figure for reference. The three dimensionality of the rotor blade is exhibited in Figure 7.

C. Positioning of the LTA Measurement

The blade passages of the compressor are ordered in a clockwise direction. In Figure 5, the laser beams are within the 16th blade passage. Generally, laser measurements were made in the fifth and seventh blade passages which are the first and third passages after the instrumented blade visible in Figure 5. The blade passages measured for each location are reported in Table 20 in Appendix C. With the multiple station capability of the LTA described in Section 4 of Appendix A, the data acquisition system could acquire laser measurements simultaneously at up to 32 different locations in two blade passages. The circumferential extent of each of these measurement windows is controllable from the data acquisition computer. Generally, measurements were made at 17 equally spaced locations across a blade passage. This resulted in the circumferential extent of one measurement being about 5.5% of the blade-to-blade distance. Particle

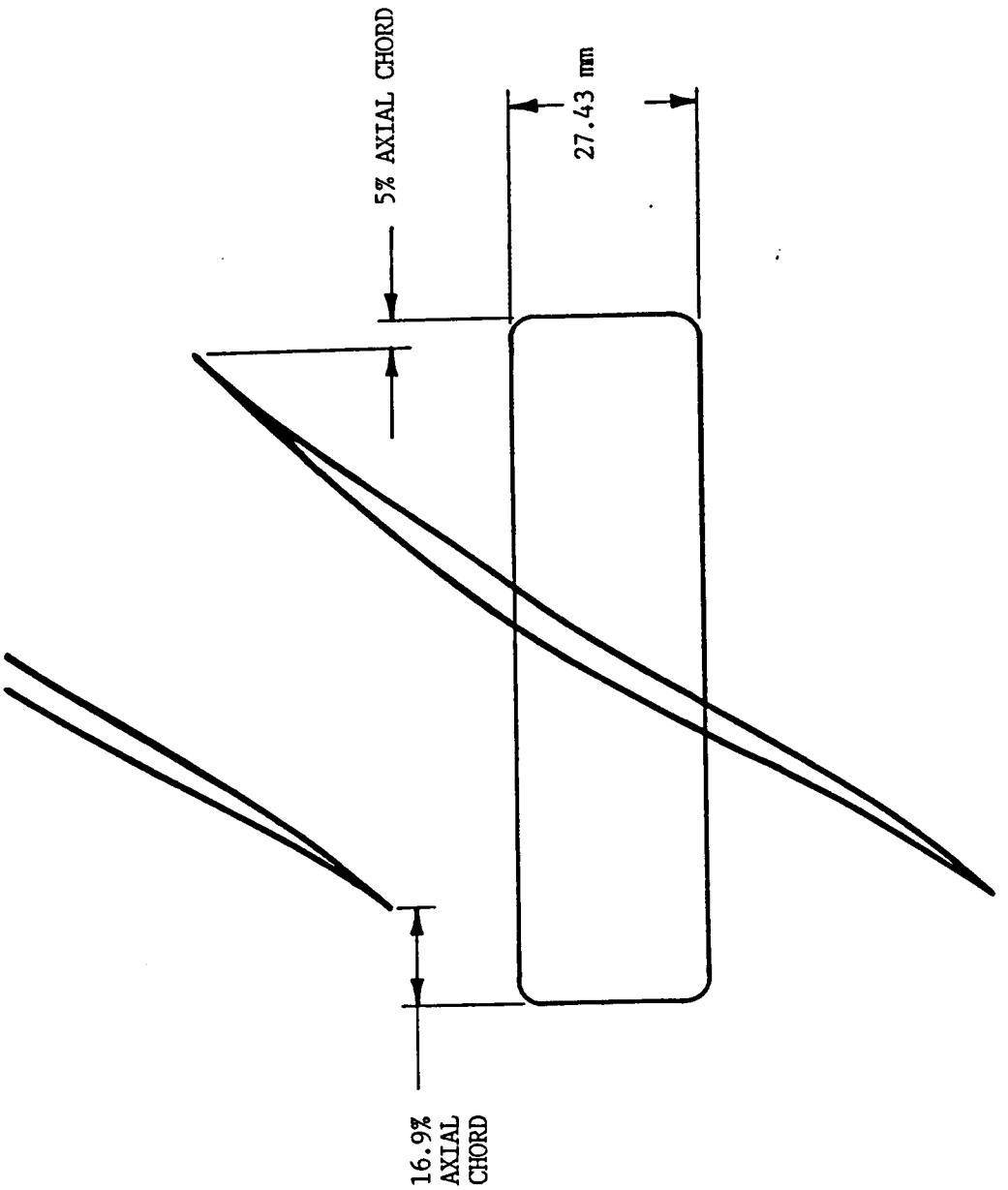

FIGURE 6 Rotor Blade Profiles at 91.7% Radius

FIGURE 7 FIRST STAGE ROTOR BLADES
OF THE TRANSONIC COMPRESSOR

transits measured anywhere along this measurement length of one station are considered to represent the velocity at the middle of the station. Once set, these measurement window locations and widths were measured as explained in Section 4 of Appendix A.

The axial and radial locations of the measurement were positioned by the traverse as previously described. For a given radial immersion, the axial position of the blade leading edge was obtained by moving the traverse upstream until the flare light from the blade surface just dissappeared. Axial positions other than the blade leading edge were located with respect to the blade leading edge at 91.7% of the blade radius by using the position read-out of the traverse table. Since the axial chord did not vary appreciably in the region of flow field measurements, the axial chord length at 91.7% of the radius was used for all radial depths. Therefore, different radial measurements for a given chord wise location were all performed at the same axial location except at the blade leading edge.

IV DATA ACQUISITION

The LTA data acquisition system used in the experiment is essentially the system as supplied by the manufacturer. Originally the LTA system was configured without a post processing capability of stored data sets. During the experimentation, data were reviewed on line, and preliminary results were recorded. Once a data set was accepted, it was stored on disk. Following the compressor test, a post-processing program was developed to recall the stored data and perform the final data analysis.

A. Laser System

The optical head of the LTA used in the investigation is shown to the left of the compressor in Figures 2 and 3. A complete description of the LTA and the details of preparatory experiments performed with the system are presented in Appendix A. References 22 and 35 describe the principles of operation of the LTA while a description of the Correlex manufactured by Spectron Development Laboratories to process the LTA signal is presented in reference 36. Basically, the LTA optical system produces two parallel beams of light from a single input laser beam with an optical power of approximately 0.7 watt. The two parallel beams are then focused in the flow field to form two small spots separated by a distance, SS. Backscattered light from dust or artificially induced seed particles is detected by two photomultiplier tubes, one viewing each spot. The term dust is used here to signify

any natural particle in the air flow that will scatter the incident laser light. Through optical rotation, the two spots are aligned to the velocity vector component in the plane perpendicular to the optical axis. The time that scattered light is observed from the downstream spot can be correlated with the time that scattered light is observed from the upstream spot to yield a histogram of particle transit times. This cross correlation is performed by the Correlex mentioned above. The Correlex used in this investigation was capable of performing up to 64 different correlations simultaneously. If the dust or artificial seed particles follow the flow, the transit time histogram, along with the spot separation, can yield the absolute flow velocity in the measurement plane perpendicular to the optical axis. From the spot rotation, αr, the flow angle can be determined.

The probe volume dimensions for the LTA were determined experimentally as described in Section 5 of Appendix A. The spot separation, SS, and beam diameter, d, were determined by measuring the linear beam power distribution at the focal point. A knife edge was translated across the two beams and the transmitted power was recorded as a function of the knife edge position. The beam diameter was measured in this manner to be 0.016 mm. The spot separation measured using the knife edge was 0.279 mm. Neglecting turbulence effects with this beam diameter-to-spot separation ratio, a particle will theoretically only pass through both spots if the spot rotation angle, αr, is within ±3.3 degrees of the absolute flow velocity vector direction projected in the plane of the measurement. This compares

favorably with the useful range of about ±3.0 degrees observed during the experiment. The depth of field or effective length of the probe volume was determined using a free jet positioned at different angles to the optical axis in the plane of the two spots. This effective length was measured to be 0.430 mm. Again neglecting turbulence effects, the dimensions for the LTA probe geometry would permit measurement of the component of the absolute velocity vector in the plane perpendicular to the optical axis if the following two conditions are met. First, the absolute flow velocity vector must be within ±57 degrees of the measurement plane. Second, the spot rotation must be aligned to within ±3.0 degrees of the absolute flow velocity component direction in the measurement plane. Therefore, the LTA can measure the velocity component in the measurement plane even though the absolute velocity vector has a significant component in the optical axis direction.

B. Velocity Calculation

The velocity calculation using the data collected by the Correlex is performed in the data acquisition computer. Each station in the Correlex has a maximum of 256 discrete time bins. The selected time window for the Correlex, along with the 256 bins, specifies the maximum particle transit time that can be measured by the system.

Each observed particle transit is added to the number of events of a given bin representing that transit time. Over time, a histogram of

particle transits is developed. The time to generate the histogram is again selectable through the data acquisition computer. For the compressor measurements reported here, it was generally three or five minutes per angle setting. An example of the output histogram is presented in Section 3 of Appendix A. The calculation of velocity is performed using the data contained in the histogram. First the bin, IPEAK, containing the most events is determined. Then a value of preliminary background, PBACK, is determined by the following:

$$PBACK = \left\{ \sum_{I=4}^{I=IPEAK\ -32} C(I) \quad + \quad \sum_{I=IPEAK\ +\ 32}^{256} C(I) \right\} / NOB$$

The population of the Ith bin is represented by C(I), and NOB represents the number of bins included in the two summations. The summations cannot go below 4 or above 256, and they exclude IPEAK and 32 bins on either side of IPEAK. Therefore, the minimum value for NOB is 189. If IPEAK is within 32 bins of either the 4th bin or the 256th bin, the calculation will increase NOB to account for the new limits in order to obtain a PBACK that is an average population for the bins outside of the region around IPEAK.

Based on this value of PBACK, the remaining bins excluded from the PBACK calculation are searched to determine if there are bins within this region with population below PBACK. If this is the case, then the region around IPEAK is narrowed to the closest bin on either side of

IPEAK that falls below PBACK. These new limits are termed HIGH and LOW. The summation for the final background, BACK, is now performed with the following relation.

$$BACK = \left\{ \sum_{I=4}^{LOW} C(I) + \sum_{HIGH}^{256} C(I) \right\} / NOB$$

Again, NOB is the number of bins included in these two summations.

The most likely transit time bin, TTB, is now determined by calculating the effective weighted center of the histogram between the LOW and HIGH limits. The calculation is as follows:

$$TTB = \frac{\sum_{LOW}^{HIGH} I\,(C(I) - BACK)}{\sum_{LOW}^{HIGH} (C(I) - BACK)}$$

This value for the transit time is then combined with the spot separation, SS, and the selected time width of the bin, DT, to calculate the measured velocity, V, from:

$$V = \frac{SS}{(TTB)\,(DT)}$$

Generally it is desirable for this calculation procedure to adjust the value of DT to position the most probable transit time to be nearly one half of the measurable maximum transit time.

C. Measurement Errors

The LTA, or any laser anemometer, can only measure the behavior of particles carried in the flow that scatter the incident laser light. If the particles do not follow the flow, then the LTA will not measure the flow behavior. Generally, the use of particles with diameters of 1.0 micron or less is desirable (13, 37). Maxwell (38) showed analytically for turbomachinery applications that 0.5 micron diameter particles with a density of 1 gm/cc would experience velocity and angular deviations generally less than 1 percent and 0.5 degree, respectively. During the compressor testing, polystyrene latex spheres of 0.48 micron diameter and 1 gm/cc density were introduced through a probe located approximately two meters upstream of the blade row (see Figure 1). This distance is about three times further upstream than what was successfully used in a similar configuration reported in reference 13. The probe could be translated in the radial direction, and through rotation, the seed could be introduced at different circumferential locations. However, during the experiment, the seed injection location and flow rate had no effect on the observed data rate of the LTA signal. Therefore, all of the compressor measurements reported here are considered to have been made using the natural particles in the atmosphere. The inlet flow to the compressor was

filtered to 5.0 microns so the particles used to measure the flow behavior are assumed to be less than this diameter. In normal atmospheric air, the number of particles with diameters between 0.1 micron and 1.0 micron is 1000 times the number of particles with diameters between 1.0 micron and 5.0 microns, according to the data provided in the Frank chart presented in reference 39. The minimum diameter of 0.1 micron is essentially the smallest seed diameter the LTA is able to measure. From the distribution of natural particles in the atmosphere, it is felt that the measurement uncertainty in the worst case would be based on the particle dynamics of 1.0 micron particles. From Maxwell (38), velocity and angle deviations for 1.0 micron diameter particles are estimated to be less than 4 percent and 3.0 degrees, respectively. This is considered to be a conservative estimate for subsonic compressors since Maxwell's predictions are for turbine blades with higher turning than compressor blades. However, the shock waves in a transonic compressor may introduce higher deviations locally.

Particle dynamics are just one of the many sources of measurement error in laser anemometry. There are three additional categories of errors that can effect the measurement. Electronic bias and precision errors can affect the measurement of the transit time and the location of the measurement stations across the blade passage. These bias and precision errors are transmitted to the mathematical data reduction algorithms and affect the outcome of the calculation of velocity. Positioning errors result from physically moving the probe volume with

respect to the compressor, as well as referencing the flow velocity direction measured by the laser to the compressor reference frame. Finally, there are statistical errors in computing the flow velocity from a finite number of particle transits.

The electronic bias and precision errors of the LTA were resolved experimentally. Employing the calibration technique presented in Section 5 of Appendix A, the electronic and calculation bias error for velocity measurement was reduced to the calibration bias using the calibration jet. There are essentially two other uncertainties associated with the LTA system configured with multi-stations. A temporal precision error exists, as well as a bias error from station to station. Both of these uncertainties are quantified in Section 5 of Appendix A. For the flow range of 100 to 300 m/sec, the LTA system is considered to be capable of measuring the flow velocity with a bias uncertainty of less than 1% and a temporal precision error of 0.12%. Additionally, the system has an uncertainty of 0.2% from station to station which is considered to be a bias term. All three terms are in percent of the measured velocity.

The number of particle transit events required for the sample population to represent the true histogram with a 95% confidence level is presented in reference 18. For a confidence level of 95%, the relationship between the uncertainty in percent, the number of measurements, N, and the turbulence level, T, is.

$$\% \text{ Uncertainty} = \frac{1.97\,T}{N^{\frac{1}{2}}}$$

For a turbulence level of 5% or less and a desired uncertainty of 2%, 25 measurements are required. If only ten measurements are used at this turbulence level, the uncertainty will increase to 3.1%. Usually more than 25 measurements were used to calculate the velocity at each location in the flow field; however, data were only excluded if less than 10 measurements were available between the HIGH and LOW limits. Therefore, the statistical accuracy is generally better than 2% but may be closer to 3.1% in some cases. Table 20 in Appendix C reports the actual number of particle transients used for each measurement.

The total uncertainty of the velocity measurement can now be determined from the stated uncertainty of particle dynamics, PDU, calibration bias uncertainty, CBU, measured station-to-station bias uncertainty, STSU, temporal precision uncertainty, TPU, and statistical uncertainty, SU. Using the method of root sum squares, as reported in reference 40, the system bias uncertainty, SBU, in percent can be estimated by,

$$SBU = (PDU^2 + CBU^2 + STSU^2)^{\frac{1}{2}}$$

The value of SBU is calculated to be 4.1%. System precision uncertainty, SPU in percent, associated with variation in time, TPU, and the statistical uncertainty, SU, can be estimated in a similar manner by

$$SPU = (TPU^2 + STSU^2)^{\frac{1}{2}}$$

The value of SPU is calculated to be 3.1%. Total system uncertainty, TSU, in percent can be estimated to a confidence level of 95% by combining the bias and precision uncertainty using the following relationship of reference 40

$$TSU = (SBU^2 + t_{95} SPU^2)^{\frac{1}{2}}$$

where t_{95} is the value of the two-tailed Student's "t" distribution. For the investigation reported here using a minimum of 10 particle transits, it is considered to have a value of 2.2. The total system uncertainty is now calculated to be ±6.2%.

Positioning errors are associated with the timing of the interblade passage locations as well as the positioning of the traverse system. As covered in Section 4 of Appendix A, the width of the station was measured to an accuracy of 0.6% of the blade passage. The distance from the suction surface to the center of a station is dependent on the reflected laser signal from the suction surface of the blade. An example of both of these measurements is contained in Section 4 of Appendix A. From the observed data, the measurement of the center of these "time-distance" windows is accurate to 0.6% of the blade passage.

The method of positioning the probe volume axially and radially is covered in Section III and Appendix B. With the probe volume dimensions presented in Section 5 of Appendix A, the maximum error in locating the blade leading edge would be equal to one half of the sum

of the spot separation distance and the beam diameter plus or minus the positioning error of the traverse. This would be 0.074 cm ± 0.00025 cm. Therefore, the accuracy of the axial movement can be considered to be ± 0.074 cm. The radial movement is dependent on the accuracy of the traverse, window effects and the accuracy of measuring the laser angle. After the experiment, the radial position was measured with the window installed at three of the immersions used. These three measurements were all within ± 0.013 cm. Therefore, the positioning accuracy of the LTA measurements is considered to be ± 0.074 cm axially, ± 0.013 cm radially and ± 0.14 degree circumferentially. The axial uncertainty of positioning is 27% of the spot separation while the radial uncertainty of positioning is three percent of the effective length of the probe volume. The uncertainty of the circumferential position is approximately 11% of the measurement window width.

In conclusion, the velocity measurement is considered to have a total system uncertainty of ±6.2% with a system precision uncertainty of ±3.1%. The uncertainty of the radial and axial location measurements are ± 1% of the probe volume effective length and ± 14% of the spot to spot distance respectively. The circumferential positioning uncertainity is ± 0.6% of the blade passage.

D. Determination of Flow Angle

The LTA system can only measure the flow velocity vector magnitude if the two spots are aligned to the velocity vector direction. As

reported in Section III, for the LTA used in this investigation, the angle of the two spots must be within 3.0 degrees of the velocity direction in the measurement plane to measure the velocity. During the experiment a limited number of angles was used to measure the flow to efficiently use the test time. Two degree increments were used to measure the flow on the upstream side of the shock wave while three degree increments were used to measure the flow on the downstream side of the shock wave. In the post processing routine, as reported in Section 5 of Appendix A, the angle with the largest contrast was selected as the flow velocity direction. This angle stepping process introduces a maximum uncertainty of ± 1.5 degrees in flow direction.

A calibration of the LTA spot angle with respect to the compressor axis is presented in Section 5 of Appendix B. The bias accuracy of this calibration is ± 1/2 degree. In Section 5 of Appendix A, it is demonstrated that the LTA precision in detecting the flow velocity direction is ± 0.2 degree. The particle dynamics, angle stepping and calibration bias uncertainties and the resolution precision uncertainty can all be combined in a manner similar to the velocity measurement uncertainties, using the root sum square method. The maximum total uncertainty in the absolute flow velocity direction is thus ± 3.4 degrees due to the combined effects of particle dynamics, discrete angle measurements, angle calibration and LTA angle precision sensitivity. This uncertainty is reduced in the relative reference frame because the speed of the blade motion is significantly larger than the absolute velocity. The relationship of the relative velocity

angle, ALPHA, with respect to the measured quantities of wheel speed, U, absolute velocity, C, and absolute flow angle, BETA, is

$$\text{ALPHA} = \text{ARC COS}\left\{\frac{\text{C COS (BETA)}}{([\text{ U+C SIN (BETA)}]^2 + \text{C}^2)^{\frac{1}{2}}}\right\}$$

By differentiating this expression numerically, the sensitivity of ALPHA to BETA can be calculated. For the values of BETA, C and U generally measured downstream from the shock wave, the sensitivity of ALPHA to BETA was conservatively calculated to be 0.3. The maximum uncertainty of the angle resolution in the relative reference frame is therefore considered to be ±1.0 degree, using this sensitivity with the angle uncertainty in the absolute reference frame.

E. Data Reduction and Non-Dimensional Treatment

The post processing of the data included the recalculation of the velocity and other basic quantities originally available on line. The software program developed further analyzed complete angle sets to select the most probable angle of the flow velocity vector for each station. The selection was performed using the calculated value of contrast as indicated in Section 5 of Appendix A. The program is not currently capable of joining different angle sets, and some manual selection for the best angle between sets was performed. Since the positioning of the measurement volume was performed manually, the values of radial and axial location were input into the data reduction software by hand. Further, the timing of the stations was measured

separately on the digital oscilloscope. Once analyzed, this information was also manually input to the data reduction software. Table 20 of Appendix C contains a summary of all of the compressor measurement data collected. The actual values of velocity are not reported but are nondimensionalized. The absolute and relative velocities are nondimensionalized by selected different values that are not reported.

V EXPERIMENTAL RESULTS

The axial and radial locations measured in the transonic compressor are shown in Figure 8 and listed in Table 19 of Appendix C. Measurements were usually made in the fifth and the seventh blade passages. The fifth passage is the first passage to the right of the instrumented blade shown in Figure 5. The seventh passage is two passages further to the right. The average blade mode described in Appendix A would decrease the time to acquire the test data by a factor of 16, equal to the number of blade passages. Attractive as this advantage is, it did not outweigh the possibility of eliminating the individuality of a single blade passage through averaging. Individual blade passages were measured to eliminate the possible flow field distortion which might result through averaging all of the blade passages together.

The circumferential distance was usually divided by the timing network into 17 circumferential locations per blade passage. This resulted in each data collection window being about 5.5% of the blade-to-blade distance. Particle transits measured anywhere along this measurement length are considered to represent the velocity at the middle of this window. Data were collected based on a time limit of three or five minutes per angle. Generally, five angles in two degree increments were used to measure the flow on the upstream side of the shock wave while six angles in three degree increments were used to measure the flow on the downstream side of the shock wave. The actual angle sets used to measure the flow field are listed in Table 19 of

Appendix C for the locations shown in Figure 8.

The laser measurements were made near the peak efficiency point of the compressor. To acquire the LTA data, the compressor was set to the desired corrected speed and then held at the respective mechanical speed during a laser measurement scan. While the LTA data were being reduced and stored, the compressor speed was adjusted to the desired corrected speed, if necessary. During the nearly 50 hours of compressor operation, the standard deviations in the pressure ratio, corrected speed, mass flow and efficiency were calculated as a percentage of the corresponding mean values to be 1.14%, 0.14%, 0.75% and 0.85%, respectively.

A. Detailed Flow Field Measurements

The inlet absolute velocity profiles for five of the radial locations measured at the leading edge of the blade are shown in Figure 9. The absolute velocity is presented as a percent of an average blade-to-blade absolute velocity within the blade row. The velocity is plotted from the suction side (0% blade passage) to the pressure side. The next suction side is at 100% blade passage in the figure. Figure 9 shows that the inlet velocity is sinusoidal across the passage near the end wall at 96.1% and 97.5% radii. The absolute velocity is generally higher nearer the suction surface than the pressure surface. As the measurements are made closer to the tip end wall, the overall magnitude decays as would be expected. A significant change in magnitude is

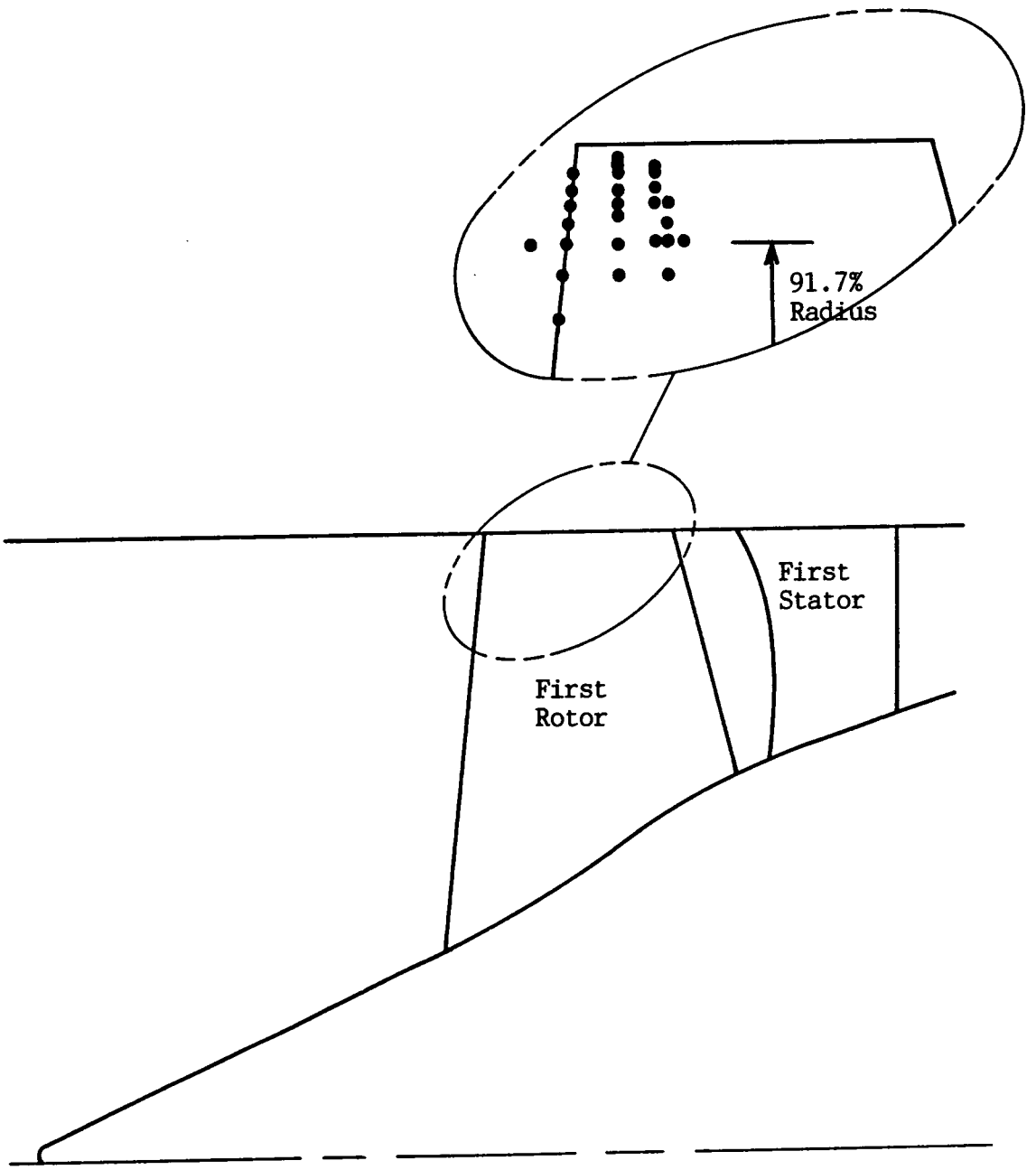

FIGURE 8 LTA Measurement Locations

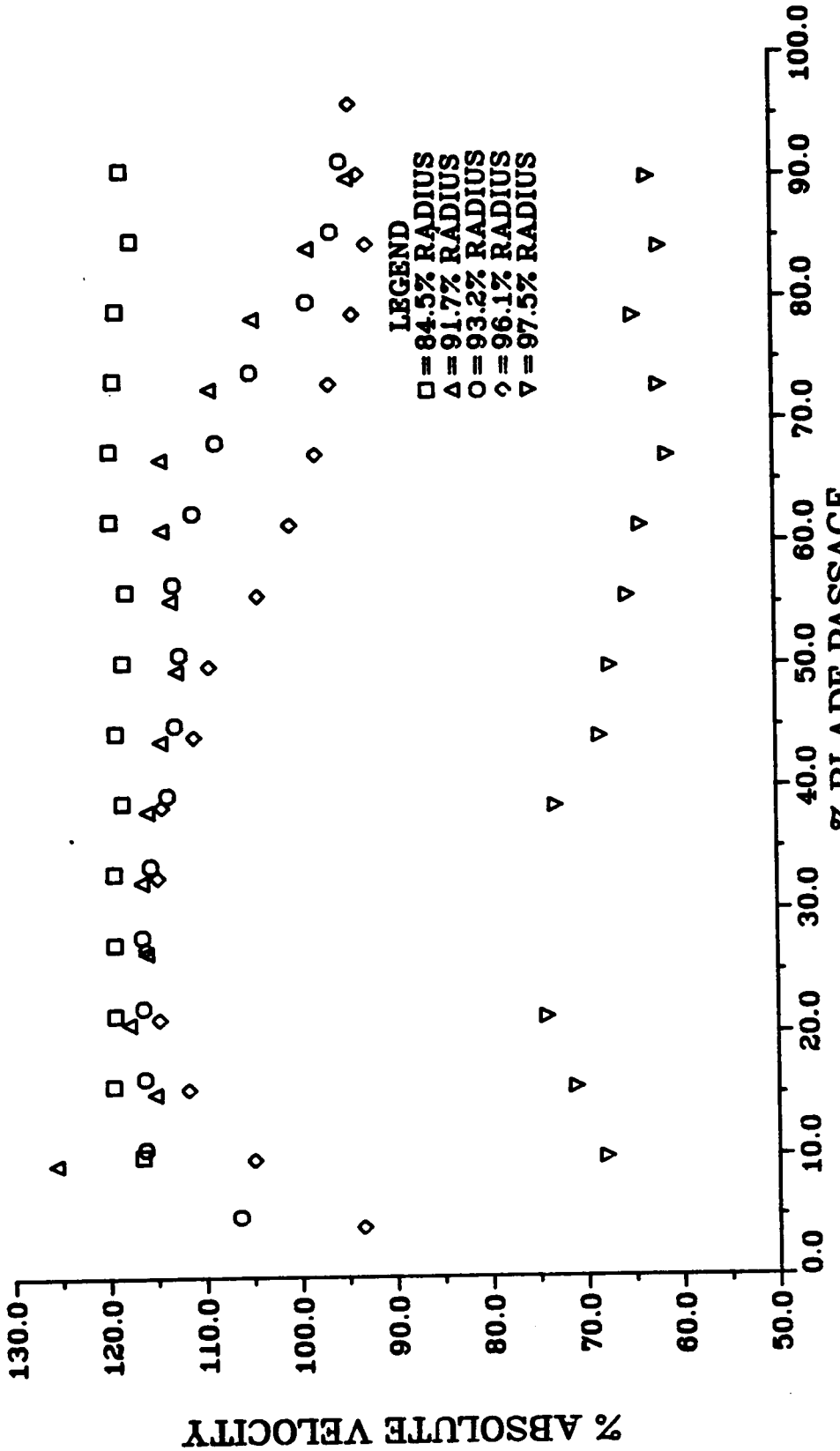

FIGURE 9 ABSOLUTE VELOCITY PROFILE, 0% CHORD, PASSAGE 5

observed between 96.1% and 97.5% of the radius. The decay in the velocity from suction side to pressure side, as well as the sinusoidal behavior, appears to be the result of the precompression waves emanating from the suction surface of the blading in the first 20% of the axial chord. A flow pattern with precompression waves is also reported in reference 10.

Figure 10 is similar to Figure 9 except it includes the profiles from both measured passages to demonstrate blade-to-blade variations. The variation in velocity from passage to passage is generally less than the estimated precision uncertainty, except at 97.5% radius. At this location, there is slightly larger variation.

Since these profiles are taken outside the blade passage, the velocity magnitudes and directions at the extremes of each profile should be the same. A closer examination of Figures 9 and 10 shows that this is essentially the case, except for the profiles at 91.7% and 93.2% radius. Figure 9 indicates that at the 91.7% radius, the velocity is essentially constant across the passage until 65% of the blade passage. Here the velocity begins to decay by approximately 20% as the pressure side of the blades is approached. This same behavior is also exhibited at 93.2% and 94.6% radius (see Table 20 in Appendix C). This observation of the profiles supports the idea that there is a series of discontinuities from the pressure side to the suction side in front of the blade between 91.7% and 94.6% of the blade radius. This is believed to be the result of the precompression waves in this region.

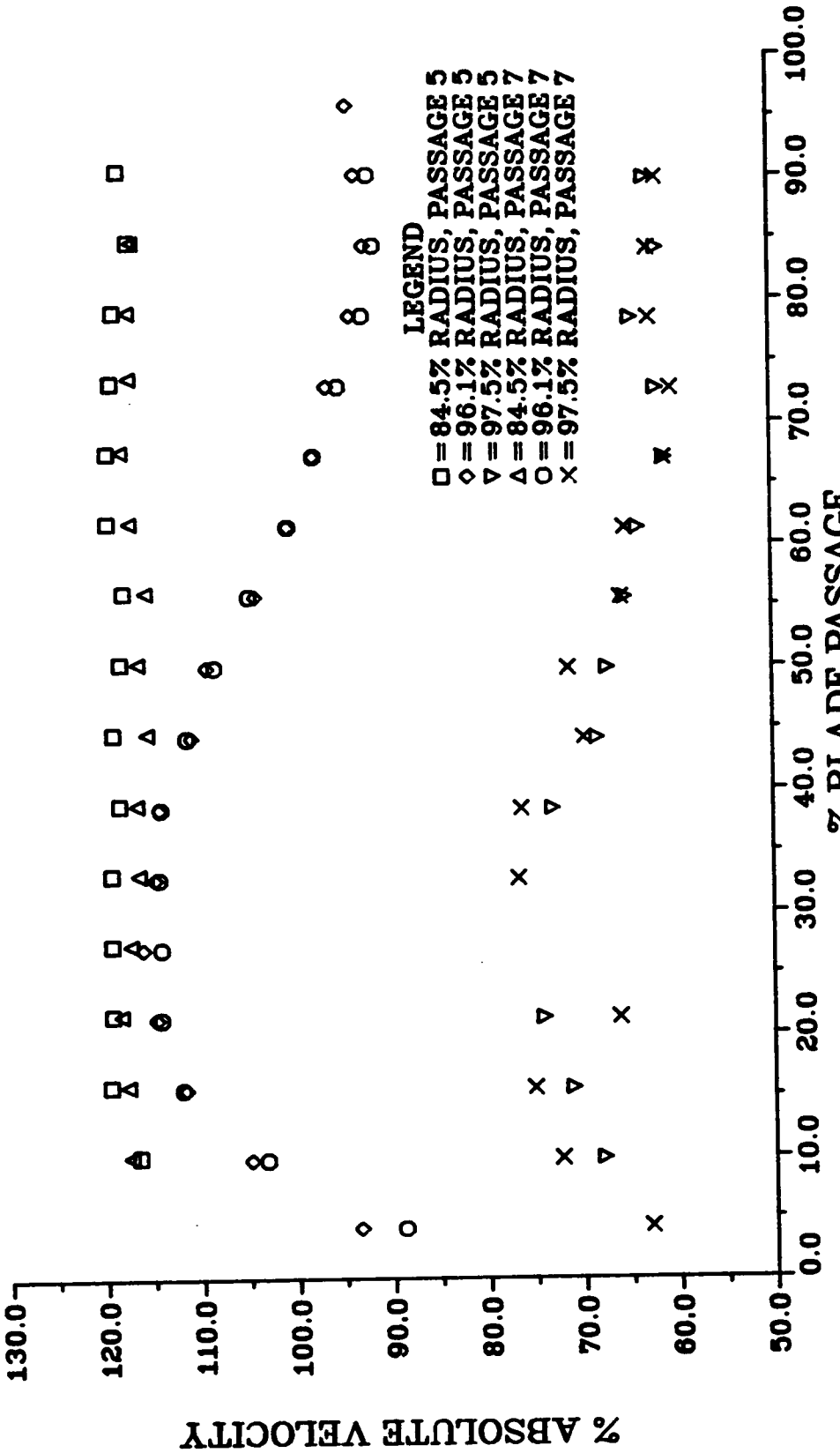

FIGURE 10 ABSOLUTE VELOCITY PROFILE, 0% CHORD, PASSAGES 5 AND 7

From the inlet data reported here, the strength, or at least the effect of these precompression waves, first increases from 88.9% to 91.7% radius and then decreases from 94.6% to 96.1% radius. The 94.6% radius appears to be where this effect is the strongest.

An inlet boundary layer profile composite using the average absolute velocity for each radius location measurement made at the leading edge is presented in Figure 11. Average absolute velocities for both passages measured are listed in Table 1. The decay in the velocity as the wall is approached is expected. Even though the flow is supersonic with respect to the blade at the compressor tip, the flow is still subsonic with respect to the inlet ducting. This subsonic flow field would permit an upstream influence from the rotor flow field.

Results for five of the radius locations measured at the 12% axial chord location are shown in Figure 12. In this figure, the relative velocity is presented as a percentage of the average blade-to-blade relative velocity within the blade row. The passage shock wave is observed to be at a constant position within the passage for all radial locations presented. Some scatter in the level of measured velocity exists on the upstream side of the passage shock wave. A closer look at this region reveals that at different depths the behavior changes. At a depth of 88.9%, the change at 42% of the blade passage is sudden and discrete, appearing similar to the passage shock wave at 64% of the blade passage. As the measurement location moves toward the end wall,

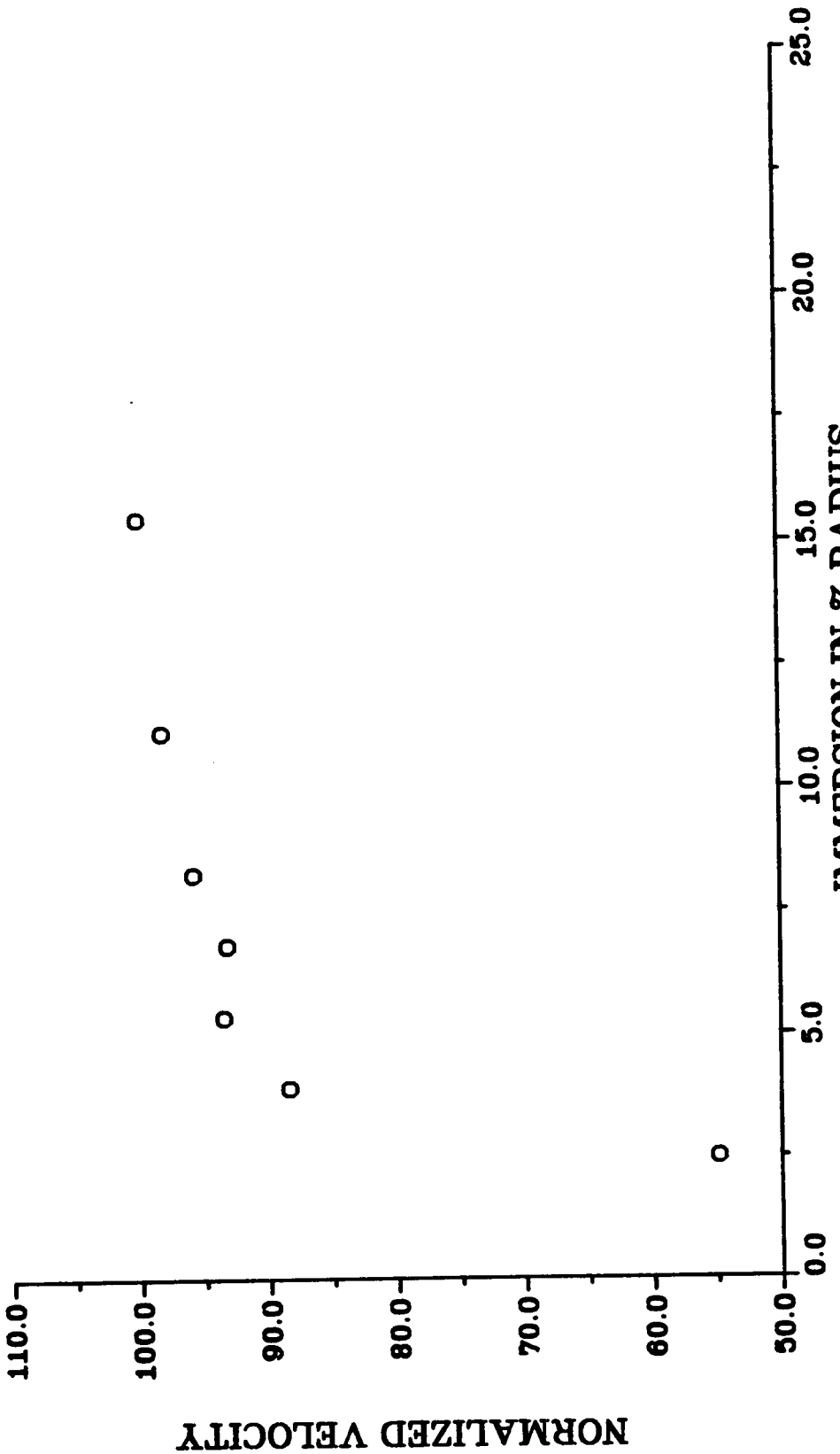

FIGURE 11 CIRCUMFERENTIALLY AVERAGED INLET
END WALL BOUNDARY LAYER PROFILE

TABLE 1

CIRCUMFERENTIALLY AVERAGED

BOUNDARY LAYER PROFILE DATA

% RADIUS	PASSAGE % ABSOLUTE VELOCITY		NORMALIZED VELOCITY IN %	
	PASSAGE #5	PASSAGE#7	PASSAGE#5	PASSAGE#7
84.5	118.6	117.0	100.0	100.0
88.9	115.6	114.8	97.5	98.1
88.9	115.2	114.8	97.1	98.1
91.7	112.1	112.0	94.5	95.7
93.2	109.5	108.0	92.3	92.3
94.6	109.7	109.3	92.5	93.4
96.1	103.7	103.4	87.4	88.4
97.5	66.4	67.4	56.8	57.6

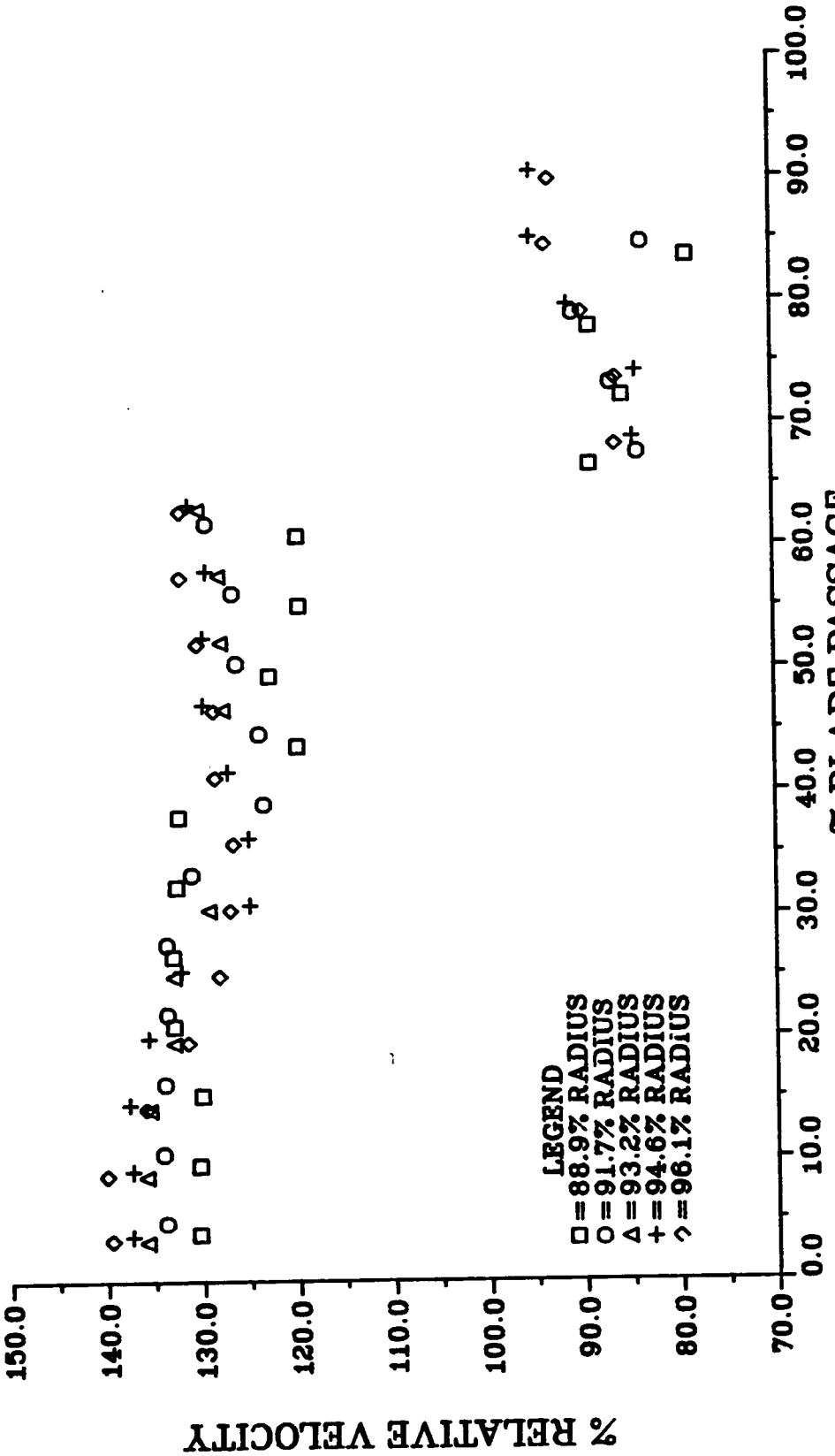

FIGURE 12 RELATIVE VELOCITY PROFILE, 12% CHORD, PASSAGE 5

the velocity changes more gradually and approaches a sinusoidal behavior similar to that observed at the leading edge. The change in relative velocity between the suction surface and the middle of the passage is again attributed to precompression waves emanating from the suction surface of the blade within the passage. The precompression waves tend to spread out across the passage as the tip end wall is approached. The coalescing behavior of the precompression waves at 12% axial chord is not repeated at the leading edge of the blades. Figure 13 shows the comparison from passage to passage at 12% axial chord for two radius positions. At this axial location, the variation from passage to passage is larger than the estimated precision uncertainty, but is less than the total system uncertainty.

When measurements were attempted at 12% axial chord and 96.8% radius, no measurements were obtained from the 17 locations across the blade passage. However, some measurements were recorded at 97.5% and 98.8% of the radius. At 98.8% of the radius, two locations in each of the blade passages produced usable data. Measurements at four locations in passage 5 and three locations in passage 7 were obtained at 97.5% radius. However, at this radius, two locations in each passage showed unusual behavior resulting in three velocity measurements of different magnitude and direction for each location. This behavior is referred to as "trimodal." A summary of the measurements at 98.8% and 97.5% of the radius, along with corresponding data from 96.1% of the radius, are presented in Table 2. Since there is a small variation in station locations between radii, Table 2

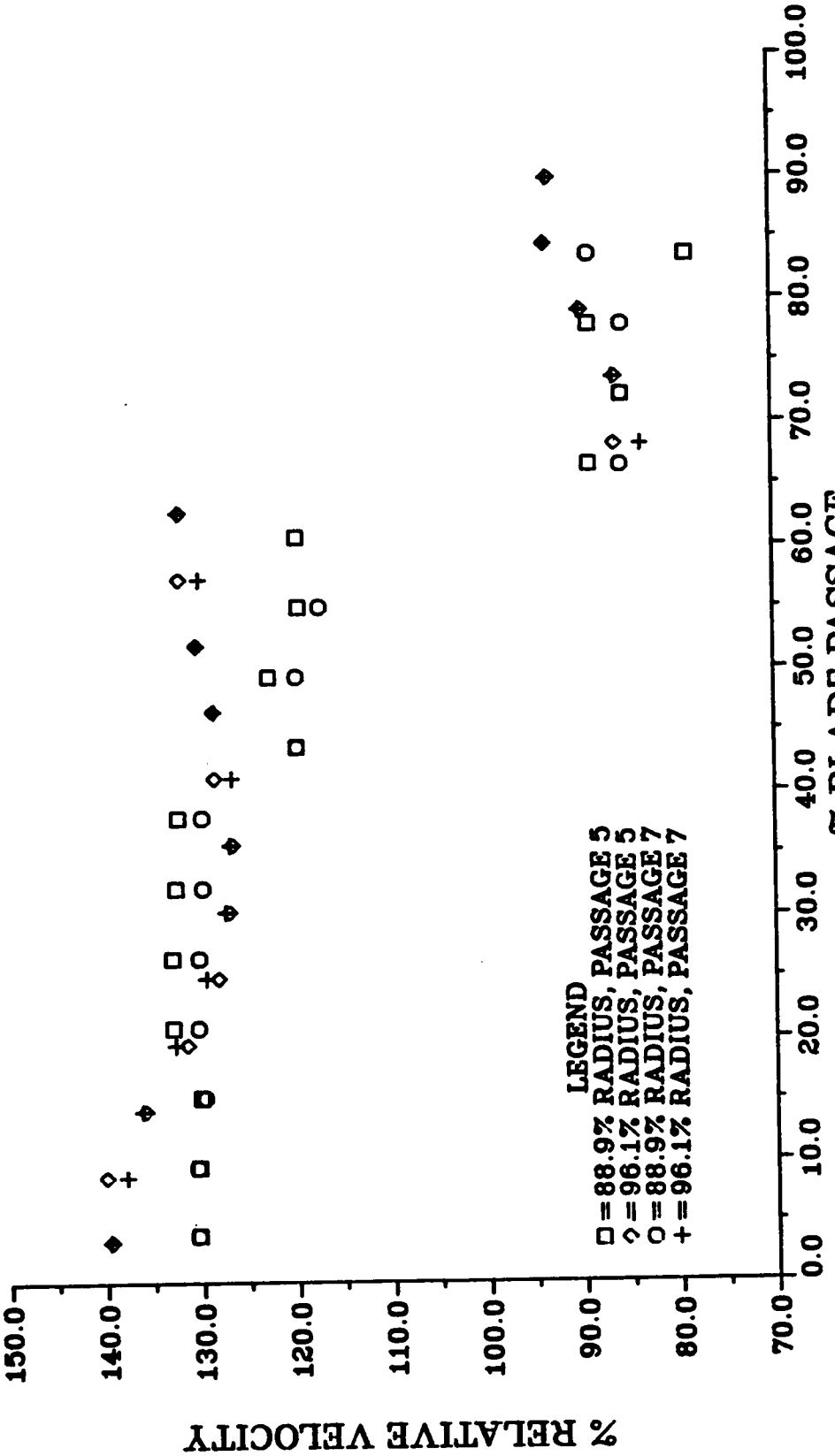

FIGURE 13 RELATIVE VELOCITY PROFILE, 12% CHORD, PASSAGES 5 AND 7

TABLE 2

COMPARISON OF ABSOLUTE VELOCITY AND FLOW ANGLE FOR RADIAL LOCATIONS AT 12% AXIAL CHORD

% BLADE PASSAGE FOR 96.1% RADIUS	RADIAL LOCATION					
	96.1%		97.5%		98.8%	
	VELOCITY (%)	ANGLE (degrees)	VELOCITY (%)	ANGLE (degrees)	VELOCITY (%)	ANGLE (degrees)
PASSAGE 5						
25.0	105.5	-4.7	123.1	1.7		
			152.9	-76.8		
			184.6	-85.6		
30.4	95.7	-6.8	107.8	1.7	102.7	-27.1
			159.0	-81.1		
			163.0	-82.6		
79.0	104.7	-42.6	163.3	-81.1		
84.4	103.0	-39.3	156.0	-81.1	101.3	-27.1
PASSAGE 7						
25.0	106.5	-6.8	130.3	1.7		
			162.8	-81.1		
			168.6	-82.6		
30.4	97.4	-6.8	111.4	1.7	151.0	-78.6
			159.4	-81.1		
			176.0	-85.6		
35.8	95.2	-6.8			168.1	-27.1
84.4	103.0	-39.3	158.2	-81.1		

contains the station positions at 96.1% radius for reference. Table 20 in Appendix C contains the actual values for the other two radii. The data in Table 2 show a definite change in the flow field behavior between 96.1% and 97.5% radius. The magnitude and direction of the velocity vector measured beyond 96.1% radius do not agree with measurements at 96.1% radius. Measurements at radial locations less than 96.1% do compare favorably from radius to radius as shown on Figure 12. The measurements made at 96.1% of the radius show no unusual behavior. Turbulence level was indicated to be essentially the same as other radial locations (less than 5%). Even though only a few velocity values are reported in Table 2 for the measurements at 97.5% and 98.8% radius, particle transit times were observed at the other locations by the LTA system. This is evidenced by the total number of events listed in Table 20 in Appendix C. These particle transits, however, were uncorrelated. The LTA spot angle search was widened and eventually included purely circumferential flow (see Table 19 in Appendix C for details); still, no additional correlated measurements were observed. Three possible reasons are offered as to why a correlated signal was not observed at more locations beyond 96.1% of the radius. First, the absolute velocity vector direction in the end wall area could be outside the region of acceptable angles for the LTA spot orientation as stated earlier (see also Section 5 of Appendix A). Second, the turbulence level could have increased to a level greater than 20%, where the LTA cannot make measurements because of its probe volume geometry as reported in Section 6 of Appendix A. Third, the flow could have decelerated to a value outside the expected velocity range of 120

to 550 m/sec. In any event, the change in the flow field behavior occurred abruptly over a distance of only 0.7% of the radius. This abrupt change indicates that there is a shear layer between the well ordered core flow region and the end wall boundary layer region. A previous study by McDonald, et al. (20) presents LTA measurements at a percent of span that would correspond to the 96.1% radial location in the compressor studied here. However, there is no report in reference 20 of measurements being made closer than this to the end wall.

Relative velocity measurements at three of the radial locations measured at 22% of the axial chord location are shown in Figure 14. Relative velocity is again nondimensionalized by the average velocity used at the previous location. All of the radial locations show essentially the same behavior. The passage shock wave is again located at the same position within the blade passage for all radial locations presented. At this chord location, there is no evidence of the precompression waves observed at the previous two locations. Figure 15 shows the comparison of the measurements made in both blade passages at this axial location for two radial locations. Here there is essentially no passage to passage variation.

When the flow field was measured at 22% axial chord and 96.8% radius, only five locations out of the possible 17 locations were measured for each blade passage. The measurement location was moved to 97.5% of the radius, and at that position, only four locations were measured. Table 3 presents these data along with corresponding values

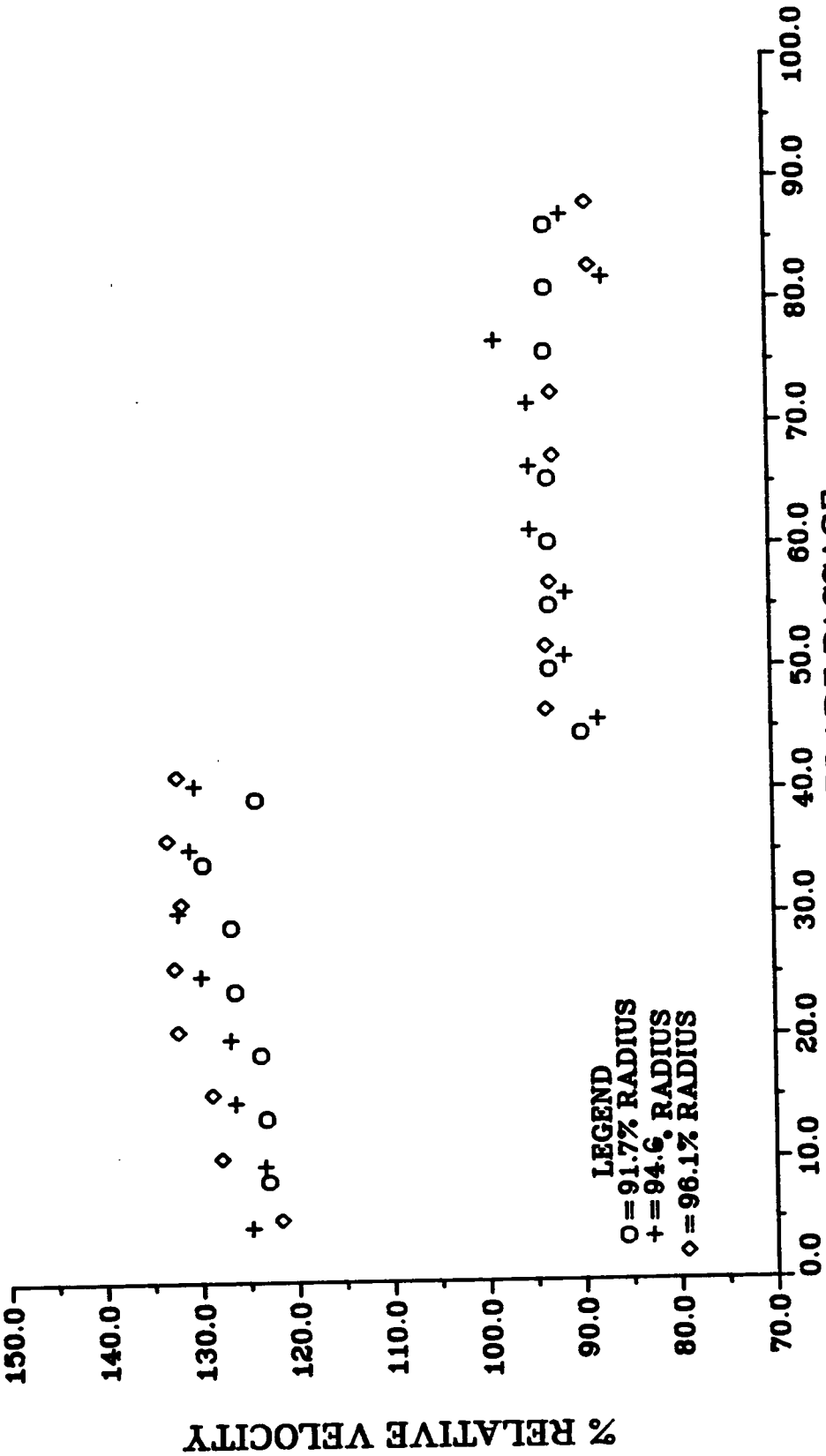

FIGURE 14 RELATIVE VELOCITY PROFILE, 22% CHORD, PASSAGE 5

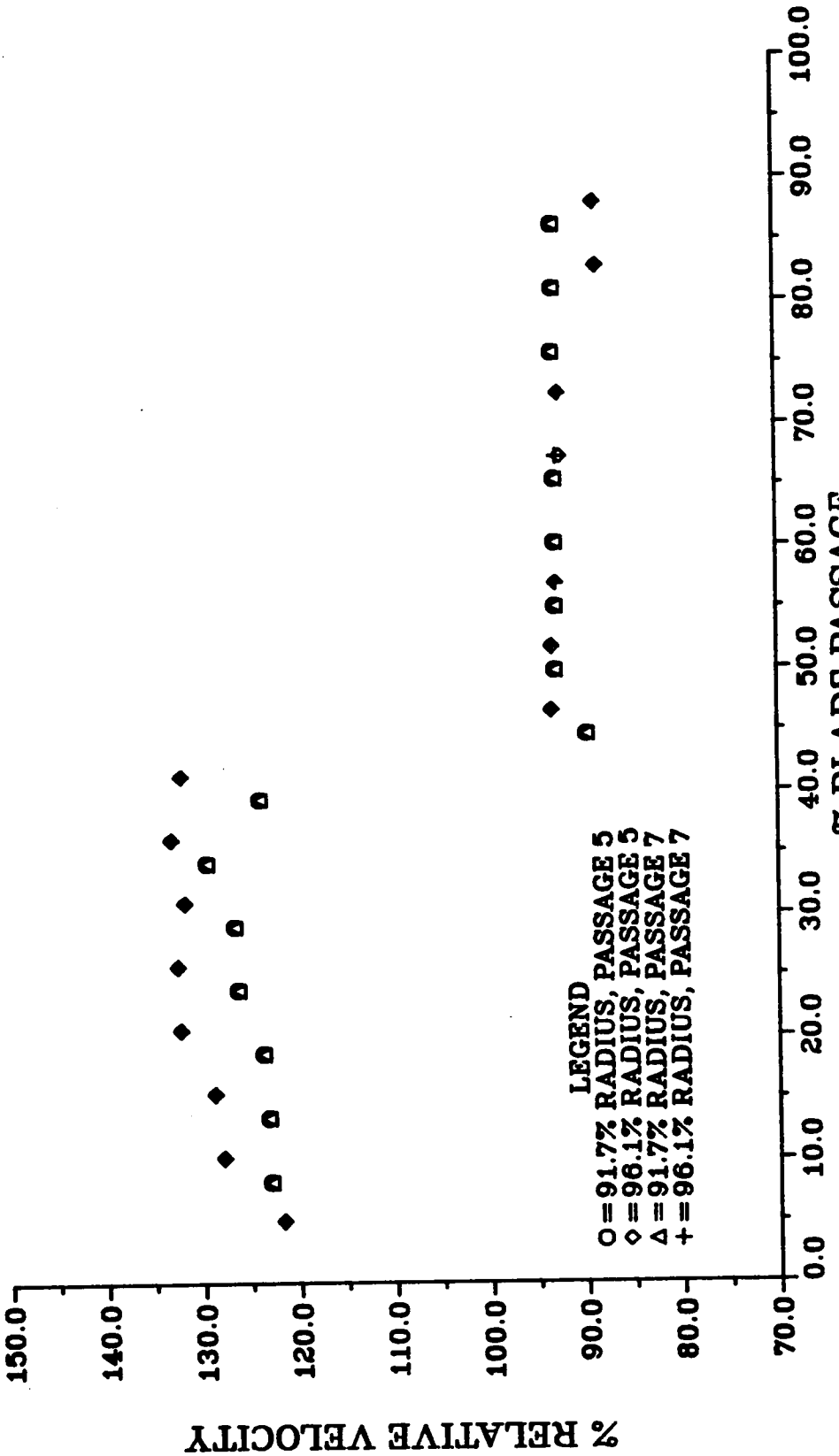

FIGURE 15 RELATIVE VELOCITY PROFILE, 22% CHORD, PASSAGES 5 AND 7

TABLE 3

COMPARISON OF ABSOLUTE VELOCITY AND FLOW ANGLE FOR RADIAL LOCATIONS AT 22% AXIAL CHORD

% BLADE PASSAGE FOR 96.1% RADIUS	RADIAL LOCATION					
	96.1%		96.8%		97.5%	
	VELOCITY (%)	ANGLE (degrees)	VELOCITY (%)	ANGLE (degrees)	VELOCITY (%)	ANGLE (degrees)
PASSAGE 5						
20.7	107.3	-4.6	108.9	-53.3	110.1	-9.0
25.9	108.5	-2.5	96.6	-53.3	96.7	-9.0
72.6	106.9	-36.4	91.3	-52.9	-	-
77.8	119.7	-43.0	107.3	-53.3	108.5	-9.0
82.9	115.0	-43.0	86.3	-53.3	-	-
PASSAGE 7						
20.7	108.8	-4.6	109.5	-53.3	107.0	-9.0
25.9	109.9	-4.6	28.3	-53.3	185.0	-9.0
41.4	100.3	-2.5	87.1	-21.9	-	-
62.2	-	-	31.9	-52.9	-	-
77.8	-	-	107.7	-53.3	103.6	-9.0

measured at 96.1% of the radius. Since there is a small variation in station locations between radii, the positions at 96.1% radius are used for reference. Table 20 in Appendix C contains the actual values for the other radii. From Table 3 it is obvious that there is a change in the flow field behavior from 96.1% to 96.8% of the blade radius. The data also indicate that this change occurs across the complete blade passage except at 20.7% and 25.9% of the blade passage. At these two locations, measurements were observed out to 97.5% of the blade radius in both blade passages measured. In blade passage 5, the value of velocity and direction for these two locations at 97.5% radius agrees favorably with the corresponding data at 96.1% radius, although the data at the intermediate region of 96.8% radius do not correspond to the other two locations. However, in blade passage 7, the value of velocity and direction at 97.5% radius only agrees favorably with the corresponding data at 96.1% radius at 20.7% of the blade passage.

At 12% and 22% of the axial chord, the flow essentially became unmeasurable between 96.1% and 96.8% of the radius, even though measurements at 97.5% of the radius were made at the leading edge of the blade (see Figures 9 and 10). This layer between measurable and unmeasurable flow was not only constant in radial position from 12% of the axial chord to 22% of the axial chord, but it was also at the same depth across the blade passage from the suction surface to the pressure surface. It is important to note that this was not a result of a low data rate in this region; rather, the particle transit times measured in this region were uncorrelated for the transit time range sampled.

An attempt was made to measure closer than 96.8% of the radius to the end wall. Similar results were observed until the probe volume was so close to window surface (99.0% radius) that the reflected light scattered from the window interface prevented any transit measurements.

Flow field measurements were made at 91.7% radius at -10%, 25% and 30% of the axial chord. These data are presented for passage 5 in Figures 16, 17 and 18, respectively. A shock wave discontinuity is only observed at the 25% axial chord location. Here, measurements were made with two station widths and both are presented for comparison. The inlet flow at -10% axial chord exhibits a gradual change in flow velocity similar to the data at the blade leading edge. The flow near the suction surface of the passage at -10% axial chord is approximately 30% lower than the center of the passage. This reduction in velocity is believed to be a result of the leading edge expansion fan. The velocity profile at 30% axial chord shows no evidence of the passage shock wave observed at 12%, 22% and 25% axial chords. The magnitude of the velocity is observed to be approximately the same as the magnitude measured downstream from the passage shock wave at the other three locations. However, as can be seen in Table 20 in Appendix C, the absolute angle is considerably different. The flow at 91.7% radius and 30% of the axial chord is at -75 degrees, only 15 degrees from being purely circumferential. At the other three locations where the passage shock wave was observed, the flow was measured to be at about -40 degrees. The leading edge of the first circumferential groove shown in Figure 4 (see also Figure 53 in Appendix B) is located at 30% of the

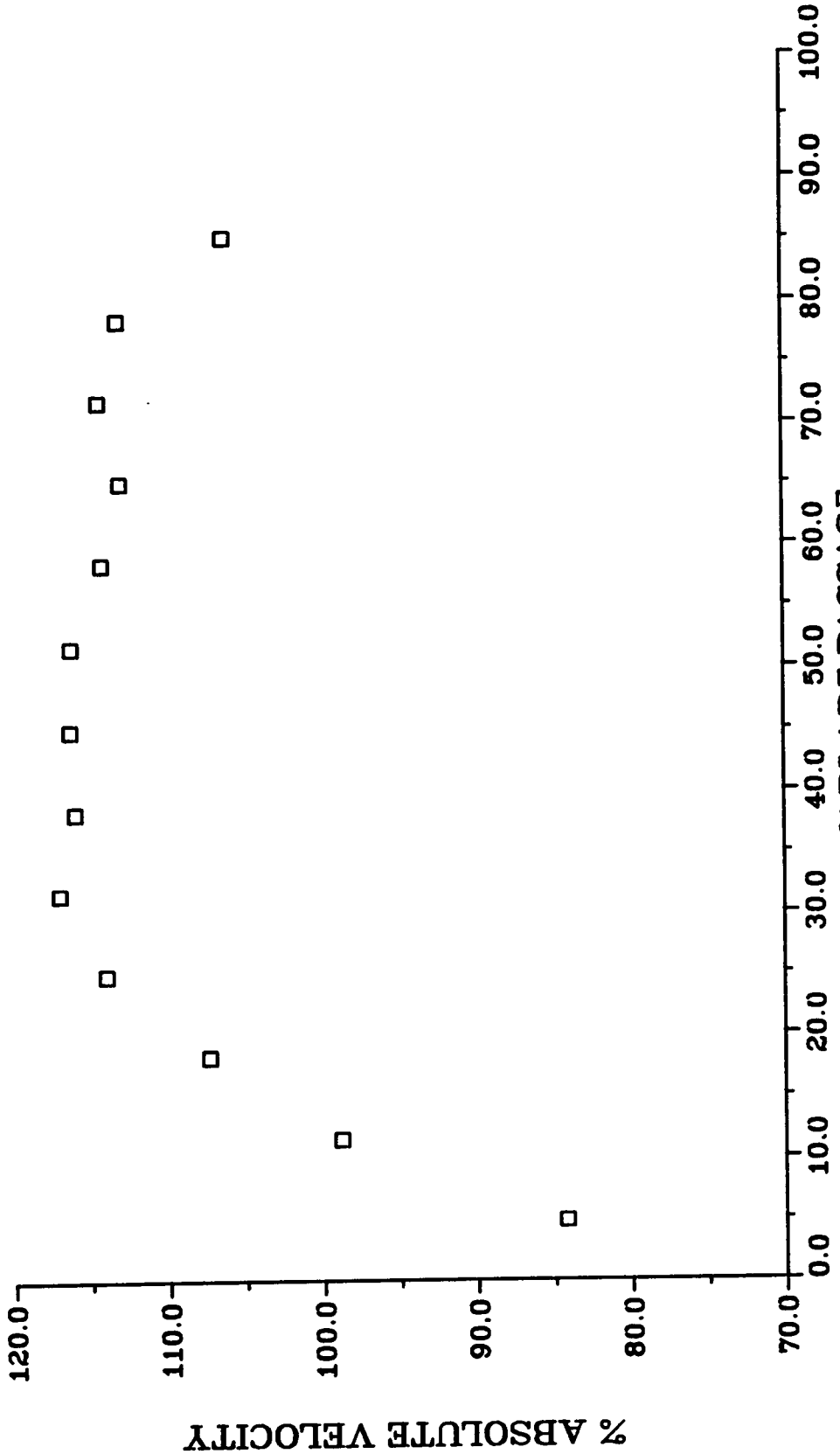

FIGURE 16 ABSOLUTE VELOCITY PROFILE,
−10% CHORD, PASSAGE 6, 91.7% RADIUS

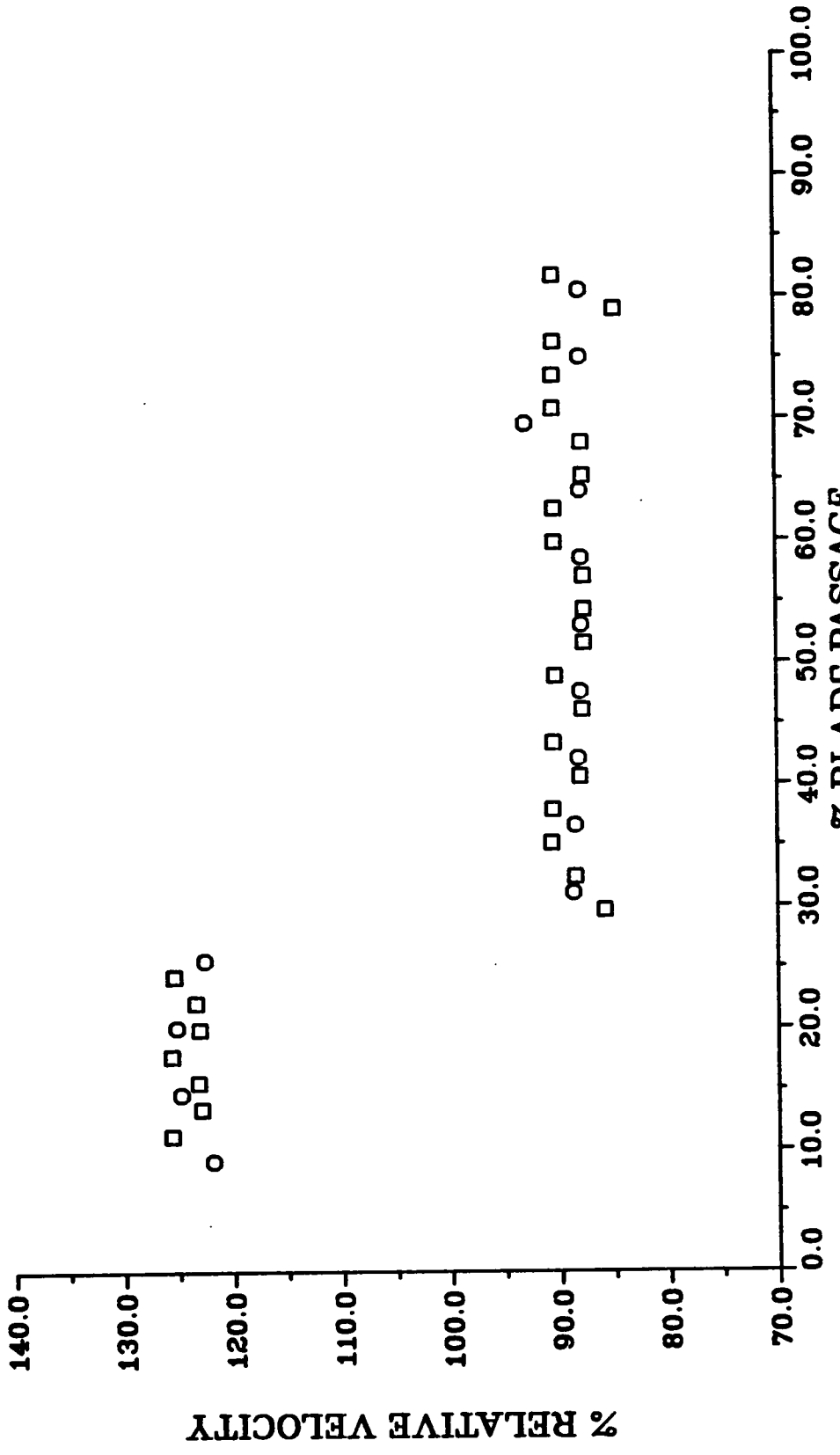

FIGURE 17 RELATIVE VELOCITY PROFILE, 25% CHORD, PASSAGE 5, 91.7% RADIUS

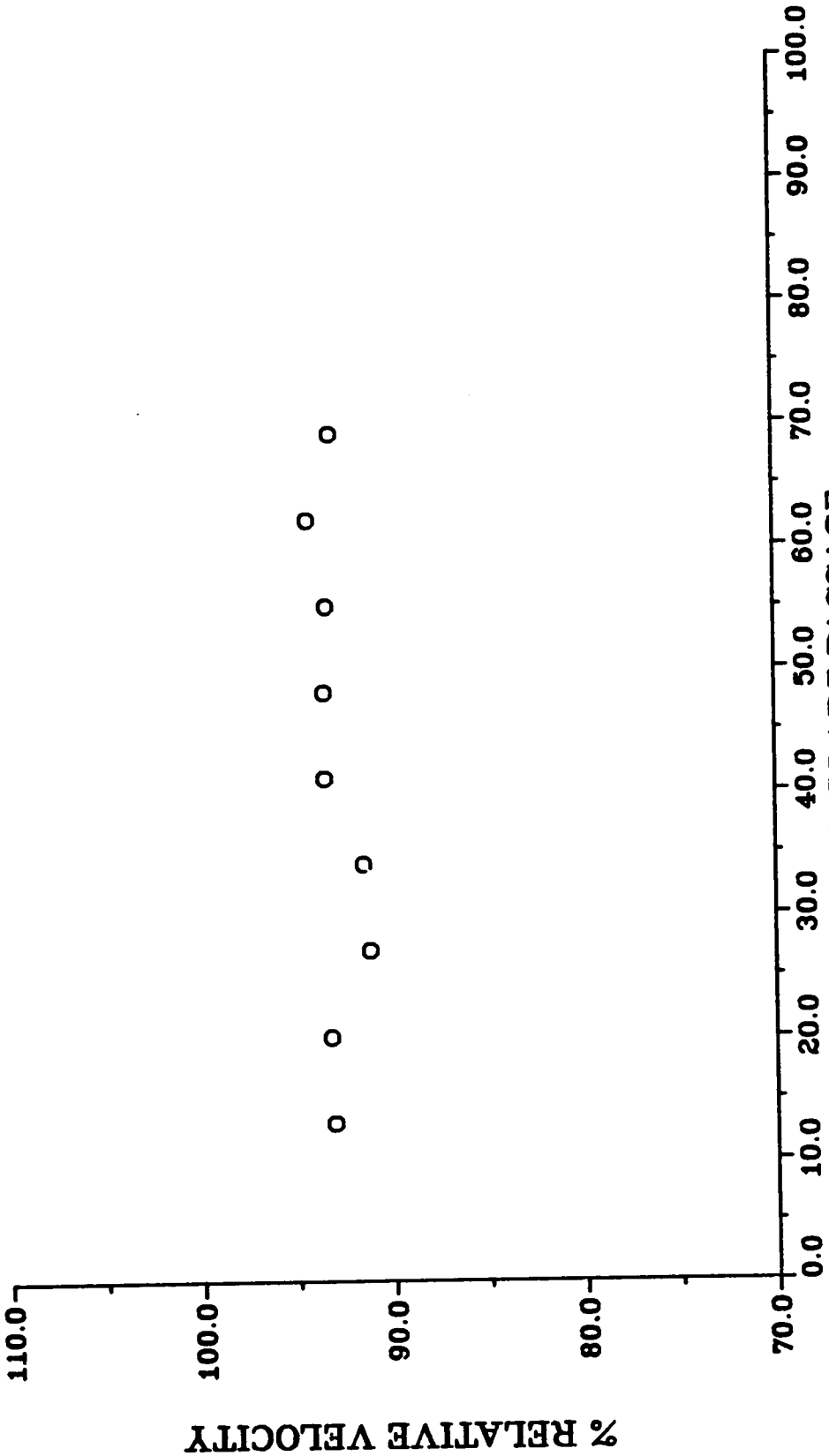

FIGURE 18 RELATIVE VELOCITY PROFILE, 30% CHORD, PASSAGE 5, 91.7% RADIUS

axial chord. The flow at 91.7% radius at this location may be affected by the flow within the groove itself.

A composite of all the measurements made at 91.7% radius is presented in Figure 19. The triangles represent discrete jumps in the relative flow velocity and a shock wave similar to that observed in Figure 17. The bands along the circumferential measurement lines indicate regions of gradual changes in the flow velocity, as shown in Figures 9 and 12, due to the leading edge expansion fan and precompression waves. The points near the blade surfaces indicate the maximum extent of the LTA measurements in the circumferential direction. From Figure 1 the passage shock wave is measured to be at an angle of about 20 degrees to the axial direction at 22% of the axial chord.

B. Data Verification:

Besides the calibration and the evaluation of measurement errors associated with the LTA system which have been discussed and presented in detail in Section IV, part C, the acquired compressor data were also verified using three independent methods. During the experiment, data were measured in two blade passages simultaneously, as described in Appendix A. The passage-to-passage variation has already been reported at 0%, 12% and 22% of the axial chord in Figures 10, 13 and 15, respectively. Further comparison between passages can be performed using the data presented in Appendix C. It is unlikely that the

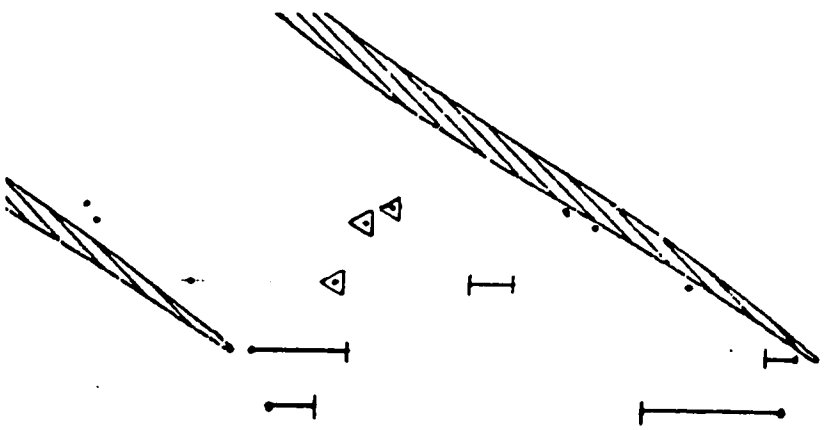

FIGURE 19 Flow Field Behavior at 91.7% Radius

variation from passage to passage and the actual measurement errors would cancel or reduce any observed variation between passages. Therefore, a pessimistic estimate of the error in the LTA system during the experiment could be estimated assuming that the passage flow fields were the same. Then the variation from passage to passage would represent the actual experimental precision. From the data in Figures 10, 13 and 15, this implied experimental precision is considered to be less than ± 2.5% of the absolute velocity. For the locations presented in these figures, Appendix C indicates that the implied precision in direction is less than ± 1.25 degrees of the absolute flow angle.

Measurement locations were also repeated from day to day and within a test day. Six locations were measured more than once (see Tables 19 and 20 in Appendix C). Figures 20 through 21a present a representation of these comparisons for five of these locations. Again the variation between repeated measurements can pessimistically be considered an indication of the precision. In these figures, the implied experimental precision is less than ± 4.5% of the absolute velocity and ± 1.5 degrees of the absolute flow direction .

One further verification technique was employed. The change in flow angle and magnitude in the relative reference frame should be related to the shock wave angle in the relative reference frame as indicated by Prince (41). Using the two dimensional shock wave relations of reference 42, the Mach number and flow directions measured upstream and downstream from the shock wave can be compared to the

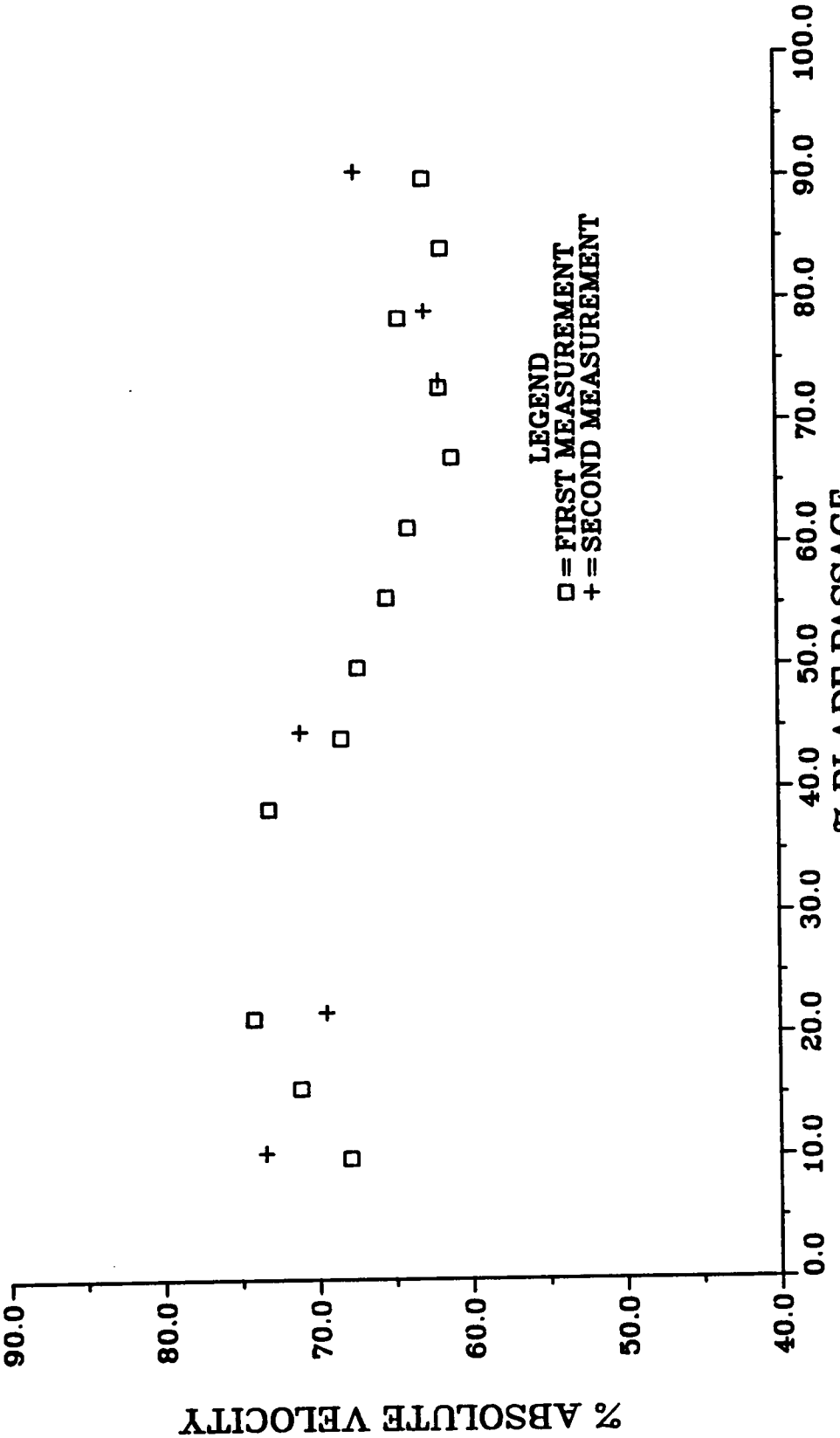

FIGURE 20 REPEATABILITY OF FLOW FIELD MEASUREMENTS
WITHIN A TEST DAY, 0% CHORD, 97.5% RADIUS, PASSAGE 5

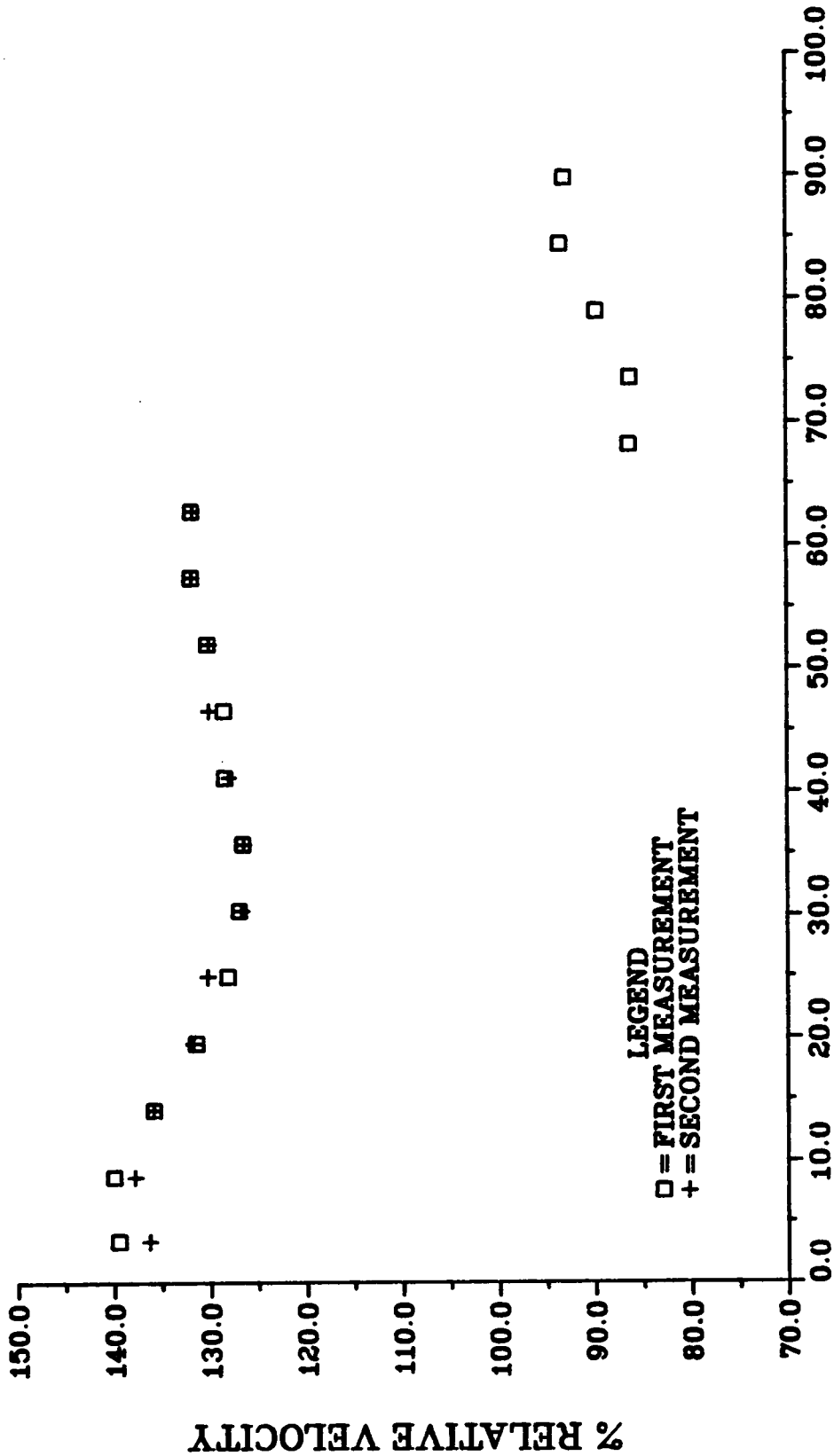

FIGURE 20A REPEATABILITY OF FLOW FIELD MEASUREMENTS
WITHIN A TEST DAY, 12% CHORD, 96.1% RADIUS, PASSAGE 5

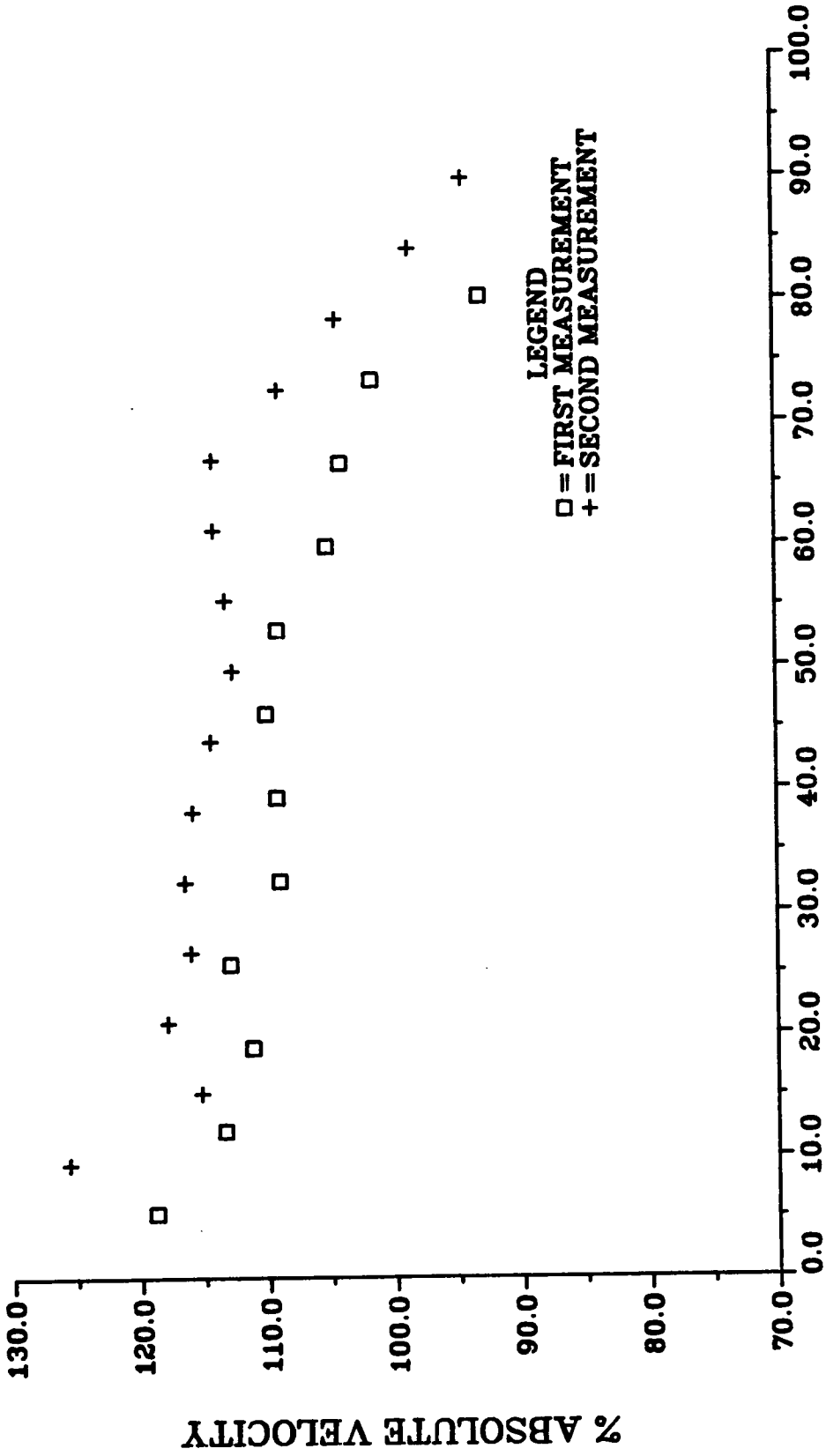

FIGURE 21 REPEATABILITY OF FLOW FIELD MEASUREMENTS
FROM DAY TO DAY, 0% CHORD, 91.7% RADIUS, PASSAGE 5

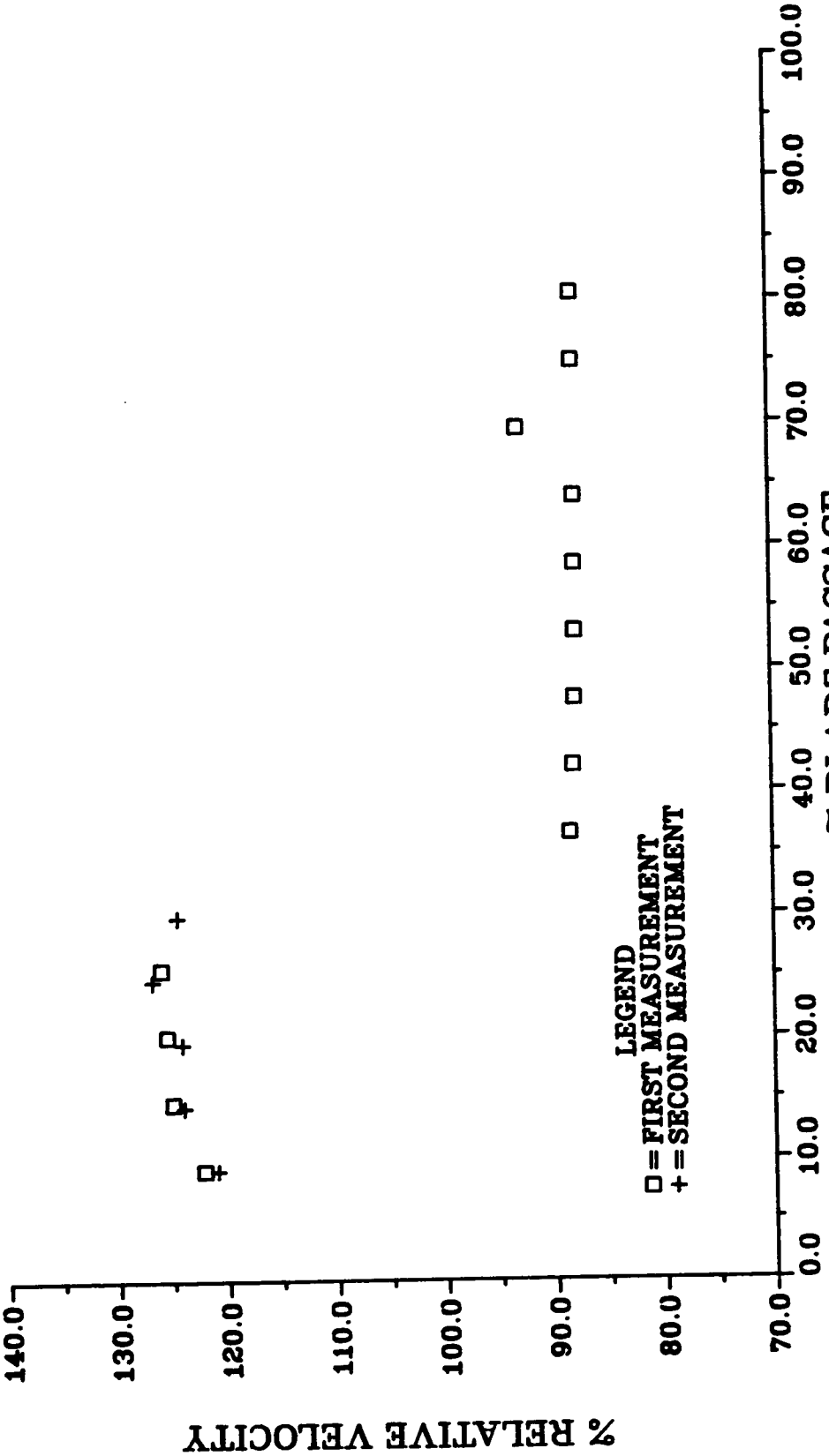

FIGURE 21A REPEATABILITY OF FLOW FIELD MEASUREMENTS
FROM DAY TO DAY, 25% CHORD, 91.7% RADIUS, PASSAGE 5

observed shock angle in the blade passage. The Mach number and flow direction changes measured across the shock wave along with the two dimensional shock wave relationships presented in reference 42 supported the representation of the shock angle shown in Figure 19. However, the shock angle can be in error because of the use of discrete stations to measure the flow across the blade passage. If the shock wave at 12% axial chord had been located in the next station toward the suction side of the passage, then the shock angle in Figure 14 would be at approximately 12 degrees if there were no corresponding change with shock wave location at 22% axial chord. Therefore, although the shock wave angle is in agreement with previous measurements (9, 11) the results are not conclusive. It is noted that the purpose of this work was not to measure the shock angle; its importance lies in the characterization of flow behavior near the end wall. In future experiments, more circumferential locations within the passage could be measured to overcome this uncertainty in shock angle.

C. Seed Effects

The size of the particles measured by the laser anemometer can be estimated if the particle deceleration distance behind the shock wave can be determined. The particle deceleration distance perpendicular to the shock wave can be estimated from the measured compressor flow field shown in Figure 17. This figure presents two sets of measurements made within the same blade passage. The distance used to make a measurement in one case is 5.5% of the blade passage, and in the other case, the

distance for a measurement is 2.7% of the blade passage. With the longer distance, the change in velocity is observed to jump from the velocity before the shock to the velocity after the shock between two adjacent measurement locations in passage 7. When the distance was 2.7% of the blade passage, the velocity changed over two measurement locations. This behavior was observed in both of the measured passages. If the deceleration distance of the measured particles is the only factor influencing this result, then a range of deceleration distance can be calculated. Referring to Figure 22, the maximum deceleration distance, Xw, perpendicular to the shock wave can be calculated from

$$Xw = SW \cos\phi$$

In this relationship, SW is the measurement length along the line of measurements used to make one velocity measurement, and ϕ is the angle between the shock wave and the normal to the line of measurements. In Figure 17, a discrete change in velocity from one station to the next is observed for a measurement length of 5.5% of the blade passage but not with a measurement length of 2.7% of the blade passage. Therefore, the particle deceleration distance must be between the maximum deceleration distances calculated using these two measurement lengths. For the results obtained in Figure 17, the particle deceleration distance would be between 2.9 mm and 5.9 mm. From these distances and the data presented by Melling (37), the particles being measured are considered to be on the order of 0.4

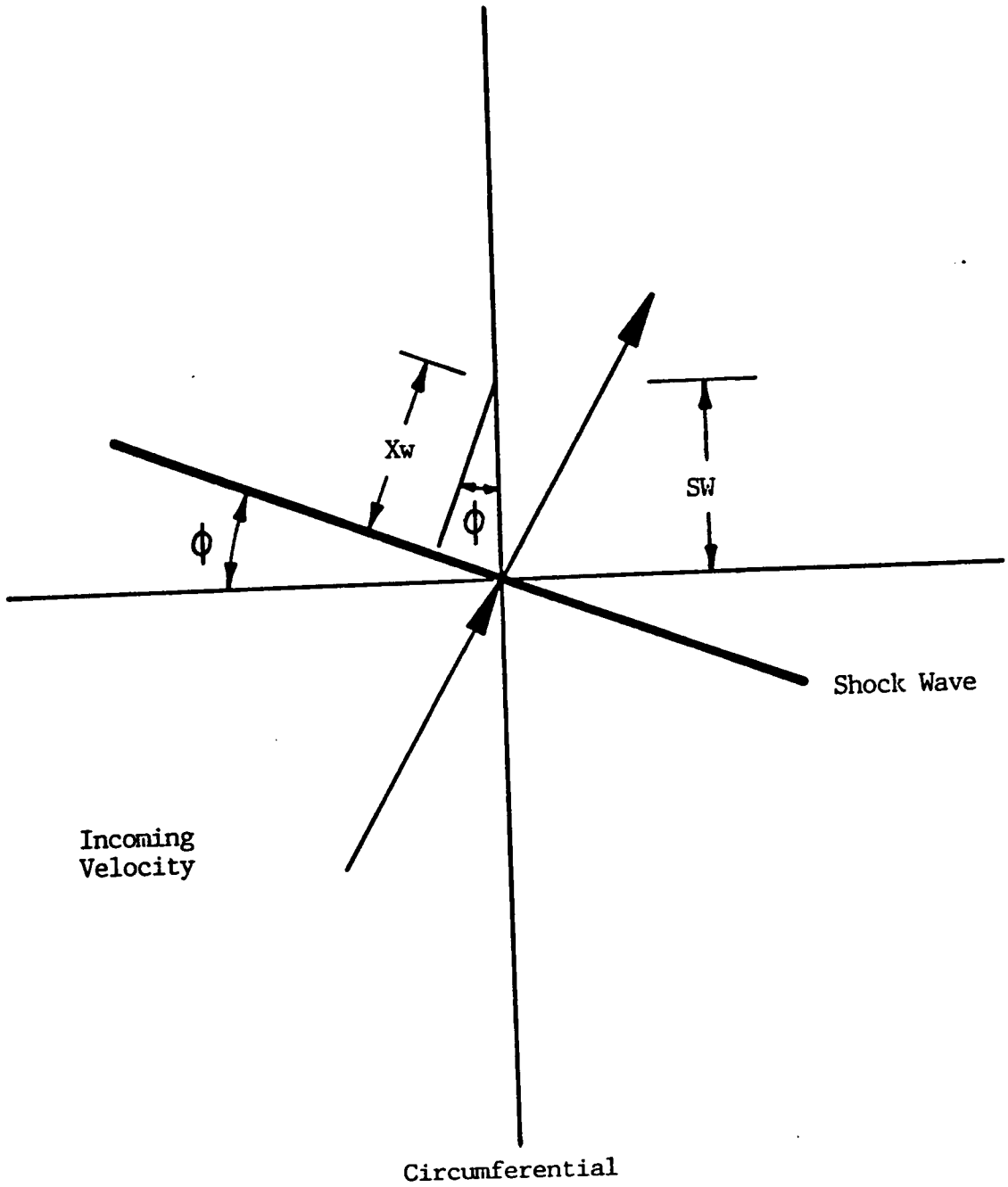

FIGURE 22 LTA Measurement Orientation to Passage Shock Wave

micron to 0.6 micron. This agrees favorably with the expected diameters based on natural dust particles.

This calculation ignores any movements in the shock location, which could also cause the loss of data in the finer step measurements. If the shock wave did move, as reported by Strazisar (16), the observed resolution of the shock location would indicate that the diameter of the measured particles would be even smaller than the range given above. The range of 2.9 mm to 5.9 mm is essentially half of the deceleration distance reported in reference 13 where the seed diameter is reported to be about 1.3 microns.

VI ANALYTICAL PREDICTIONS

The two dimensional Reynolds-averaged Navier-Stokes computer model developed by Richardson (43) was used to guide the LTA setup during the experiment and to analyze the test results. Since the program assumes two dimensional flow behavior, the analysis was only performed at the 91.7% radius. The original design codes used for the compressor considered the flow to be two dimensional at this radius (33).

A. Program Overview

The Reynolds-averaged Navier-Stokes equations in vector form were solved using a CRAY XMP-12 computer. These equations in mass-averaged variables take the following form for general curvilinear coordinates:

$$\frac{\partial \vec{U}}{\partial t} + \frac{1}{\delta}\left(\frac{\partial \vec{E}}{\partial x} + \frac{\partial \vec{F}}{\partial y}\right) = 0$$

where the vector components are:

$$\vec{U} = \begin{bmatrix} \rho \\ \rho u \\ \rho v \\ \rho e \end{bmatrix}$$

$$\vec{E} = \begin{bmatrix} \delta\rho u \\ \delta\rho u^2 - \sigma_{xx} \\ \delta\rho uv - \tau_{xy} \\ \delta\rho ue - u\sigma_{xx} - v\tau_{xy} - \dot{q}_x \end{bmatrix} \qquad \vec{F} = \begin{bmatrix} \delta\rho u \\ \delta\rho uv - \tau_{xy} \\ \delta\rho v^2 - \sigma_{yy} \\ \delta\rho ve - v\sigma_{yy} - u\tau_{xy} - \dot{q}_y \end{bmatrix}$$

where the normal and shear stresses, σ and τ, and the heat flux components $\dot{q}_x$ and $\dot{q}_y$ are:

$$\sigma_{xx} = 2.6\mu\frac{\partial(\delta u)}{\partial x} + 0.6\mu\frac{\partial(\delta v)}{\partial y} - \delta P$$

$$\sigma_{yy} = 2.6\mu\frac{\partial(\delta v)}{\partial y} + 0.6\mu\frac{\partial(\delta u)}{\partial x} - \delta P$$

$$\tau_{xy} = \tau_{yx} = \mu\left[\frac{\partial(\delta u)}{\partial y} + \frac{\partial(\delta v)}{\partial x}\right]$$

$$\dot{q}_x = K\frac{\partial(\delta T)}{\partial x}, \quad \dot{q}_y = K\frac{\partial(\delta T)}{\partial y}$$

and δ is the streamtube contraction distribution taken from the design streamtube prediction (33).

The program uses the MacCormick explicit algorithm and the Baldwin-Lomax algebraic eddy viscosity turbulence model for closure. With the MacCormick explicit algorithm, a predictor and a corrector step are used. The predictor step is:

$$\vec{U}_{i,j}^{n+1} = \vec{U}_{i,j}^{n} - \frac{\Delta t}{\Delta x}\left(\vec{E}_{i+1,j}^{n} - \vec{E}_{i,j}^{n}\right) - \frac{\Delta t}{\Delta y}\left(\vec{F}_{i,j+1}^{n} - \vec{F}_{i,j}^{n}\right)$$

and the corrector step is:

$$\vec{U}_{i,j}^{n+1} = \frac{1}{2}\left(\vec{U}_{i,j}^{n} + \vec{U}_{i,j}^{n+1}\right) - \frac{\Delta t}{\Delta x}\left(\vec{E}_{i,j}^{n+1} - \vec{E}_{i-1,j}^{n+1}\right) - \frac{\Delta t}{\Delta y}\left(\vec{F}_{i,j}^{n+1} - \vec{F}_{i,j-1}^{n+1}\right)$$

where i and j are the grid indices, n is the time step index, and Δt is the time step determined by the Courant - Fredericks - Levy stability criteria. The upstream relative total temperature and pressure were specified along with a constant value of the wheel speed. A "no slip" condition on the blade surfaces was enforced and it was required that derivatives of static pressure and temperature with respect to the normal to the blade be zero near the blade surface. Blade passage periodicity was specified in the flow field upstream and downstream of the blades. The operating condition of the compressor for a given wheel speed was set to the test conditions by specifing the downstream static pressure as determined from the test results.

B. Flow Field Predictions

The analytical prediction of the flow field at 91.7% radius for the compressor operating conditions of the LTA experiment is shown in Figure 23. The region shown in Figure 23 is essentially the area investigated during the experiment. From these predicted pressure and Mach number contours, precompression waves and the passage shock wave are visible. Figure 24 shows a combination of the experimental data presented in Figure 19 and the analytical results presented in Figure 23. Here it is seen that the two do not exactly match, but the structure of the flow field from the analytical predictions compares favorably with the measured flow field behavior. Both the analytical results and the measurements show an obvious passage shock wave. Also,

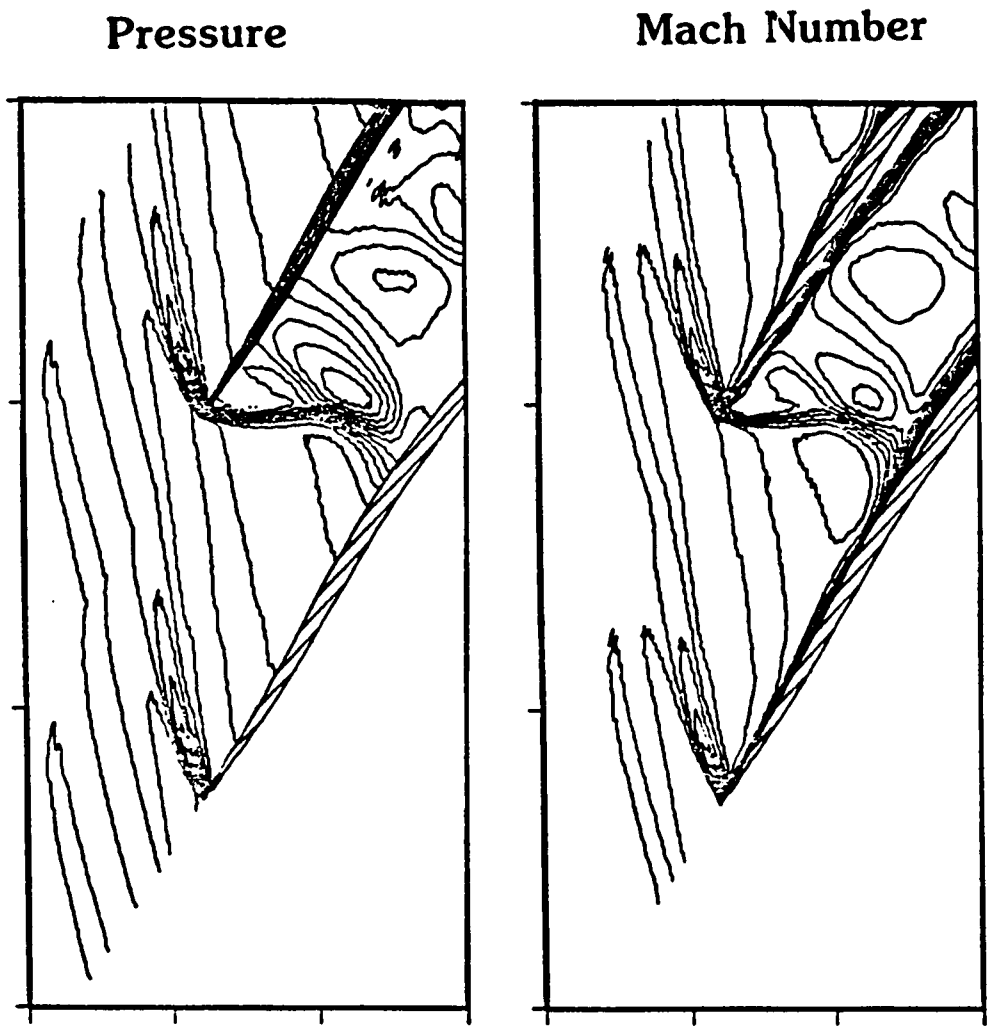

FIGURE 23 Analytical and Experimental Comparison

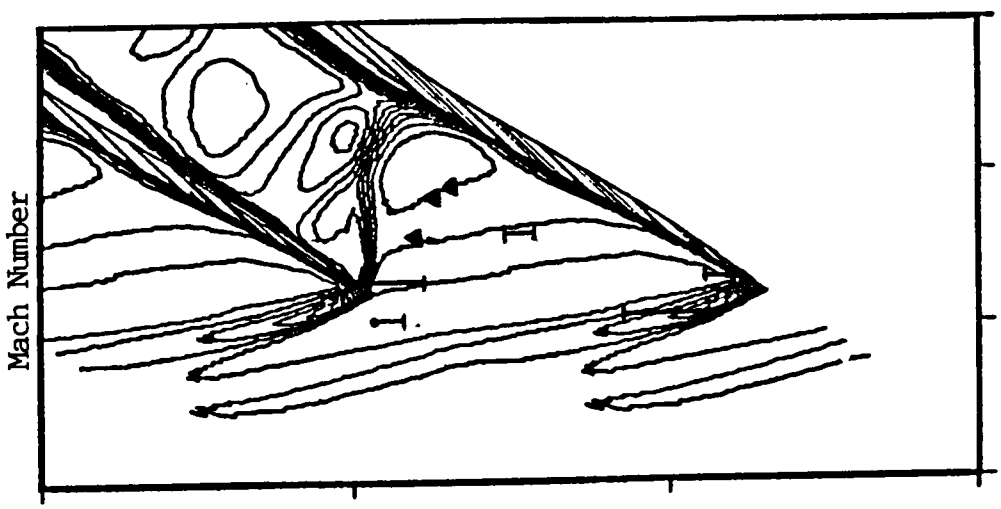

FIGURE 24 Analytical and Experimental Comparison

both show a series of precompression waves. Figures 23 and 24 show a strong gradient in the flow at about 10% of the axial chord in front of the blade leading edge. This behavior was not seen in the LTA experiment, but the indicated bow shock may have been outside the region of circumferential measurements at this location.

VII DISCUSSION OF RESULTS

A somewhat unexpected result was obtained with respect to the passage shock wave end wall boundary layer interaction. Measurements revealed that the passage shock wave and all ordered flow in this transonic compressor ended abruptly at a shear layer located between 96.1% and 96.8% of the blade radius. The position of the shear layer appears to be constant across the passage from suction side to pressure side. It was also observed to be at this same depth at both 12% and 22% of the blade axial chord (see Tables 2 and 3). Further, the passage shock wave does not change its angle with respect to the end wall in the outer 90% of the blade radius (see Figures 12 through 15). It intersects the end wall boundary layer at normal incidence. This is evidenced by the fact that the location of the passage shock wave remains constant within the blade passage at different radial locations. The passage shock wave did not reach the end wall but dissipated at the shear layer separating the well ordered core flow from the end wall boundary layer. No reflected waves were observed from the measured passage shock wave boundary layer interaction.

Wood and Strazisar (44) measured and predicted the passage shock wave location from mid span to 90% of the radius for a NASA transonic compressor. In their investigation, the shock wave is at an angle of about 70 degrees to the end wall between 40% and 80% of the blade radius. It then turns nearly normal to the end wall by 90% radius. Their investigation did not continue to determine the interaction of

the passage shock wave with the tip end wall boundary layer. The present investigation carries the measurements within the end wall boundary layer and shows that the passage shock wave remains at normal incidence to the end wall from 90% of the blade radius until its dissipation at a shear layer separating the well ordered core flow from the tip end wall boundary layer.

The observed passage shock wave pattern, at 91.7% radius, compares favorably with other transonic compressor rotor studies near peak efficiency. References 9, 11, 14, 16, and 20 all present data at or near the peak efficiency. The passage shock wave is reported to be axial in references 14, 16 and 20. Reference 9 reports a shock wave angle of 20 degrees, similar to that seen in Figure 19, for 90% speed and part flow which should be near the peak efficiency point. The data presented by Moore, et al. (11) show that, for different pressure ratios in their compressor, the angle of the shock wave can vary along the 90% speed line from axial to 35 degrees. All of these references (9, 11, 14, 16, and 20) observed that the shock wave turns toward the suction surface as shown by the shock wave location at 25% axial chord in the present investigation, and seen in Figure 19.

The holographic studies reported in references 9 and 11 indicate a leakage vortex developing in the leading edge region of the rotor passage. No evidence of this vortex was observed in the present study, unless it occurred beyond 96.1% of the radius where few measurements were correlated (see Tables 2 and 3). For a low speed compressor, Hah

(29) shows in his numerical study of the end wall and tip clearance flows that there would be no effect of the leakage at 95% of the radius. Only very near the tip at 99.4% of the radius was the tip clearance effect noticed. Similar results for the inlet region of the passage in a low speed compressor were reported in reference 15.

The behavior of the observed precompression waves in the first 20% of the rotor passage changed with radius. This wave pattern first appeared to be a coalescent shock wave, then changed to a series of weak shock waves as the end wall was approached. This behavior appears to be due to the end wall boundary layer since the blade geometry is nearly constant in this region. It is further observed that these waves influence the upstream flow field. At 10% of the axial chord ahead of the leading edge of the blade, the flow field is already adjusting to the presence of the compressor. In some locations across the passage the flow was observed to have turned by as much as 4 degrees from its upstream direction. This turning is a result of the upstream influence of the precompression waves and the passage shock wave. Similar behavior was observed in the analytical predictions.

The general structure of the flow field observed in the analytical prediction compares favorably with the measured flow field behavior (see Figure 24). Both show a clean passage shock wave and both exhibit the precompression wave structure. The analytical prediction substantiated the observed turning of the flow field at 10% of the axial chord ahead of the leading edge. It also indicated that the

passage shock wave was so close to the pressure side of the passage at the blade leading edge that it was outside of the range of LTA measurements. Therefore, the LTA did not measure a discrete change in velocity at this location.

In the tip region of the flow at 12% axial chord and 97.5% radial position, a "trimodal" velocity behavior is reported (see Table 2). This behavior was observed at approximately 25% and 30% of the blade passage in both blade passages. This passage location is at the same position as the precompression waves measured in the core flow. This trimodal velocity behavior could be the result of the precompression waves terminating in the end wall boundary layer with a lamda shock wave. If the station width was wide enough, all three velocities within the lamda shock wave pattern could be measured simultaneously. Another possible explanation could be that the lamda shock wave is oscillating back and forth across the measurement station. Three velocities from each of the three regions within the lamda shock wave could also be measured in this case. The measurements at 22% axial chord do not show this trimodal velocity behavior (see Table 3). From Table 20 in Appendix C it can be observed that the most dominant absolute velocity at this location is at nearly -80 degrees. This means that the flow at 25% and 30% of the blade passage at 12% chord has at least some indication of being nearly circumferential in the direction of the blade motion. Similar results of circumferential flow were observed completely across the passage at 30% of the axial chord and 91.7% radius which is nearly at the first groove leading edge. At

this location, the passage flow may be significantly influenced by the circumferential flow within the tip treatment grooves.

There were regions within the flow field that exhibited correlated flow velocities at two substantially different angles. This behavior is termed "bimodal". Bimodal behavior was generally observed in this experiment to be near a shock wave. It is believed that the bimodal velocities were either a result of measurements being made on both sides of a shock wave within one station or evidence of the shock wave moving. These data are not reported because the method of selecting the measured velocity based on contrast excluded them from the reduced data. It is interesting to note that a laser doppler anemometer system will use these bimodal velocity distributions to calculate the reported average velocity while the LTA system does not have a method of using both measurements and chooses only one. Neither method is correct. The data reduction methods for both measurement techniques need to be improved to properly account for complex multimodal flow fields.

The uncertainty of the flow field measurements was empirically predicted for the expected natural particle behavior to be ± 6.2% of absolute velocity and ± 3.4 degrees in direction. During the investigation, the particle diameter was estimated to be about 0.5 micron. This diameter would reduce the uncertainty to ± 4.8% of absolute velocity and ± 1.6 degrees in flow direction. Repeated data points (see Figures 20 and 20a) reveal that the repeatability is

approximately ± 2.5% of absolute velocity and ± 1.25 degrees on a given test day. This is similar to the repeatability from passage to passage shown in Figures 10, 13 and 15. The data from day to day repeated to ±4.5% of the absolute velocity and ±1.5 degrees in flow direction, as shown in Figures 21 and 21a. Other factors besides instrument error could cause the difference from passage to passage, from test to test and from day to day. For example, any change in the size of naturally occurring particles would cause a shift in the measured flow field behavior. The variation in the data exhibited in Figures 10, 13, 15, and 20 through 21a, helps to confirm the empirically predicted uncertainty. It is interesting to note that if the seed material followed the flow ideally, the uncertainty in absolute velocity would be ±4.7% and flow angle uncertainty would be ±1.6 degrees. This is essentially the uncertainty predicted for the seed diameter inferred from shock wave measurements. The uncertainty in absolute flow velocity could further be reduced to about ±3% if greater than 25 particle transits were required for a velocity measurement.

If the complete flow field behavior is important, the number of circumferential measurement locations should be increased. The resolution, $\Delta\phi$, of the measured shock wave angle, ϕ, can be related to the station width, SW, and the distance between axial measurement locations, AL, as follows:

$$\Delta\phi = \phi - \tan^{-1}\left\{\tan - \frac{SW}{AL}\right\}$$

For the present condition of 17 circumferential measurement positions and the length between 12% and 22% of the axial chord, this resolution is about 10 degrees.

However, increasing the number of circumferential positions results in a direct increase in measurement time. In order to obtain the increased measurement resolution without a significant sacrifice in measurement time, these studies could have used a two step measurement approach as follows. First, the maximum data in a minimum amount of time could be obtained. The blade average mode with a few (perhaps only ten) circumferential locations and maximum angle step, could be used to obtain more precise flow field measurements. With the maximum of 32 circumferential positions, the resolution would be 6 degrees, assuming measurements were obtained in each circumferential position. This would require smaller diameter seed particles than were apparently measured in this investigation.

With the LTA concept, the measurement time is directly impacted by the number of angles measured to capture the velocity direction. However, this angle search can be used to an advantage in locating the blade orientation with respect to the circumferential measurement stations. During this investigation, the two spots could have been rotated until both flare signals were in phase with one another. This measurement would have then represented the blade angle and position of the suction surface with respect to the measurement stations to within

the diameter of one focal point. A more precise measurement of the station location would have been obtained.

VIII SUMMARY AND CONCLUSIONS

The flow field near the tip end wall of a high performance transonic compressor rotor was investigated to characterize the passage shock wave end wall boundary layer interaction. A laser transit anemometer measurement system was successfully used to measure the flow velocity from 10% of the blade axial chord in front of the blade leading edge to 30% of the blade axial chord into the blade passage. At the blade leading edge, and at 12% and 22% of the axial chord, different radii locations were investigated to determine the behavior of the passage shock wave interaction with the end wall boundary layer. The well ordered core flow was found to be separated from the end wall boundary layer by what appears to be a shear layer where the flow behavior changes abruptly. The shear layer appears to be at a constant depth between 96.1% and 96.8% of the radius from 12% to 22% of the axial chord. At the leading edge, no evidence of this flow discontinuity was observed in the data taken at the 97.5% radial location. However, the 97.5% radius location is definitely within the end wall boundary layer at the leading edge. The flow discontinuity within the passage also appears to be at a constant depth across the blade passage at 12% and 22% of the axial chord.

The precompression waves produced by the compressor rotor were also studied. The behavior of the precompression waves in the entrance region and at 12% of the axial chord changed with the radial location.

Between the 88.9% and 96.1% radial locations at 12% of the axial chord, the precompression waves went from what appears to be a coalescent shock wave to a series of weak shock waves across 50% of the passage. The behavior of a series of weak shock waves was also observed at the blade leading edge. As the end wall was approached at the blade leading edge, the precompression wave behavior resulted in a sinusoidal velocity profile.

A method to estimate the seed diameter from the actual LTA measurements was presented. By varying the measurement length, the measured particle deceleration distance can be determined. If the shock wave is measured discretely, then the deceleration distance of the measured particles must be less than the maximum deceleration distance for that measurement length. The largest particle diameter could be predicted if the measurement length was considered as the maximum deceleration distance. It was estimated in this manner that the diameters of the natural particles in the atmosphere measured in this experiment were on the order of 0.4 micron to 0.6 micron.

IX REFERENCES

1 Koch, C.C. and Smith, L. H. Jr., "Loss Sources and Magnitudes in Axial-Flow Compressors", Journal of Engineering for Power, July 1976, pp 411-424.

2. Johnson, I. A. and Bullock, R. O. Editors, "Aerodynamic Design of Axial-Flow Compressors" NASA SP-36, 1965

3. Simon, C. and Grahl K. G., "Comparison of End Wall Boundary Layer Calculation Methods for Axial-Flow Compressor STAGE", ISABE 85-7071, 1985

4. Epstein, A. H., Kerrebrock, J. L. and Thompkins, W. T. Jr., "Shock Structure in Transonic Compressor Rotors", AIAA Journal, Volume 17, Number 4, April 1979.

5. Lakshminarayana, B., Pouagare, M. and Davino, R., "Three-Dimensional Flow Field in the Tip Region of a Compressor Rotor Passage - Part I: Mean Velocity Profiles and Annulus Wall Boundary Layer", Journal of Engineering for Power, Volume 104, October 1982, pp 760-771.

6. Lakshminarayana, B., Davino, R. and Pouagare, M., "Three-Dimensional Flow-Field in the Tip Region of a Compressor Rotor Passage" - Part II: Turbulence Properties. Journal of Engineering for Power, Vol. 104, October 1982.

7. Pouagare, M., Galmes, J. M. and Lakshminarayana, B., "An Experimental Study of the Compressor Rotor Blade Boundary Layer", Journal of Engineering for Gas Turbines and Power, Vol 107 April 1985.

8. Hunter, I. H. and Cumpsty, N. A., "Casing Wall Boundary-Layer Development Through an Isolated Compressor Rotor" Journal of Engineering for Power, Vol. 104, October 1982.

9. Wuerker, R. F., Kobayashi, R. J., Heflinger, L. O. and Ware, T. C., "Application of Holography to Flow Visualization within Rotating Compressor Blade Row", NASA CR 121264, February 1974.

10. Benser, W. A., Bailey, E. E., Gelder, T. F., "Holographic Studies of Shock Waves within Transonic Fan Rotors", Journal of Engineering for Power, January 1975, pp 75-84.

11. Moore, C. J., Jones D. G., Haxell, C. F., Bryanston-Cross, P. J. and Parker, R. J., "Optical Methods of Flow Diagnostics in Turbomachinery", ICIASF '81 Record, September 1981.

12. Wisler, D. C., "Shock Wave and Flow Velocity Measurements in a High Speed Fan Rotor using the Laser Velocimeter", Journal of Engineering for Power, April 1977, pp 181-186.

13. Strazisar, A. J. and Powell, J. A., "Laser Anemometer Measurements in a Transonic Axial Flow Compressor Rotor", Journal of Engineering for Power, Volume 103, Number 2, April 1981, pp 430-437.

14. Pierzga, M. J. and Wood, J. R., "Investigation of the Three-Dimensional Flow Field within a Transonic Fan Rotor: Experiment and Analysis", Journal of Engineering for Gas Turbines and Power, April 1985, Volume 107, pp 437- 449.

15. Murthy, K. N. S. and Lakshminarayana, B., "Laser Doppler Velocimeter Measurements in the Tip Region of a Compressor Rotor", AIAA Journal, Volume 24, Number 5, May 1986, pp 807-814.

16. Strazisar, A. J., "Investigation of Flow Phenomena in a Transonic Fan Rotor Using Laser Anemometry", Journal of Engineering for Gas Turbines and Power, April 1985, Volume 107, pp 427-435.

17. Williams, M. C., "Laser Velocimetry Study of Stator/Rotor Interaction in a Multi-stage Gas Turbine Compressor", AGARD CP-399, Advanced Instrumentation for Aero Engine Components, 1986.

18. Strazisar, A. J., "Laser Fringe Anemometry for Aero Engine Components", AGARD CP-399, Advanced Instrumentation for Aero Engine Components, 1986.

19. Chima, R. V. and Strazisar A. J., "Comparison of Two-and-Three-Dimensional Flow Computations with Laser Anemometer Measurements on a Transonic Compressor Rotor", Journal of Engineering for Power, Vol. 105, pages 596-605 July 1983

20. McDonald, P. W., Bolt, C. R., Dunker, R. J. and Weyer, H. B., "A Comparison Between Measured and Computed Flow Fields in a Transonic Compressor Rotor", Journal of Engineering for Power, October 1980, Volume 102, pp 883-891.

21. Dunker, R. J., Strinning, P. E. and Weyer, A. B., "Experimental Study of the Flow Field Within a Transonic Axial Compressor Rotor by Laser Velocimetry and Comparison with Through-Flow Calculations", Journal of Engineering for Power, April 1978, Volume 100, pp 279-286.

22. Smart, A. E., Wisler, D. C. and Mayo, W. T. Jr., "Optical Advances in Laser Transit Anemometry", Journal of Engineering for Power, Volume 103, Number 2, April 1981, pp 438-444.

23. Schodl, R., "A Laser Two Focus (L2F) Velocimeter for Automatic Flow Vector Measurements in the Rotating Components of Turbomachines", Measurement Methods in Rotating Components of Turbomachinery, ASME 1980.

24. Schodl, R., "Laser Two Focus Velocimetry", AGARD CP-399, Advanced Instrumentation for Aero Engine Components, 1986.

25. Denton, J. D. "The Calculation of Fully Three Dimensional Flow Through Any Type of Turbomachinery Blade Row", AGARD.

26. Hirsch, C. and Denton, J. D. Editors, "Through Flow Calculations in Axial Turbomachines" AGARD Advisory Report No. 175, October 1981.

27. Surugue, J., Editor, "Boundary Layer Effects in Turbomachines", AGARDograph No. 164, December 1972

28. Horlock, J. H. and Perkins, H. J., "Annulus Wall Boundary Layers in Turbomachines", AGARDograph No 185, May 1974.

29. Hah, C., "A Numerical Modeling of Endwall and Tip-Clearance Flow of an Isolated Compressor Rotor", Journal of Engineering for Gas Turbines and Power, January 1986, Volume 108, pp 15-21.

30. Schafer, H. J. "The Application of Laser Anemometry to the Study of Transonic Shock Boundary-Layer Interactions", Second International Symposium on Applications of Laser Anemometry to Fluid Mechanics, July 2-4, 1984, Lisbon, Portugal.

31. Liepmann, H. W. and Roshko, A., Elements of Gasdynamics, John Wiley and Sons, Inc., 1967.

32. Shapino, A. H., The Dynamics and Thermodynamics of Compressible Fluid Flow, The Ronald Press Company, 1953.

33. Sullivan, T. General Electric Company, Evendale, Ohio, Private Communications November 1985.

34. Wennerstrom, A. J., "Experimental Study of a High-Throughflow Transonic Axial Compressor Stage" Journal of Engineering for Gas Turbines and Power, Vol. 106, July 1984.

35. Mayo, W. T. Jr., Smart, A. E. and Hunt, T. E., "Laser Transit Anemometer with Microcomputer and Special Digital Electronics; Measurements in Supersonic Flows", 8th ICIASF, Naval Post Graduate School, Monterey CA, September 24-26, 1979.

36. Mayo, W. T. Jr. and Smart, A. E., "Photon Correlation: A Fast New Digital Processor for Optical Measurements", Poster Paper, CLEO 1982, Phoenix, Arizona.

37. Maxwell, B. R., "Particle Flow in Blade Passages of Turbomachinery with Application to Laser-Doppler Velocimetry", NASA CR 134543.

38. Melling, A., "Seeding Gas Flows for Laser Anemometry", AGARD CP-399, Advanced Instrumentation for Aero Engine Components, 1986.

39. Air Pollution Engineering Manual, 2nd Edition, Environmental Protection Agency, Research Triangle Park, N.C. 1973.

40. Abernethy, R.B. and Thompson, J.W. Jr., "Handbook, Uncertainty in Gas Turbine Measurements". AEDC-TR-73-5, February 1973.

41. Prince, D.C. Jr., "Three Dimensional Shock Structures for Transonic/Supersonic Compressor Rotors" Journal of Aircraft Vol. 17, No 1 Article No 79-0043R, January 1980.

42. NASA Ames Research Staff, "Equations, Tables, and Charts for Compressible Flow", NACA Report 1135, 1953.

43. Richardson, S. M., "A Numerical Study of Unsteady Flow Effects in a Supersonic Compressor Cascade" AGARD CP-401, Transonic and Supersonic Phenomena in Turbomachines, 1986.

44. Wood, J. R., Strazisar, A. J. and Simonyi, P. S., "Shock Structure Measured in a Transonic Fan Using Laser Anemometry" AGARD CP-401, Transonic and Supersonic Phenomena in Turbumachines, 1986.

45. Rabe, D.C., and Dancey, C.L., "Comparison of Laser Transit and Laser Doppler Anemometer Measurements on Fundamental Flows" AIAA 86-1650 presented at the 22nd Joint Propulsion Conference Huntsville Alabama 16-18 June 1986.

APPENDICES

APPENDIX A

LASER TRANSIT ANEMOMETER SYSTEM

Laser anemometry is one of the most powerful measurement techniques available for measuring fluid flow, especially when the flow is physically or practically inaccessible by conventional probes. In particular, it is the only practical method of measuring the detailed flow field within rotor passages. Since the early 1970s, there have been two laser measurement techniques. These two techniques are currently known as the laser transit anemometer, LTA, or the laser two-focus velocimeter; and the laser doppler anemometer, LDA, or laser fringe anemometer. A comparison of the LTA used in the reported experiments and an LDA "three-color, three-component" measurement system, manufactured by TSI, Incorporated, is reported in reference 45. This section will explain more fully the LTA used for the present fluid-flow measurements.

1. System Description

The LTA measurement system used in the experiments has been commercially available for approximately ten years. The system was manufactured by Spectron Development Laboratories, Incorporated, Costa Mesa, California. It consists of an optical head, manual controller, two high-voltage photomultiplier tube power supplies, data management computer, Correlex and digital oscilloscope. A schematic of the laser anemometer system and a picture of the control system are shown in

Figures 25 and 26, respectively. The optics and signal processing of the system have been the subject of a number of papers in the literature. References 22 and 35 describe the principle of operation of the LTA system while reference 36 presents a description of the Correlex used for signal processing. Basically, the LTA optical system produces two parallel beams from a single input beam. These two parallel beams are then focused in the flow field to form two small spots separated by a distance, SS. A picture of the two spots in a calibration jet is presented in Figure 27. Backscattered light from dust or artificially induced seed particles is detected by two photomultiplier tubes, one viewing each spot. Since the plane containing the two spots can be rotated for different flow directions, the two spots can be aligned to the velocity vector in the plane perpendicular to the optical axis. The scattered light from particles passing through the two spots can then be cross-correlated to yield a histogram of particle transit times. This cross-correlation is performed by the Correlex described in reference 36. If the dust or artificial seed particles are small enough to follow the flow, the transit time histogram, along with the spot separation, can yield the absolute flow velocity in the plane perpendicular to the optical axis. From the spot rotation, αr, the flow angle can be determined. The geometry of the LTA probe volume is shown schematically in Figure 28. The probe volume is considered to be a rectilinear volume d high by SS wide and l_{eff} long.

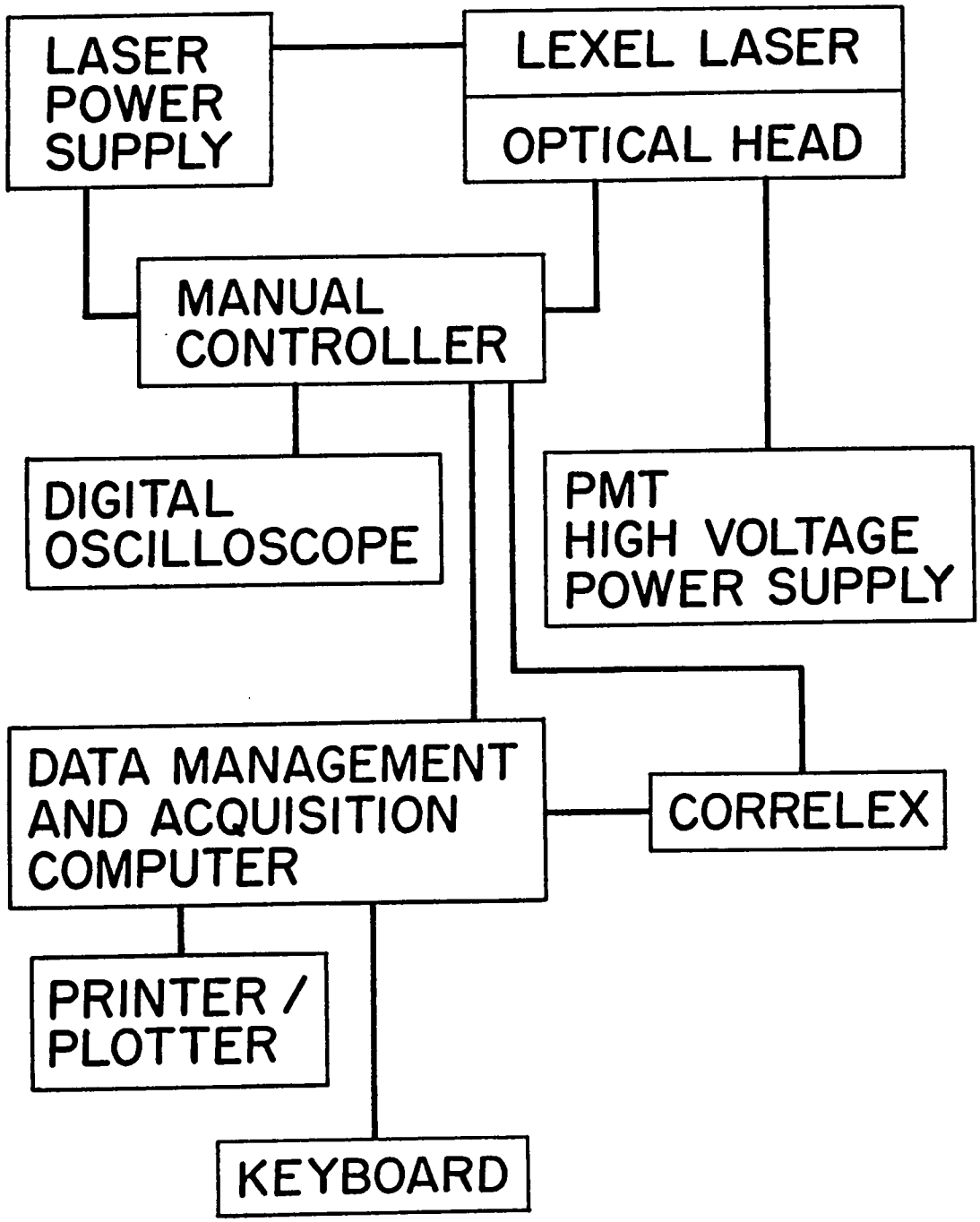

FIGURE 25 Schematic of LTA System

FIGURE 26 LTA CONTROL
AND DATA ACQUISITION SYSTEM

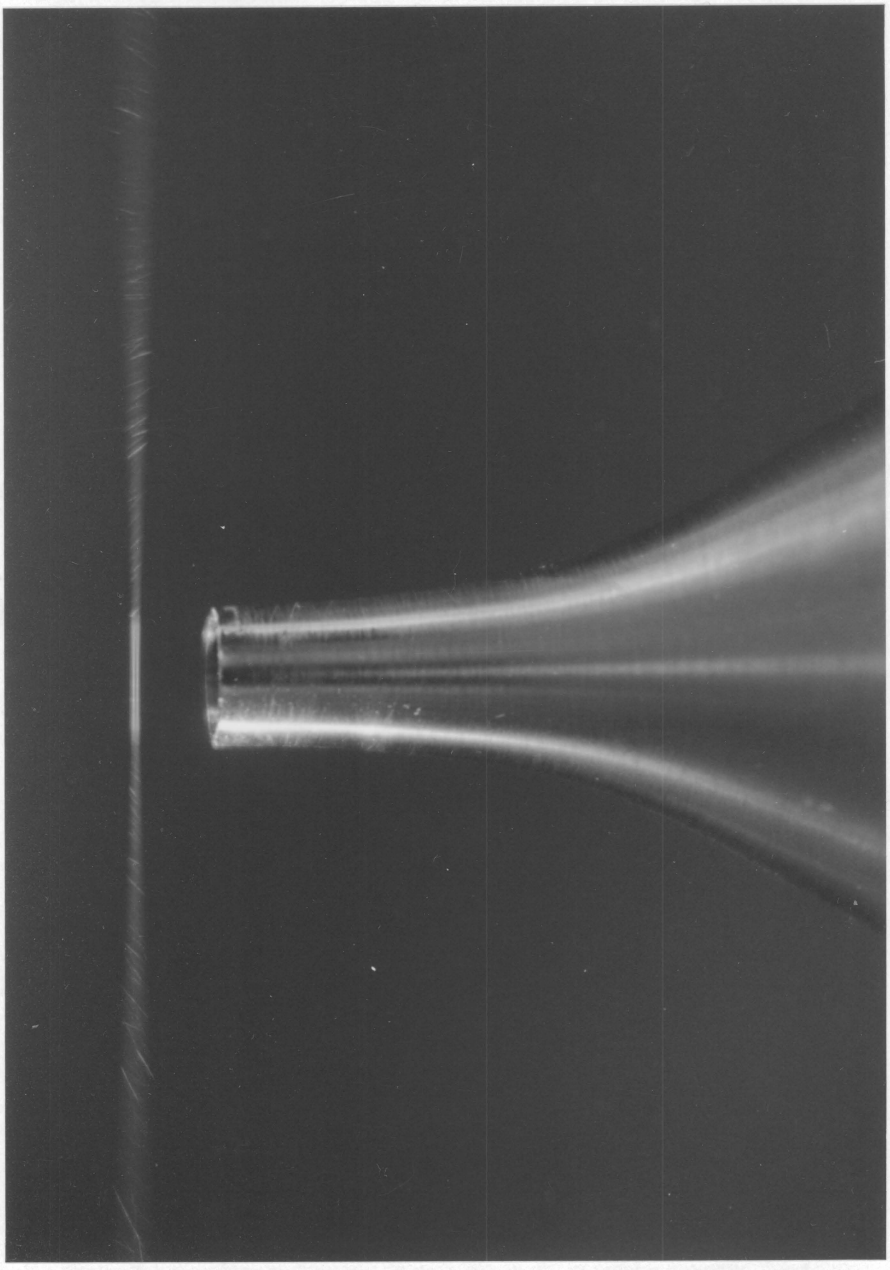

FIGURE 27 LTA PROBE VOLUME

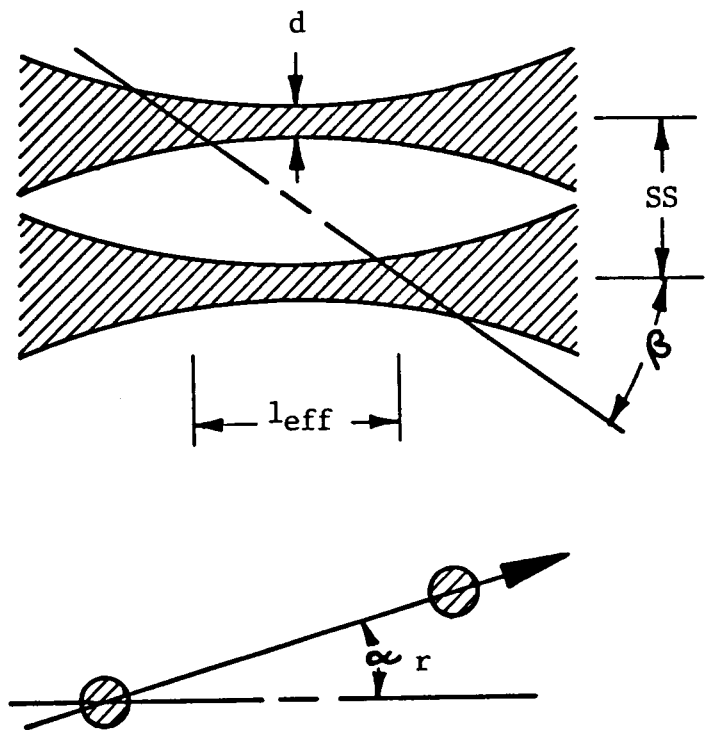

FIGURE 28 LTA Probe Volume Geometry

2. Optical Head

A schematic of the optical head is shown in Figure 29, and a picture of the system is presented in Figure 30. The optical system may logically be divided into the projection and the receiving systems with several of the components in common. The laser light originates in a Lexel model 85 argonion laser shown in Figure 29. Four turning mirrors are used to direct the light into the Wallaston prism where the single input beam is split into two parallel beams according to polarization. The two beams are then focused and expanded through the rotator prism assembly which can rotate the two parallel beams about their common center. The beams are collimated by the inner transceiver lens and focused to two spots at the desired location in the test space by the outer transceiver lens (see Figure 29). Scattered light from particles in the flow is then collected by the outer transceiver lens and focused by the inner transceiver lens. Passing back through the rotator prism assembly, the scattered light is rotated to its original orientation, independent of the prism's rotation. The scattered light passes by the transceiver mirror which separates the outgoing light from the incoming light. Flare light from one spot in the flow, or its illuminating beam, is prevented from entering the receiving path of the other channel by the cross-stop. The field stop helps to prevent stray light from the transmission optics from being received by either photomultiplier. It contains two small holes slightly larger than the returned spot images. Magnification of the beams through the enlarging objective serves to separate and enlarge the spot images so the fiber

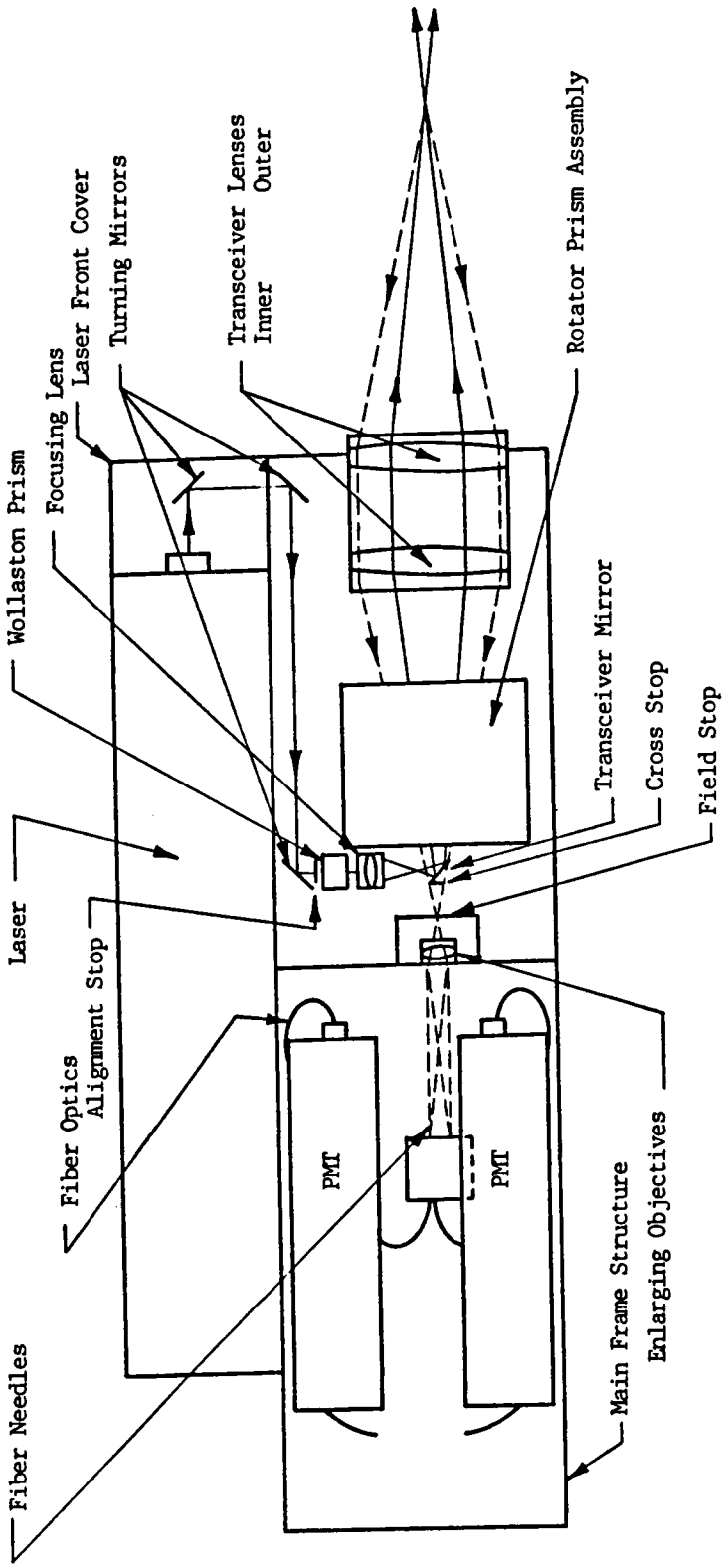

FIGURE 29 Schematic of the Optical Head of the LTA System

FIGURE 30 LTA OPTICAL HEAD COMPONENTS

optics needles can be used as the final field stop. These fiber optics bundles transmit the reflected light to the photomultiplier tubes, one viewing each spot. The photomultiplier tubes then convert incoming light to an analog electrical signal.

The electrical signal from each of the photomultiplier tubes is amplified and sent to a discriminator. The discriminator takes the analog signal from each of the photomultiplier tubes and selects the most probable peak time of the particle transit using an optimum filtering technique described in references 35 and 46. Each discriminator outputs a high-level train of digital pulses corresponding to the most probable particle transit time for each spot in the flow field, along with an analog monitor signal. The two sets of signals are sent to the manual controller (see Figure 25). The digital signal is sent to the Correlex for further signal processing while a monitor signal is sent to the digital oscilloscope where it is observed in real time to assist in the setup of the instrument. The Correlex performs the pulse cross-correlation between the digital train of events from one photomultiplier tube to the other. The process of digital correlation is covered in an introductory manner in reference 47, and the Correlex operation is specifically presented in reference 36.

3. Data Management System

The Correlex sends its information in digital form to the data

management and acquisition computer shown in Figure 25. Here, the correlation data from the Correlex is used to calculate the velocity and turbulence level in the flow field. An example of the data management output is shown in Figure 31. The correlogram in this figure displays a population distribution or histogram of observed particle transits as a function of time per unit time step. The value of time per unit time step is discrete. There are 256 bins along the abscissa, and each has a time width equal to the time step. The overall maximum transit time is set by the number of bins and the time width of the bins. An event is added to the population of a bin if the transit time for that event lies within the bin width. This means that the actual transit time could be in error by ± ½ of the bin width itself.

Using only the location in time of the bin with the maximum population, IPEAK, the velocity can be simply calculated for a given time step, DT, and spot separation, SS, as

$$V = \frac{SS}{IPEAK\ DT}$$

However, this calculation can be in error since IPEAK is uncertain by as much as ±½ of the bin width, DT. This uncertainty in velocity can be represented by

$$\% \text{ Uncertainty} = \frac{V\ (IPEAK) \pm V\ (IPEAK - .5)}{V\ (IPEAK)} \quad (100)$$

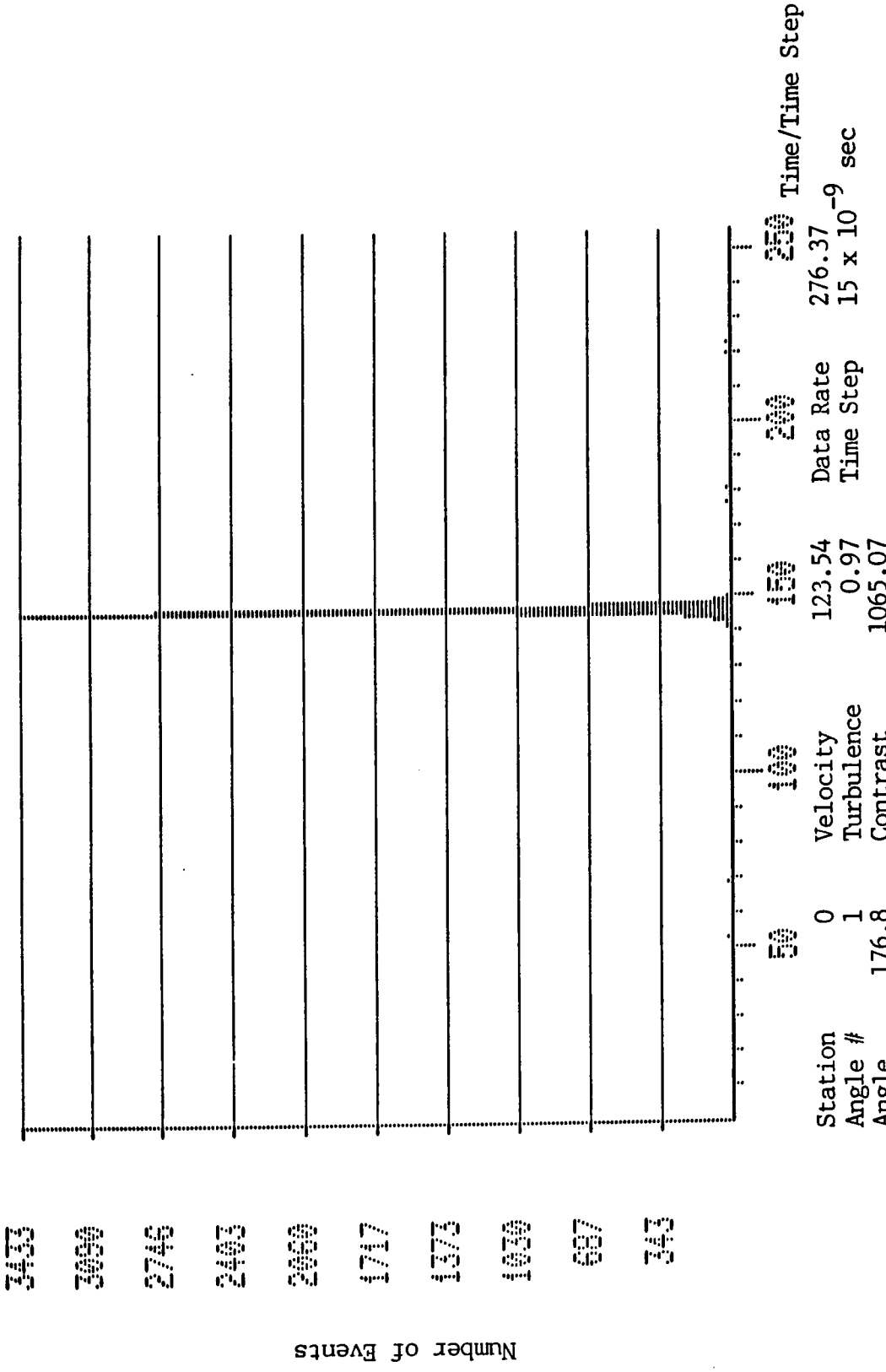

FIGURE 31 LTA Correlogram

which for a constant DT and SS reduces to

$$\% \text{ Uncertainty} = \pm \frac{.5}{IPEAK + .5} (100)$$

Now, if the bin with the maximum population is always greater than 100, as it was in the present experiments, this error would be ± .5% of the actual velocity. For higher values of IPEAK, this error becomes smaller, and in Figure 31, the error is estimated to be ± 0.26% of the actual velocity. The actual calculation of velocity is based on a number of the bins to either side of the bin with the maximum population; and, therefore, the error of ± .5% of the velocity should be an overestimate of the actual error caused by the discrete time bins.

The correlogram display in Figure 31 also includes the measured velocity in meters per second and the turbulence level in percent of the measured velocity. The data rate presented is the average number of events per second measured during the data acquisition. The contrast is an indication of the signal-to-noise ratio of the correlogram. The noise in the correlogram is considered to be the average population of the background along the abscissa that is mathematically excluded from the velocity and turbulence level calculations. If C (I) is the population in a specific bin I, then the contrast is calculated as

$$\text{contrast} = \frac{C(IPEAK) + C(IPEAK - 1) + C(IPEAK + 1)}{3\ (BACK)}$$

The spot orientation angle is also recorded, along with the angle number which is used to store the data. The value of station will be explained next.

The advantage of the Correlex process is that it can be programmed to accept many separate correlations. For application to turbomachinery, this time multiplexing capability permits a number of correlations at different stations within a rotor blade passage to be measured simultaneously. In the present experiment, up to 56 stations were evenly divided between two blade passages. The Correlex can be operated to take up to a maximum of 32 stations in each of two blade passages for a total of 64 stations. It can also be operated in an average mode where all blade passages contribute to a maximum of 32 stations representing an average blade passage.

4. Phasing of Data Acquisition

The phasing of these stations to the blade location, as well as to one another, is performed by the phase address card (PAC) in the Correlex. The PAC receives a once-per-revolution (OPR) pulse and a once-per-blade (OPB) passage pulse from the compressor and generates windows in time that events can be measured by different Correlex

stations. The time that a station can measure particle transits and the time between stations can be selected. These two parameters, along with the number of stations per blade passage, specify the geometrical resolution of the velocity measurement in the circumferential direction. Obviously, for a given flow velocity, the particle transit time between the two spots in the flow field is the minimum time that a station must be able to measure particle transits.

A schematic of the PAC operation is shown in Figure 32. This diagram is for an eight bladed compressor using four stations. The time control is provided by a 5 MHz crystal oscillator clock. The scale at the top of Figure 32, labeled METRIC, is the result of this clock dividing the time between blades into the number or intervals specified by N1. The OPR and OPB are shown for an eight-bladed compressor. At the bottom of the figure are two lines labeled two-blade mode and average blade mode. In the two-blade mode, two individual blade passages are measured similar to the measurements performed in the present work. The average mode permits the specified number of stations to measure particle transits from any of the blade passages resulting in an average velocity from all the blade passages. In both cases, the N2 parameter specifies the number of stations to be measured within one blade passage. For the two-blade mode, the PA parameter specifies the number of blade passages after the OPR pulse where the first measurements will be made. The N3 parameter sets the number of blade passages to be skipped to the second set of measurements. All of the other parameters in the figure are in terms

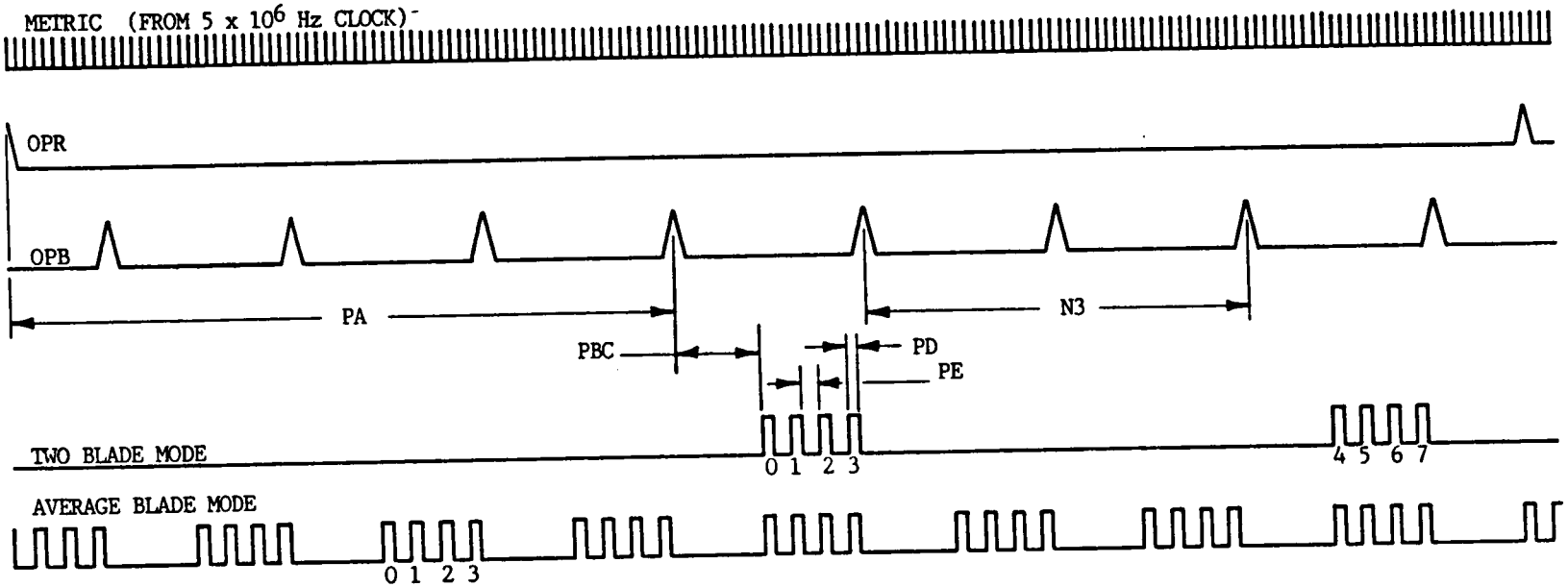

REFERENCE VALUES FOR THIS DIAGRAM

N1 = 20	PBC = 9
N2 = 4	PD = 1
PA = 4	PE = 2
N3 = 2	

FIGURE 32 PAC Timing Diagram

of N1 cycles. The value of PBC specifies the length of time between the OPB and the first measurement station. The time that a station is able to make measurements of the particle transits is specified by PD.

Finally, the interval between stations is set by the PE parameter. In an average mode, the values of PA and N3 are not used, and the other parameters set up the stations for every blade passage.

Timing Errors

The errors in timing, and consequently in the circumferential positioning of the measurement, could come from five different sources: the clock cycles, the OPB measurement and circuit, the PAC itself, inconsistency of the physical blade geometry, and the measurements of these signals. Since all of the setups of the stations are referenced to the clock, any error in the clock cycles will shift the actual measurement location within the blade passage.

For the present case of a 16-blade compressor rotating at 11,000 revolutions per minute, the 5 MHz clock would generate about 1700 cycles per blade passage. These cycles are then used to create the N1 cycles per blade passage. The clock should be accurate to one cycle; and, therefore, the accuracy in timing would be 0.06% of the blade passage. However, the N1 cycles are triggered from the OPB signal which can introduce timing errors. Further, the physical geometry of the blades can vary from blade to blade due to machining errors and

mechanical response of the blade due to the aerodynamic and centrifugal loading. These errors were eliminated by measuring the blade location and station location with a Nicolet model 2090 digital oscilloscope. With a Nicolet Model 205A amplifier, this scope was able to digitize at a rate of 50 MHz. To obtain the time between stations, the time from the beginning of the first station to the beginning of the last station was measured and divided by the number of stations minus one. Figure 33 shows this oscilloscope measurement. The reflected laser light detected from the blade was used to measure the time between the suction surface and the center of the first station. A typical signal of the blade flare and the first station signal are presented in Figure 34 showing the measurement from the blade to the center of the first station. The time between the two blades was also measured from the blade flare data in Figure 33. With this final value, the time between stations and the time to the first station were converted to a percentage of the blade passage and are included in the tables of test data in Appendix C. From this process, the distance to the center of the stations within a blade passage is accurate to 0.6% of the blade passage.

The PAC could introduce additional errors by accepting particle transits for a given station outside the specified time window. No estimate of this error is presented; however, it is assumed to be small with respect to the station width of about 5% of the blade passage. From Figure 33, it is seen that the station acceptance window is precise to 0.5 microseconds or .15% of the blade passage width and it

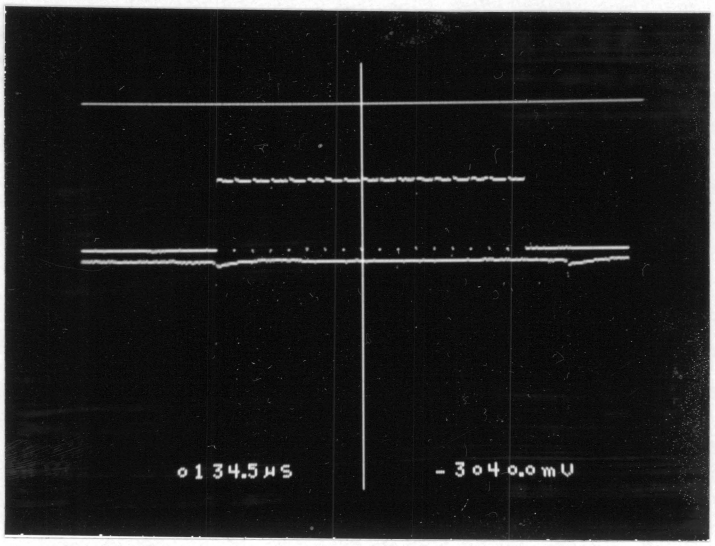

FIGURE 33 Oscilloscope Trace of
Blade to Blade Flare and Station Signal

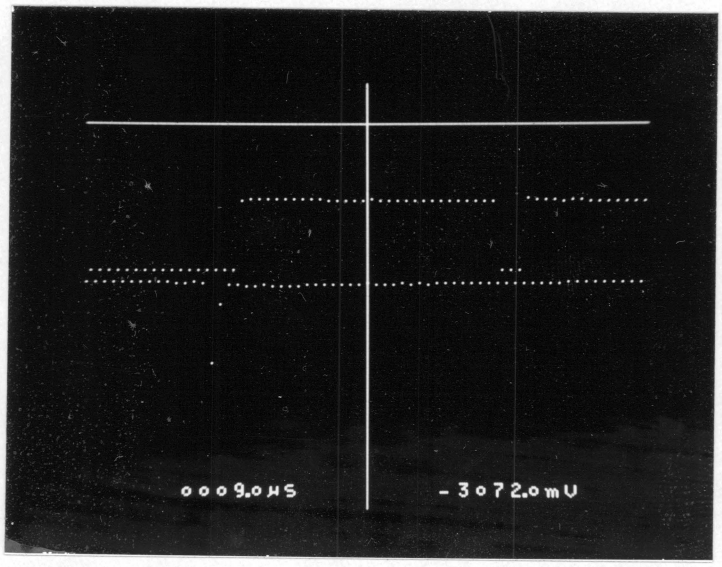

FIGURE 34 Oscilloscope Trace of
Blade Flare and First Station Signal
(Time from blade to center of first station is 9 microseconds)

is assumed that the timing of the acceptance is similar to this value.

5. Probe Volume Dimensions

a. Spot Separation

The probe volume dimensions shown in Figure 28 for the LTA were determined experimentally. The spot separation was first determined by an experimental technique presented in the LTA manual. Since the two parallel beams are designed to be polarized at right angles to each other, the placement of a polarizer in the beams, rotated to an appropriate angle, produces contrasting fringes on a distant screen. Spot separation is then related to the wavelength of light, λ, the distance from the focal point to the screen, L, and the spacing on the screen, dn, for n_f fringes. The spot separation, SS, can be calculated from these known or measured values as follows

$$SS = \frac{n_f \lambda L}{dn}$$

With an output lens of 400 mm focal length, the spot separation was measured in this manner to be 0.273 mm. As reported in reference 45, this technique was found to be inaccurate.

The spot-to-spot separation and spot diameter were more accurately determined by measuring the linear beam power distribution at the focal

point. A knife edge was traversed through the beam and the transmitted power was recorded as a function of the knife edge position. The precision of the traverse was 0.0001 mm. Figure 35 shows the linear beam power distribution from spot to spot, and Figure 36 shows the beam distribution within one spot. The data for Figures 35 and 36 are presented in Table 4. The center-to-center spot separation distance, SS, was measured from the data in Figure 35 to be 0.279 mm which is 2.2% larger than the value determined by the polarization test mentioned above.

Velocity Calibration

In order to determine the velocity measurement accuracy of the LTA, the system was calibrated using the Dantec Model 55D90 calibrator shown in Figure 27. A $12mm^2$ nozzle was used to produce velocities ranging from 10 to 325 m/sec. The supply air to the plenum of the calibrator was fed by a TSI model 9360 six-jet atomizer using 0.48 micron diameter PSL spheres dispersed in isopropanol. To ensure that the laser system measured only the PSL particles rather than unevaporated isopropanol, free jet tests were conducted with pure isopropanol, and a zero data rate was observed. The velocity was measured in the jet with the laser system and also calculated using the plenum chamber pressure and temperature and the atmospheric pressure. The exit plane velocity, V, was calculated from the following

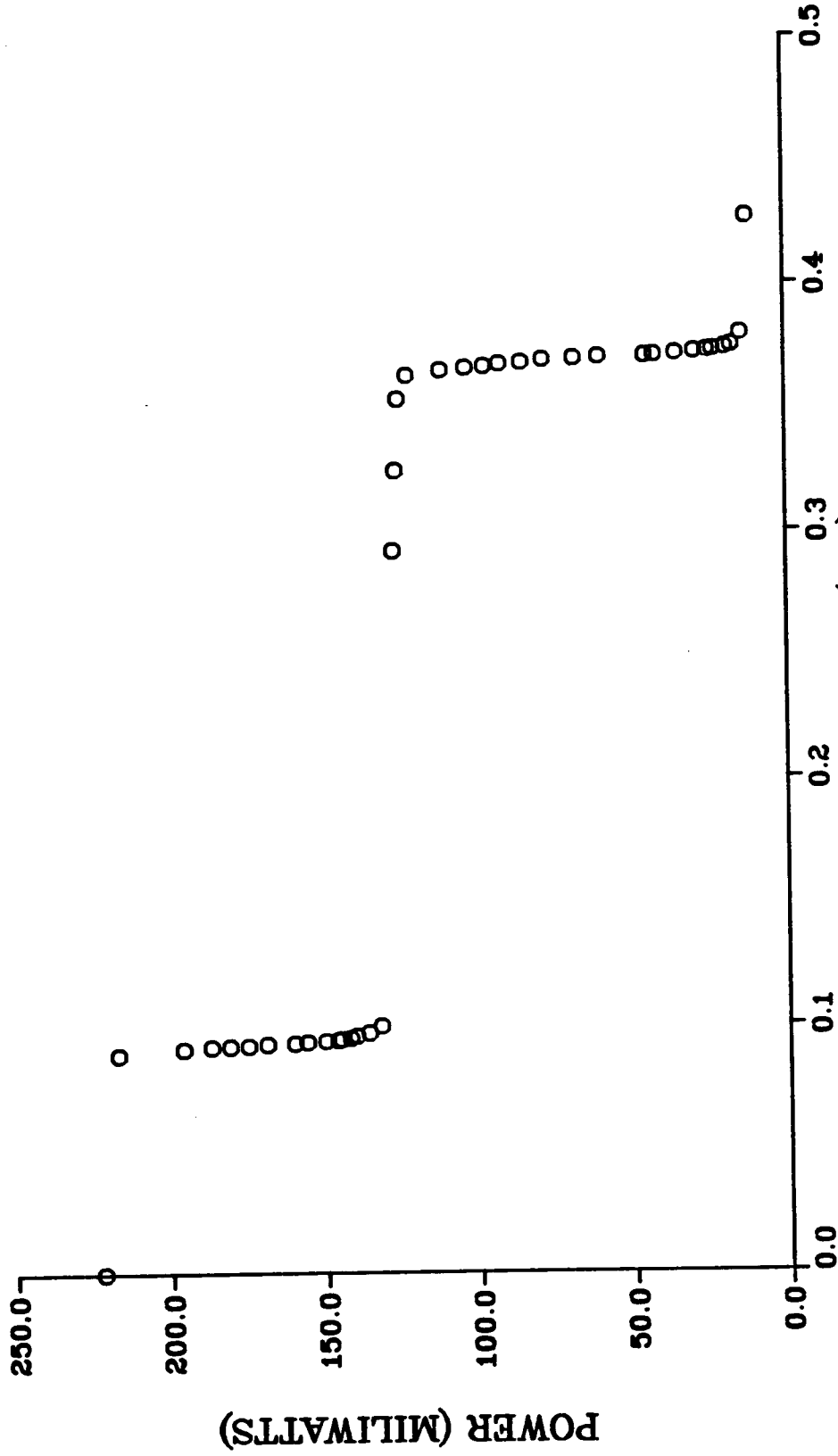

FIGURE 35 BEAM POWER DISTRIBUTION
FROM SPOT TO SPOT

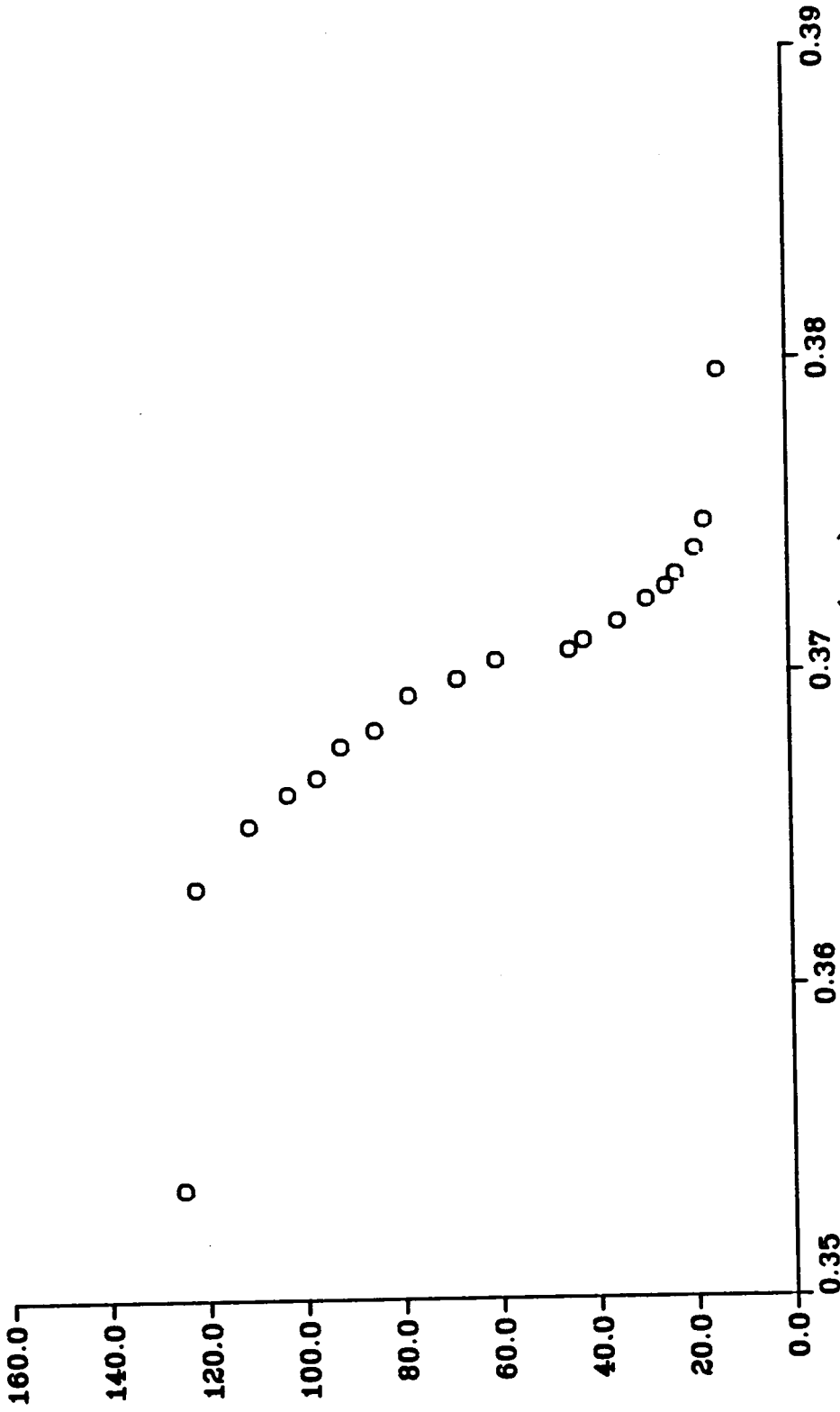

FIGURE 36 BEAM POWER DISTRIBUTION WITHIN ONE SPOT

TABLE 4

BEAM POWER DISTRIBUTION AT FOCAL POINT

LINEAR POSITION (mm)	INDICATED POWER (milliwatts)
0.0000	222
0.0888	217
0.0910	196
0.0918	187
0.0920	181
0.0922	175
0.0928	169
0.0932	160
0.0936	156
0.0940	150
0.0943	146
0.0947	145
0.0951	142
0.0960	140
0.0972	136
0.1000	132
0.2923	127
0.3247	126
0.3536	125
0.3632	122
0.3652	111
0.3662	103
0.3667	97
0.3677	92
0.3682	85
0.3693	78
0.3698	68
0.3704	60
0.3707	45
0.3710	42
0.3716	35
0.3723	29
0.3727	25
0.3731	23
0.3739	19
0.3748	17
0.3796	14
0.4270	12

one-dimensional isentropic energy equation

$$V = 2\,cp\,T_0 \left\{ 1 - \left(\frac{P}{P_0} \right)^{\frac{\gamma - 1}{\gamma}} \right\}^{\frac{1}{2}}$$

In this equation, P_0 and T_0 are the plenum chamber total pressure andtemperature, and P is the static pressure which is assumed to be the atmospheric pressure. The ratio of specific heats, γ, was assumed to be constant at 1.4, and the specific heat of air at constant pressure, cp, was assumed constant at 1.0 KJ/(Kg K). The effect of the alcohol in the air stream was assumed to be negligible on the values of γ and cp.

The results of these tests with a spot separation of 0.279 mm are tabulated in Table 5 and shown in Figure 37 where the relative error is plotted as a function of the computed velocity. The relative error is the difference between the computed and measured velocity divided by the computed value. It is observed in this figure that the relative error of the LTA system is very well behaved with little scatter in the data. However, the error would be biased 2.2% higher if the polarization method had been used to measure SS, as shown in reference 45. It is suggested here as well as in Reference 45, that the spot separation of the LTA system should be either determined or confirmed using a calibration jet. Since the relative error shown in Figure 37

TABLE 5
LTA VELOCITY CALIBRATION
Atmosperic pressure 98.250 N/m²

MEASURED VELOCITY (m/sec)	INDICATED TURBULENCE (%)	CALCULATED VELOCITY (m/sec)	P (N/m²)	TO (C°)	MEASUREMENT ERROR in %
28.16	0.71	28.80	498.0	23.0	1.79
28.20	0.70	28.81	498.0		1.75
28.20	0.71	28.82	498.0		1.72
28.28	0.76	28.90	498.0		1.45
27.92	0.68	28.53	498.0		2.71
27.92	0.67	28.53	498.0		2.71
28.38	0.70	29.00	498.0		1.11
28.39	0.69	29.01	498.0		1.07
28.44	0.72	29.07	498.0		.87
28.25	0.72	28.87	498.0		1.55
28.25	0.74	28.87	498.0		1.55
63.15	0.96	64.54	2491.0		.94
63.25	0.98	64.64	2491.0		.79
88.81	1.16	90.76	4982.0		.72
88.77	1.17	90.72	4982.0		.76
108.1	1.28	110.48	7473.0		.56
107.9	1.22	110.27	7473.0		.75
123.8	1.45	126.5	9964.0		.63
123.9	1.51	126.6	9964.0		.55
123.9	1.46	126.6	9964.0		.55
123.5	0.97	126.2	9964.0		.87
123.3	1.24	126.0	9964.0		1.03
123.3	0.93	126.3	9964.0		.80
123.7	0.86	126.4	9964.0		.72
170.2	0.83	173.9	19928.0		.58
170.0	0.85	173.7	19928.0		.69
187.6	0.92	191.7	24910.0		.64
187.6	0.92	191.7	24910.0	22.0	.47
222.7	1.09	227.6	37365.0		.40
222.0	1.12	226.9	37365.0		.71
222.1	1.13	227.0	37365.0		.67
249.9	0.76	255.4	49322.0		.08
248.7	0.77	254.2	48824.0		.01
272.8	0.86	278.8	62275.0		.03
273.5	0.88	279.5	62275.0		.29
291.7	0.90	298.1	74730.0		.17
290.5	0.91	296.9	74730.0		.25
170.8	0.81	174.6	19928.0		.06
171.1	0.81	174.9	19928.0		.12

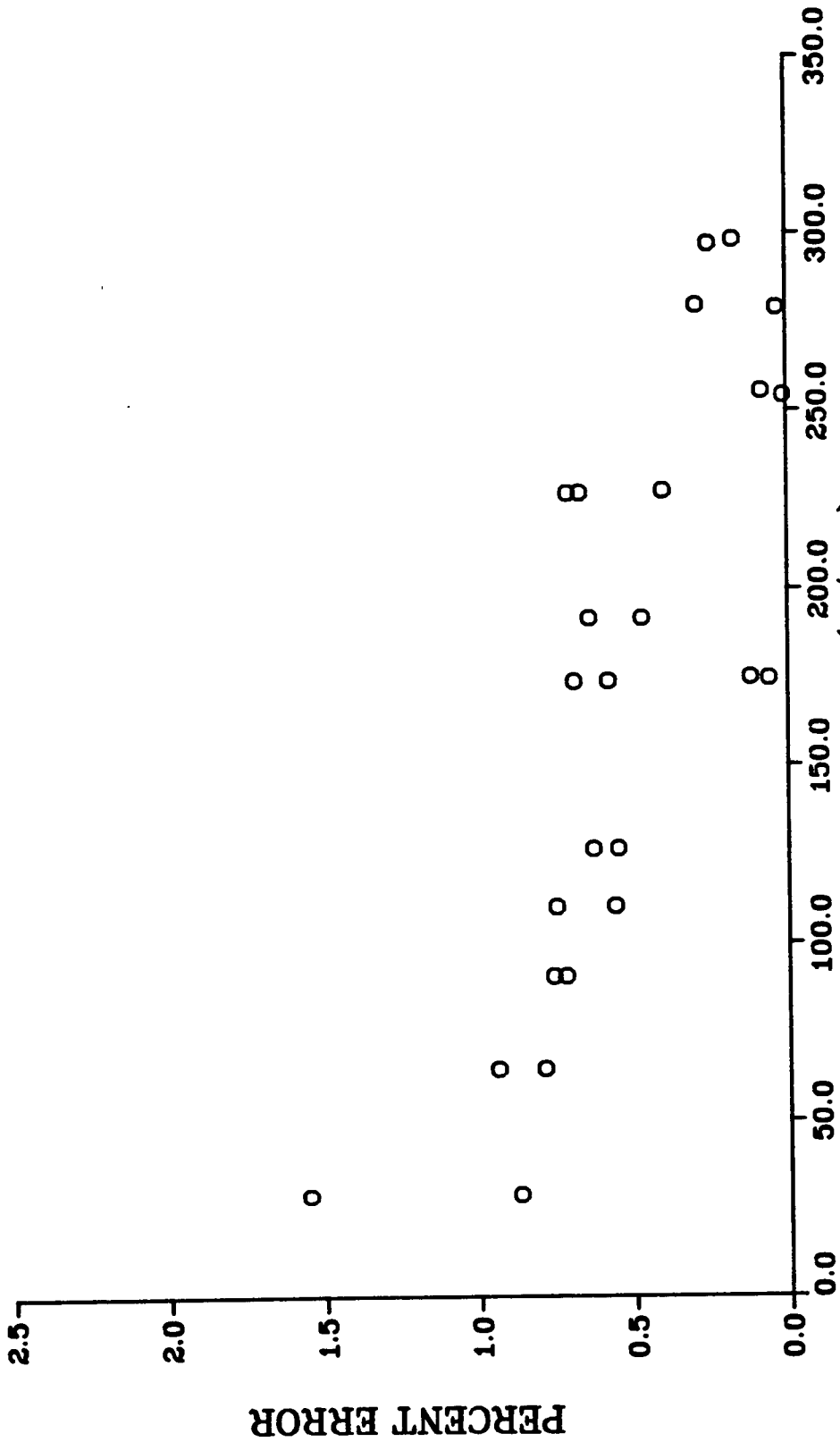

FIGURE 37 LASER SYSTEM MEASUREMENT ACCURACY

is well behaved, a calibration curve could be used in the data reduction routines. However, since the error is relatively small in the region of measured velocity above 100 m/sec, no calibration curve was used in the present experiment.

b. Spot Diameter

The width of the beam passing 95.9% of the total power was selected as the beam diameter. The diameter of each spot was determined to be 0.016 mm from the data presented in Figure 35. With an output power per spot of approximately 120 miliwatts, the power density in each focal point would be about 600 watts/mm^2.

c. Effective Length

The effective length of the probe volume was determined using the calibration jet. The jet was positioned at different angles to the optical axis in the plane of the two spots. The minimum angle, β_{min}, between the optical axis and the jet axis for which velocity measurements could be made dependent on the effective length, l_{eff}, and spot separation, SS, is as follows:

$$l_{eff} = \frac{SS}{\tan \beta_{min}}$$

The velocity of the free jet measured as a function of the jet angle to the optical axis is presented in Figure 38. The data for this figure

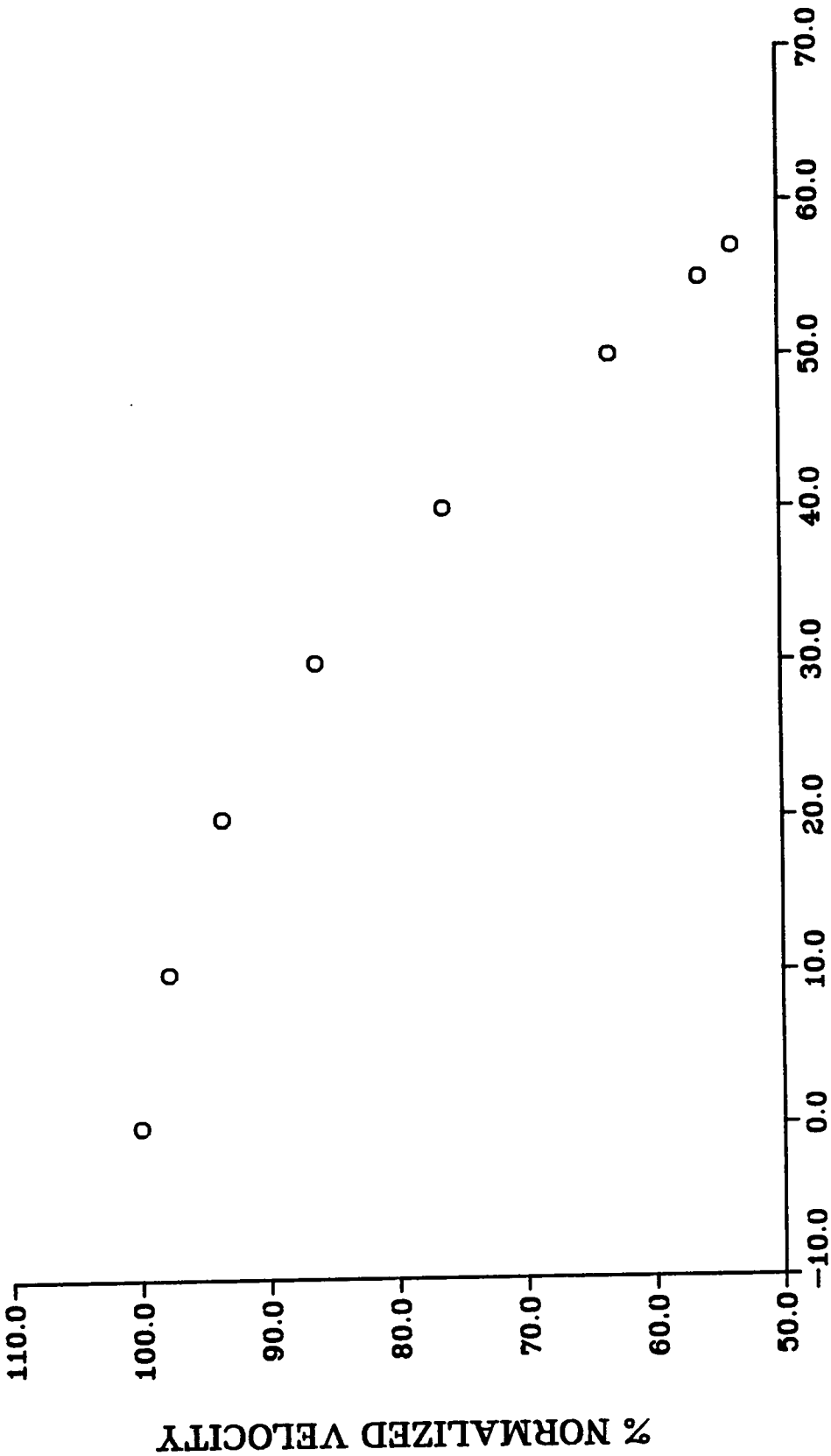

FIGURE 38 LTA SENSITIVITY TO AXIAL VELOCITY

are tabulated in Table 6. With a minimum angle measurement of 33 degrees, the effective length for the LTA probe volume in this optical configuration is calculated to be 0.430 mm.

d. Angle Resolution

The two spots in the measurement space can be aligned to the direction of the actual flow. Presently, the angle resolution of the system is about 0.2 degree. The system's sensitivity to the spot rotation was determined in the calibration jet. Figures 39 and 40 show two series of correlograms to demonstrate the system's sensitivity to spot rotation at two different turbulence levels. The different turbulence levels were obtained by measuring at two different axial locations in the Dantec calibration jet using the 60.0 mm^2 nozzle. The low turbulence level measurements in Figure 39 were obtained at 0.2 mm downstream from the nozzle exit, while the measurements in Figure 40 were obtained at 30 mm downstream from the nozzle exit. Figures 41 and 42 show the sensitivity of the measured velocity and contrast to spot angle. The velocity measured is essentially uneffected by angle and only varies ± ½% over the range of spot angles presented. On the other hand, the contrast is much more dependent on the spot angle and is a better indication of the actual flow angle.

The repeatability of the sensitivity of the contrast to the spot angle is shown in Figure 43. Here, two test runs for angle variation were performed in the calibration jet. Both of these runs, as well as

TABLE 6

SENSITIVITY OF LTA TO AXIAL VELOCITY COMPONENT

JET ANGLE (degrees)	MEASURED VELOCITY (m/sec)
0.0	28.27
10.0	27.63
20.0	26.45
30.0	24.37
40.0	21.49
50.0	17.86
55.0	15.87
57.0	15.15

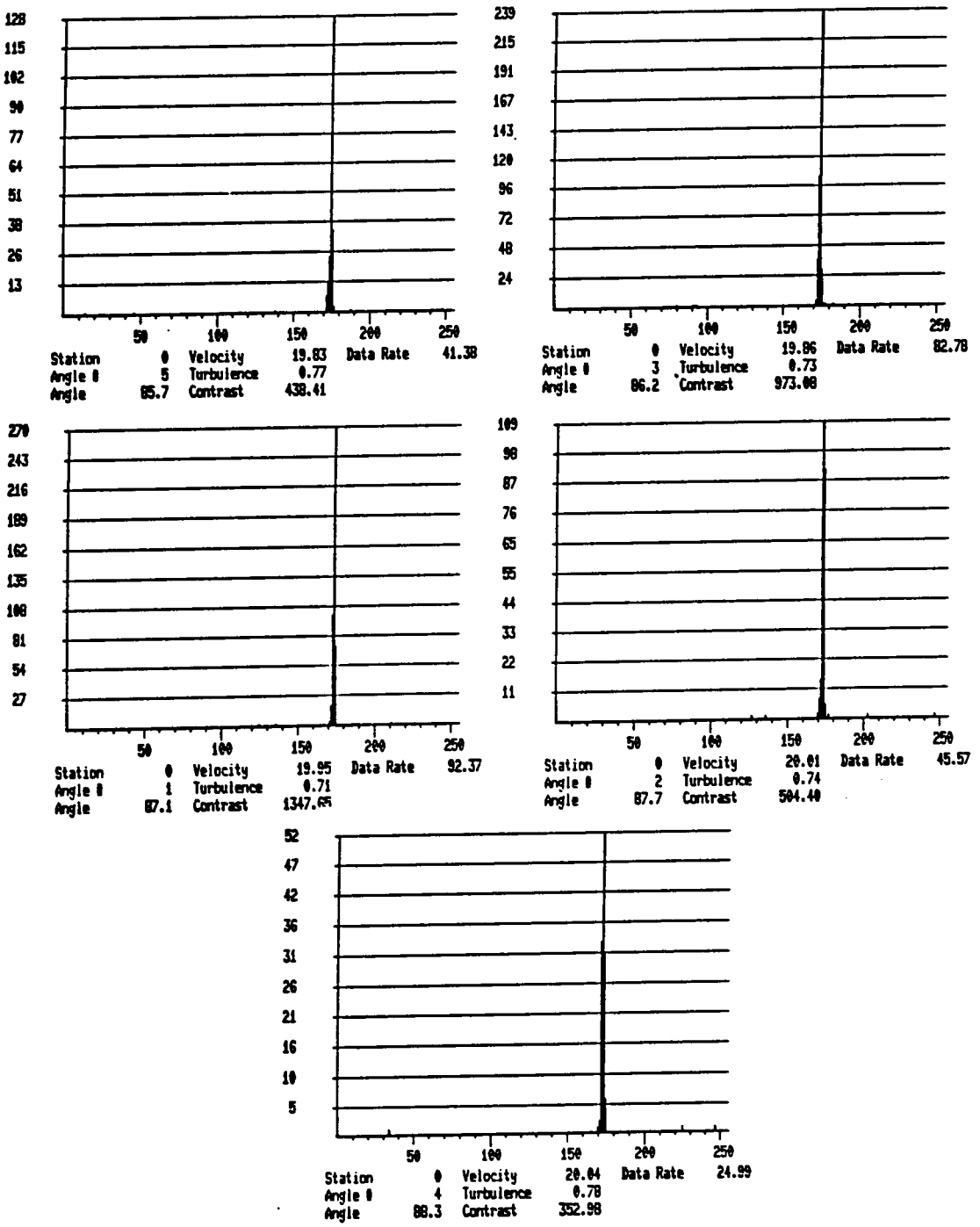

FIGURE 39 Correlogram Sensitivity to Angle at Low Turbulence

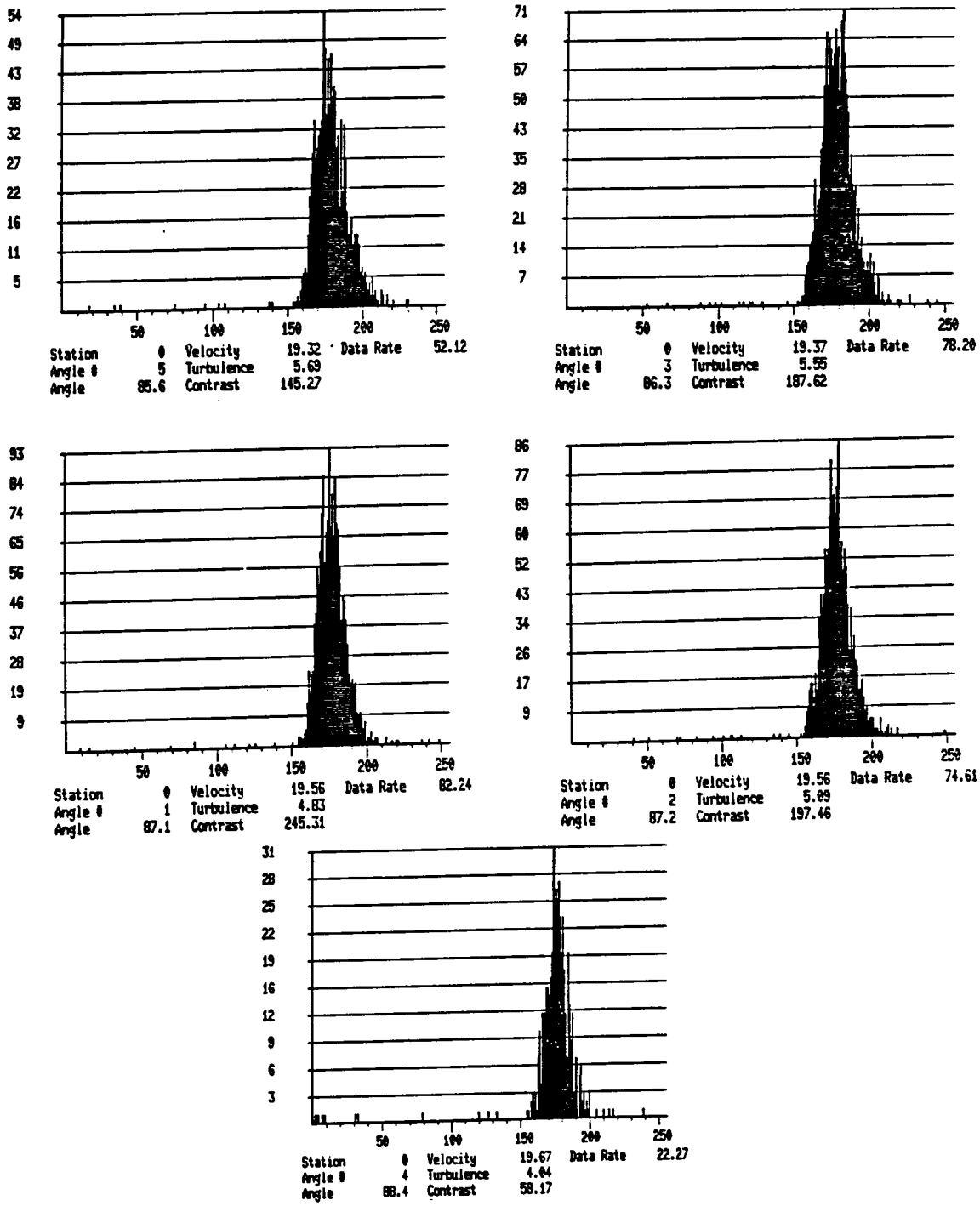

FIGURE 40 Correlogram Sensitivity to Angle at Moderate Turbulence

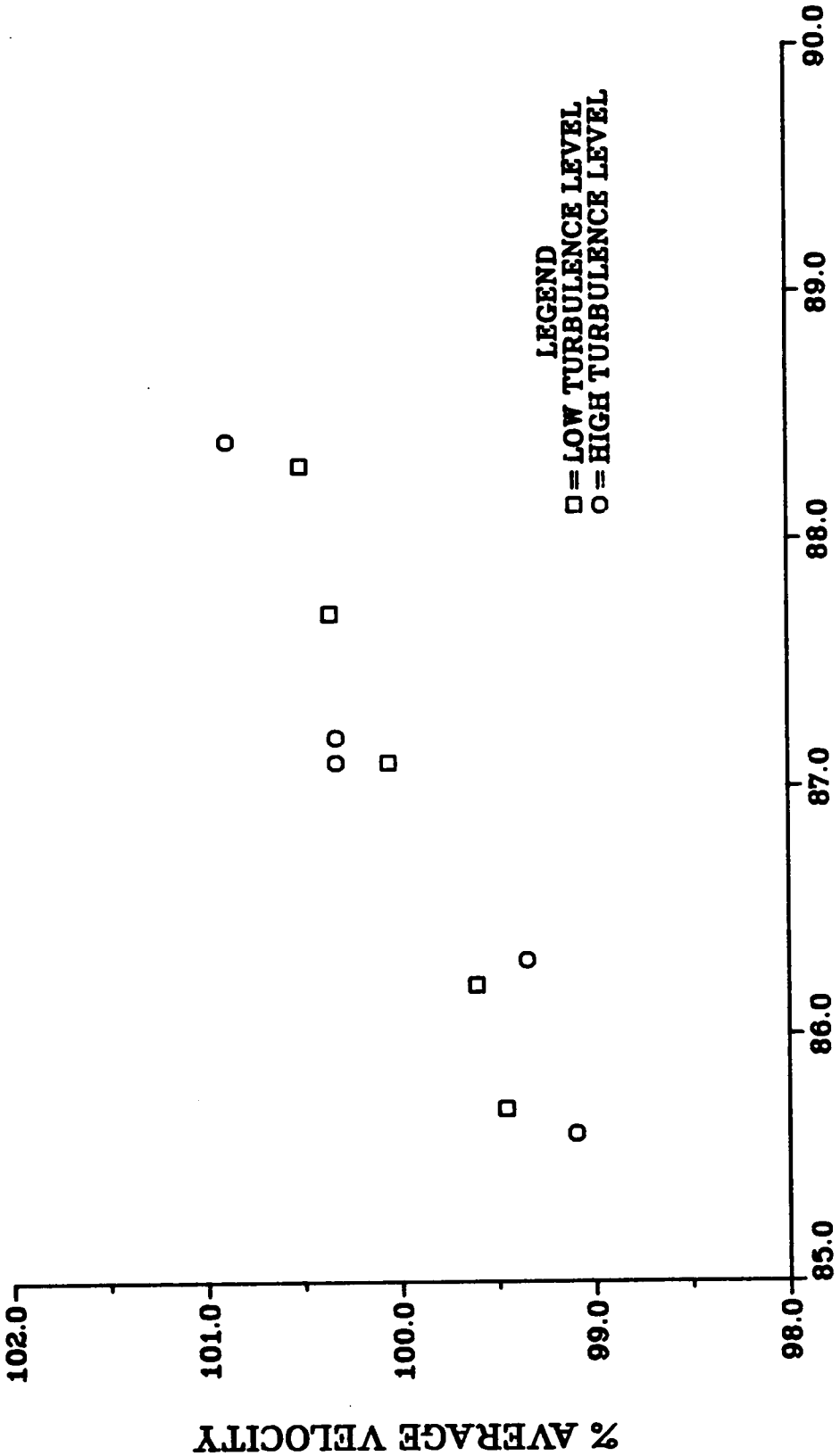

FIGURE 41 VELOCITY SENSITIVITY TO LTA SPOT ANGLE

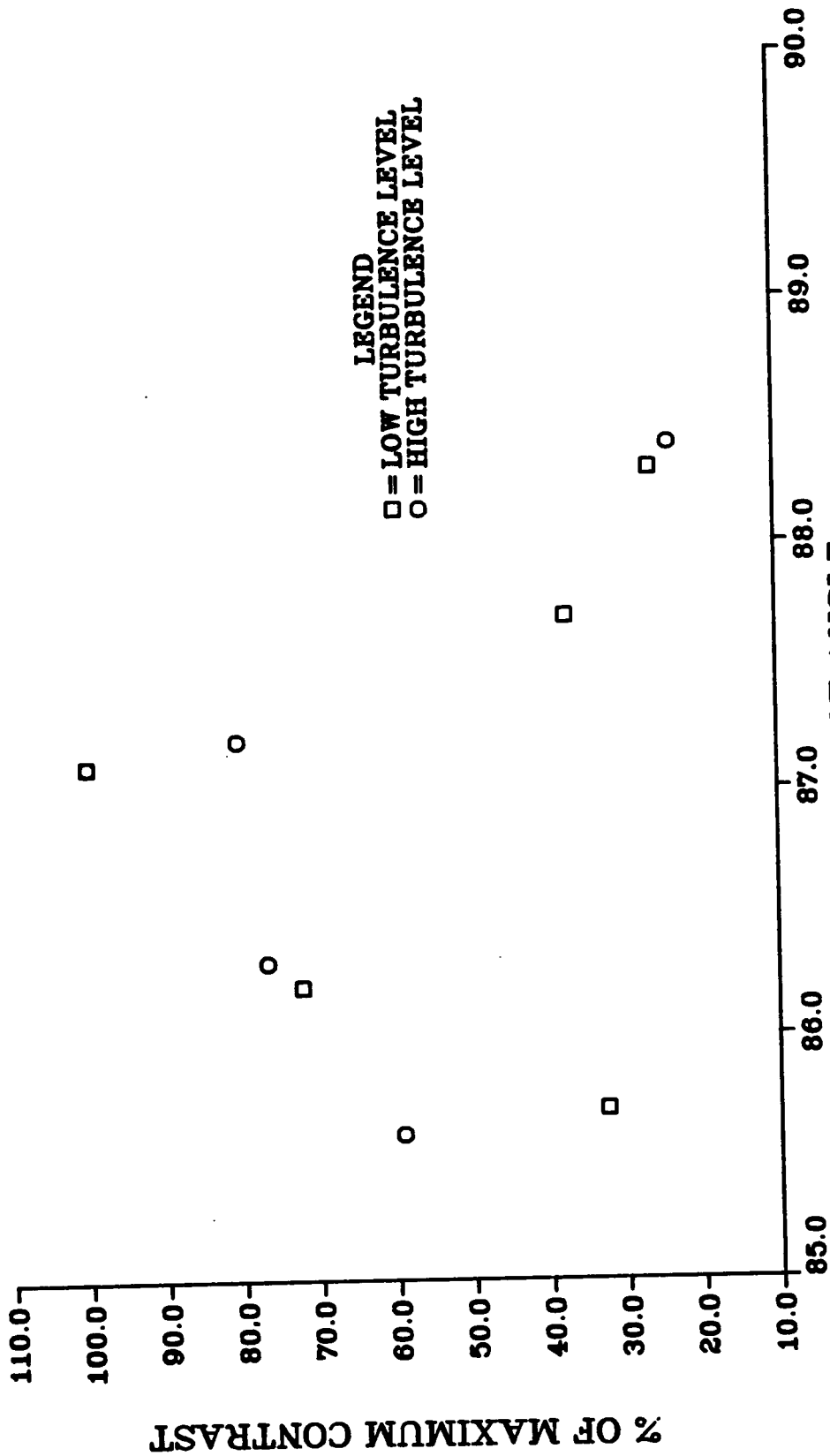

FIGURE 42 CONTRAST SENSITIVITY TO LTA SPOT ANGLE

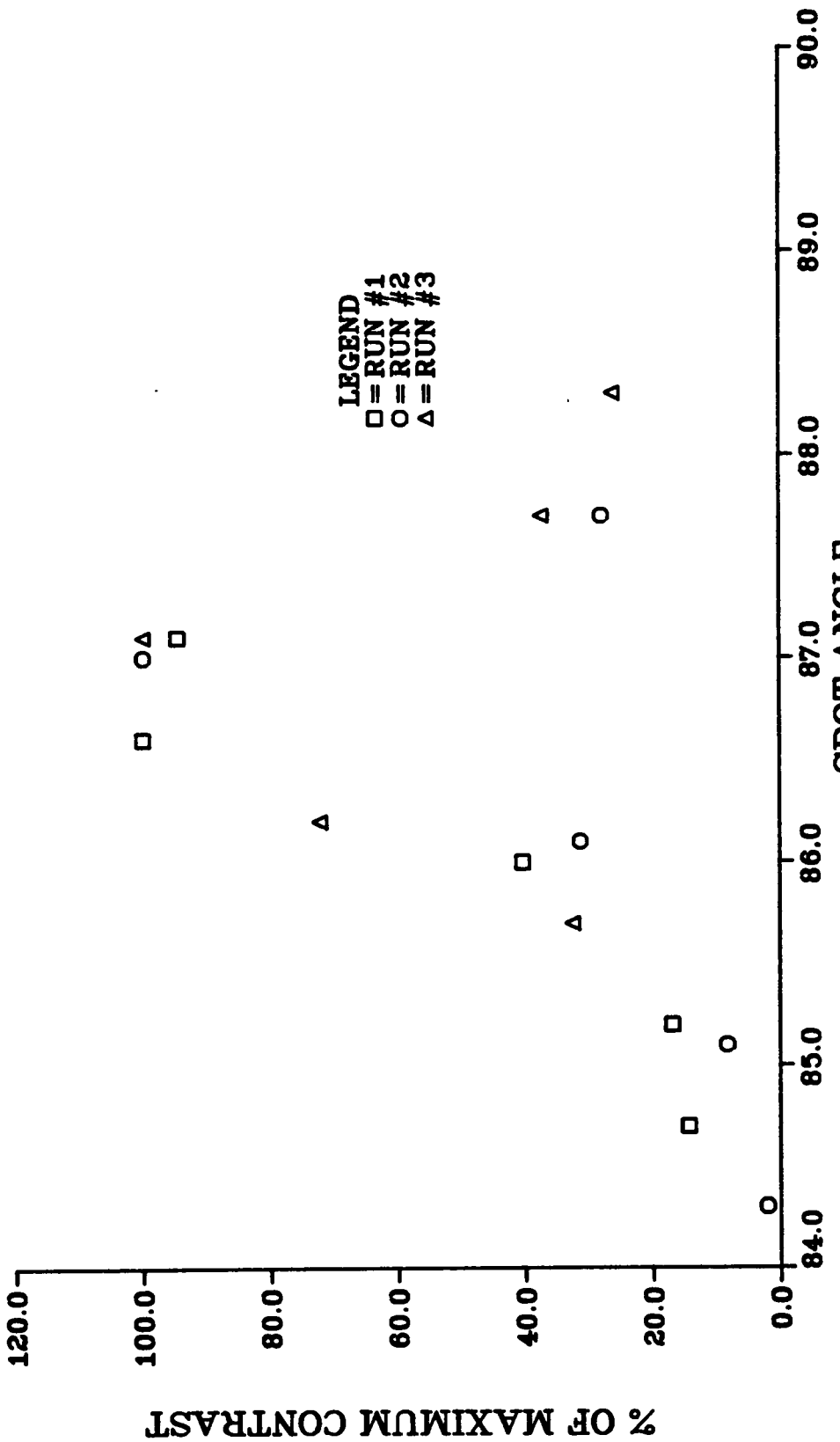

FIGURE 43 REPEATABILITY OF CONTRAST SENSITIVITY TO LTA SPOT ANGLE

both runs in Figure 42, indicate the actual flow velocity would be about 86.9 degrees. The data for Figures 41-43 are presented in Table 7. Figures 42 and 43 indicate that the actual flow angle could be predicted with a curve fit routine to a value different from an actual measured angle. In practice, this was not done. The flow angle used for the compressor data presented in Appendix C was the actual spot angle with the largest contrast for a series of spot angles. The increments used during the compressor testing were 2 degrees and 3 degrees which would measure the absolute flow angle to within ± 1.5 degrees.

e. Temporal and Station-to-Station Uncertainty

The station-to-station precision bias uncertainty of the LTA velocity measurement was determined by taking a series of station measurements in the calibration jet. With a constant velocity in the jet, each station should provide the same velocity measurement. Table 8 presents the values measured by the LTA system in this manner. The temporal precision error uncertainty can also be measured using the system to make velocity measurements over time in a constant velocity jet. Table 9 presents the data obtained during the temporal precision error check of the LTA system. From these tests, it is estimated that the temporal precision uncertainty for the measurement of velocity using the LTA system is less than ± 0.12% with a confidence level of 95%. The bias uncertainty from station to station is also considered to be less than 0.2% with a 95% confidence level.

TABLE 7

LTA MEASUREMENT SENSITIVITY

TO SPOT ANGLE

ANGLE (degrees)	VELOCITY (m/sec)	CONTRAST	INDICATED TURBULENCE (%)
LOW TURBULENCE			
85.7	19.83	438	.77
86.2	19.86	973	.73
87.1	19.95	1347	.71
87.7	20.01	504	.74
88.3	20.04	353	.78
HIGH TURBULENCE			
85.6	19.32	145	5.7
86.3	19.37	188	5.6
87.1	19.56	245	4.8
87.2	19.56	197	5.0
88.4	19.67	58	4.0
LOW TURBULENCE REPEAT RUNS			
RUN #1			
84.7	19.91	220	.74
85.2	19.89	259	.76
86.0	19.93	619	.76
86.6	19.96	1532	.73
87.1	20.01	1449	.73
RUN #2			
84.3	19.78	50	.90
85.1	19.81	204	.74
86.1	19.88	768	.74
87.0	19.96	2451	.71
87.7	20.03	686	.70

TABLE 8

STATION-TO-STATION BIAS UNCERTAINTY CHECK

STATION	VELOCITY (m/sec)	INDICATED TURBULENCE (%)	CONTRAST	DATA RATE (samples/ sec)
0	27.53	.77	260	3.0
1	27.54	.84	380	2.8
2	27.53	.80	324	3.2
3	27.51	.80	282	2.7
4	27.55	.83	354	3.2
5	27.53	.76	245	2.8
6	27.53	.87	302	2.7
7	27.53	.84	325	2.9
8	27.52	.79	193	3.0
9	27.52	.75	394	3.2
10	27.53	.77	271	2.8
11	27.54	.86	369	2.8
12	27.51	.79	485	3.2
13	27.53	.83	667	2.7
14	27.51	.83	349	2.4
15	27.52	.91	229	2.5
16	27.54	.83	354	2.9
17	27.51	.75	302	3.0
18	27.52	.87	388	3.0
19	27.54	.88	295	3.3
20	27.53	.86	453	2.7
21	27.52	.81	398	3.1
22	27.55	.92	229	3.0
23	27.52	.79	339	2.9
24	27.55	.85	239	3.0
25	27.54	.81	330	2.4

TABLE 9

TEMPORAL PRECISION UNCERTAINTY CHECK

TIME (min:sec)	VELOCITY (m/sec)	INDICATED TURBULENCE (%)	CONTRAST	DATA RATE (samples/sec)
0:00	194.10	1.45	1417	407
1:44	194.30	1.47	1088	360
3:14	194.31	1.48	764	248
4:49	194.26	1.52	710	262
6:29	193.86	1.59	528	162
8:47	194.10	1.60	540	151
10:20	193.96	1.50	507	158
12:20	194.46	1.55	307	83
13:54	194.97	1.45	317	85
15:54	193.97	1.44	249	83
17:20	194.19	1.40	249	87
18:52	194.50	1.55	264	80
20:30	194.15	1.38	306	84
22:00	194.00	1.41	248	77
23:44	194.06	1.46	274	78
25:05	194.14	1.55	300	82
26:05	194.35	1.47	244	83
27:53	194.38	1.44	293	75
29:10	193.73	1.50	323	93
30:46	194.18	1.57	286	102
32:02	194.60	1.66	418	106
33:29	194.34	1.57	319	83
34:50	194.16	1.46	267	87
36:15	194.10	1.66	270	87
37:40	194.02	1.54	404	71
38:59	194.16	1.49	355	83
--	194.29	1.42	316	104
41:45	194.22	1.56	234	177
43:13	193.97	1.57	313	85
44:33	194.34	1.55	353	84

6. Axisymmetric Jet Traverses

The LTA system was first used in an axisymmetric jet to gain experience with the system and determine the system's advantages and limitations. These initial experiments were also performed using a TSI six-beam LDA and a hot wire. The comparison results were presented in reference 45. To provide a comprehensive background of the LTA capability, some of the information in reference 45 will be included here.

The two laser systems, along with the hot wire, were used to traverse the free jet produced by the Dantec calibrator with the 60 mm^2 nozzle. The radial distribution of the mean axial velocity and axial turbulence intensity was measured at two axial locations corresponding to an L/D of 0.23 and 1.15. For these tests, the measurement volume was centered in the middle of the velocity profile measured at an L/D of 0.23. Figures 44 and 45 show the mean velocity test results. For both figures, the mean velocity is normalized by the centerline velocity. At an L/D of 0.23, the results are nearly identical for all three measurement systems, and the thin shear layers at the jet edges are clearly resolved. The thickness of the measured shear layer is considerably less than 0.1 cm at this axial location.

At an L/D of 1.15, the jet has developed somewhat. The edge shear layers are much thicker, and the turbulence intensity at the centerline is an order of magnitude larger than at an L/D of 0.23. At an L/D of

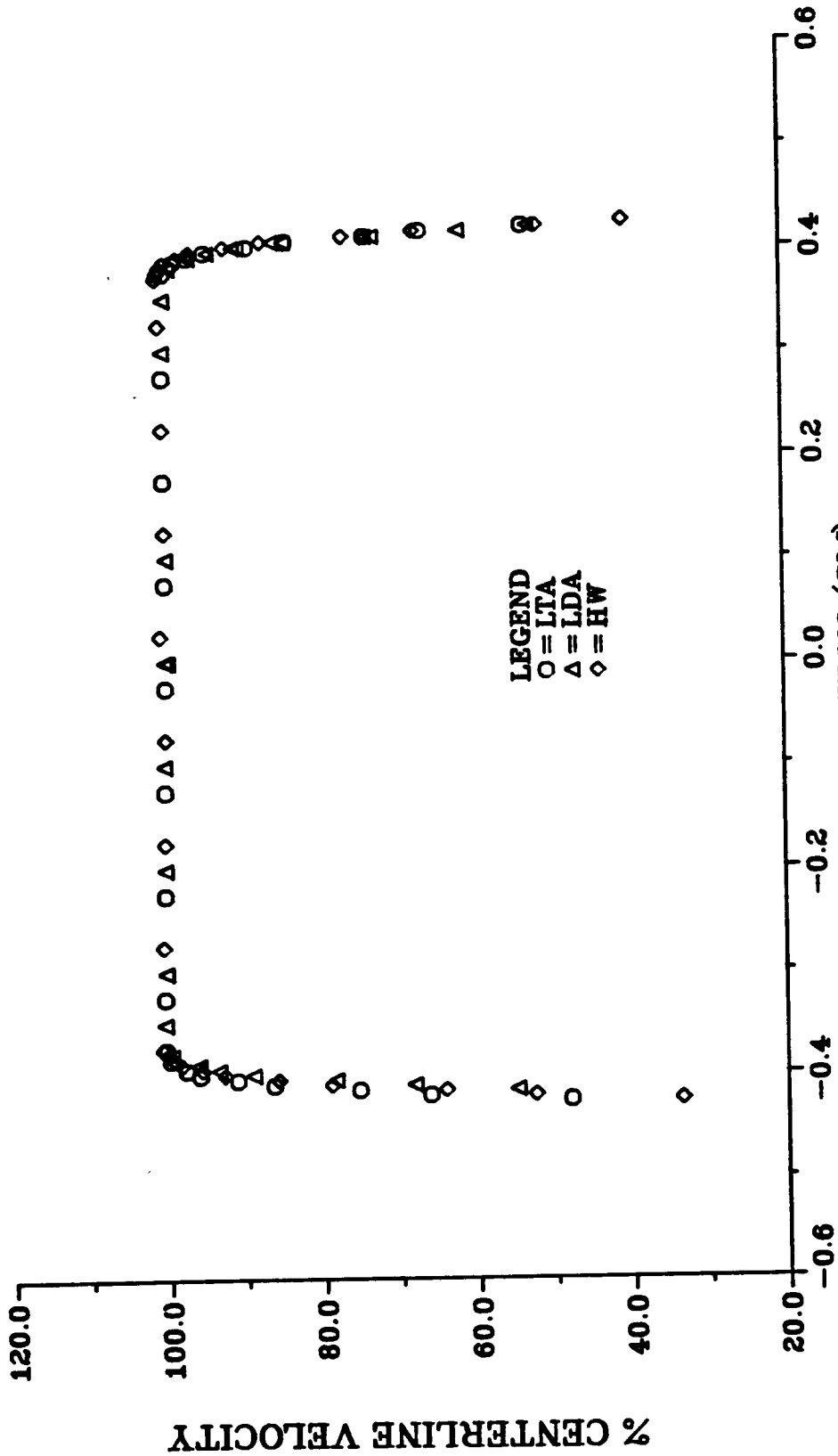

FIGURE 44 VELOCITY PROFILE OF THE 0.871 CM DIA JET, Z=0.20 CM

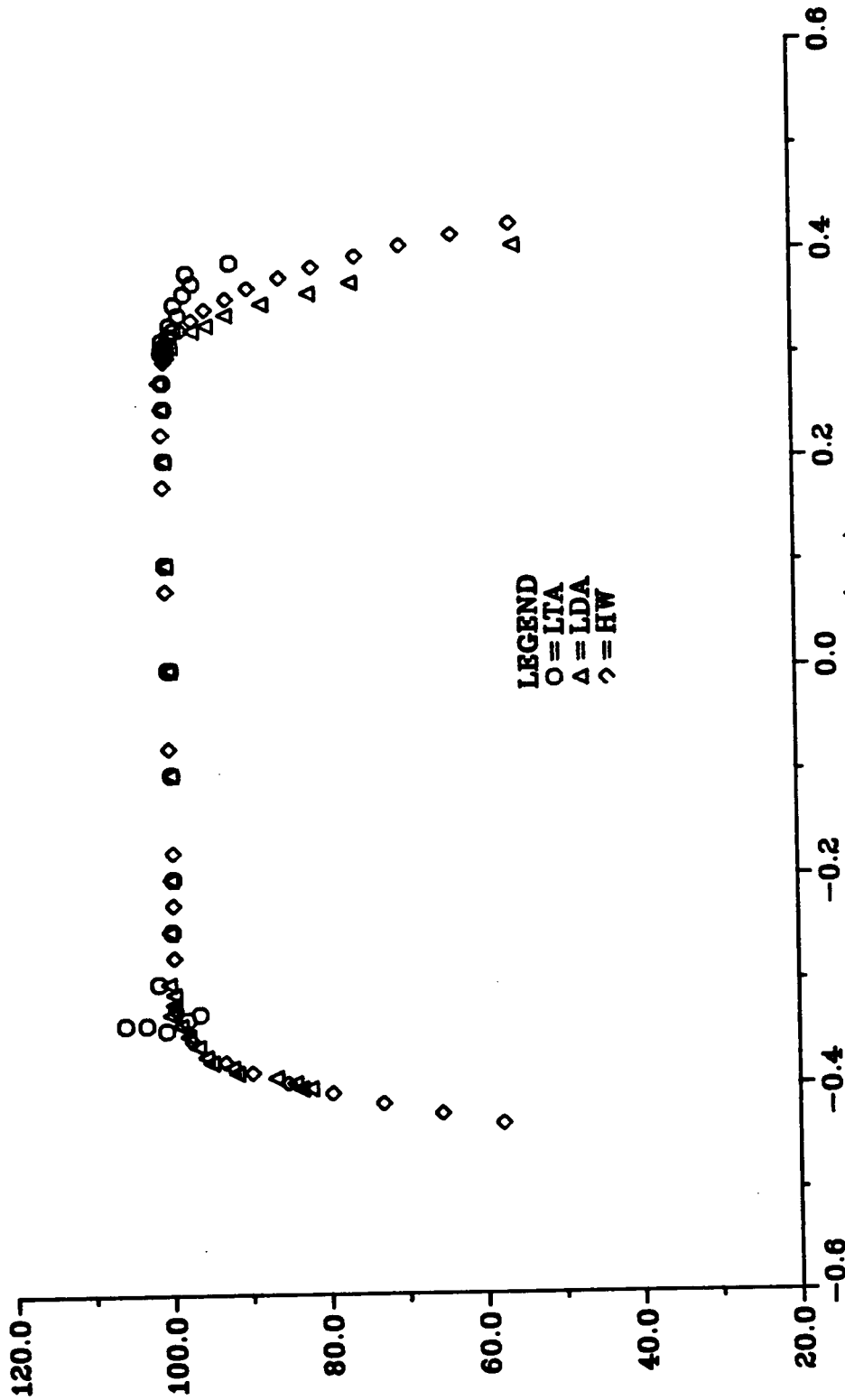

FIGURE 45 VELOCITY PROFILE OF THE 0.871 CM DIA JET, Z= 1.00 CM

1.15, the laser systems measure different behavior at the edges of the jet. The LDA and hot wire measurements yield very similar results; however, some asymmetry is observed. The LTA measures a different profile near one edge of the jet. It should be noted that the LDA and LTA systems will measure conditional velocities, as the external flow entrained by the free jet is unseeded except for naturally occurring ambient dust. The LDA does not detect naturally occurring particles, except for extremely large sizes, while the LTA can detect smaller natural particles due to its higher power density in the measurement volume. This behavior may account for some of the differences between the three systems near the jet edges. High turbulence levels at the jet edges may also adversely effect the LTA measurements.

Radial turbulence intensity profiles at the two axial positions are shown in Figures 46 and 47. In these figures, the turbulence level intensity is normalized using the local mean velocity and not the centerline value. At an L/D of 0.23, the hot wire measures a turbulence of 0.2% at the centerline. Both laser systems measure higher turbulence levels at this location. As the turbulence level increases to about 2% in the shear layer, all three systems begin to measure essentially the same value. Presumably the laser systems have a lower limit beyond which turbulence levels cannot be measured reliably.

At an L/D of 1.15, the centerline turbulence level is clearly above the threshold of both the LTA and LDA, and all three systems

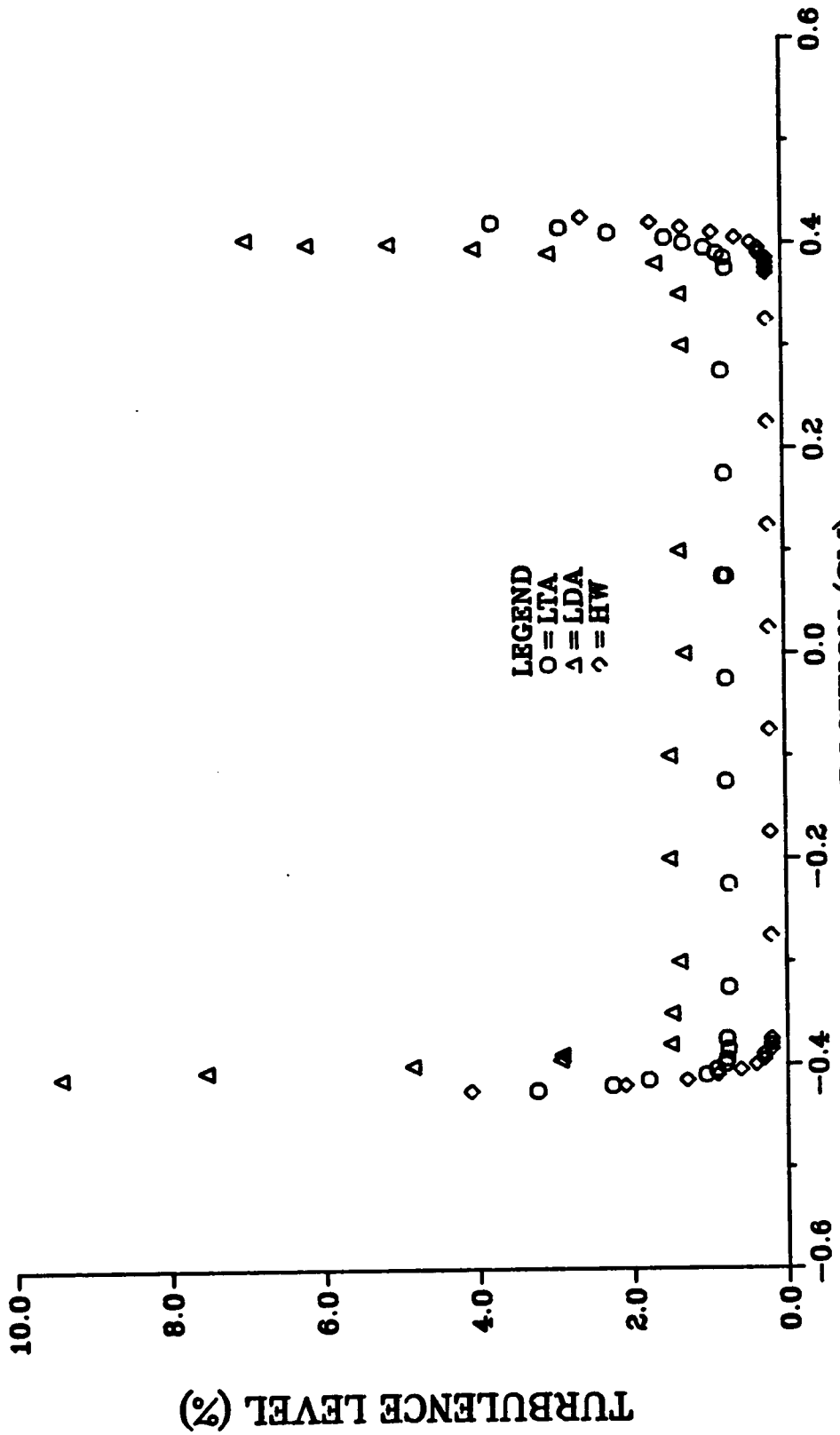

FIGURE 46 TURBULENCE LEVEL PROFILE
OF THE 0.871 CM DIA JET, Z=0.20 CM

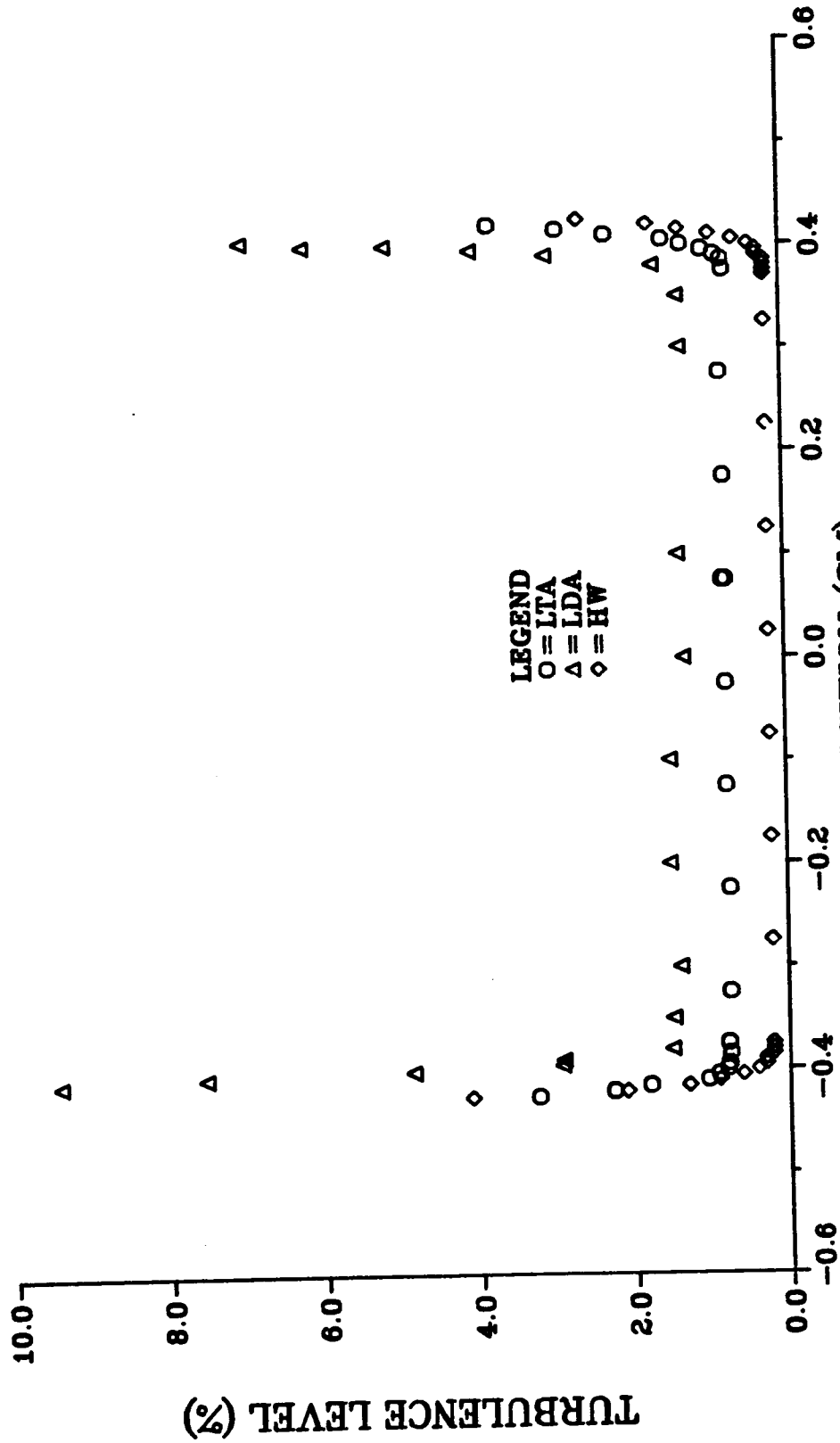

FIGURE 47 TURBULENCE LEVEL PROFILE
OF THE 0.871 CM DIA JET, Z= 1.00 CM

measure essentially the same level near the centerline. The results at the centerline also agree with reference 48. As the jet edges are approached, the hot wire and LDA measure nearly the same behavior. The LTA measures the same behavior on one edge but not on the other, possibly due to the high turbulence levels. The distortions in the LTA turbulence intensity profile are observed to be on the opposite side from the distortions in the LTA velocity profile. There was some indication in these experiments that the LTA was measuring ambient particles which may have lead to the distortions in these measured jet profiles. It is unknown at this time why these effects would be asymmetrical. The data for all of these free jet tests are contained in Tables 10-15.

7. Boundary Layer Flows

Subsequent to the free jet flows, experience with the system was gained with flat plate, boundary layer flows. Only the two laser systems were used to measure these flows. For these boundary layer measurements, a flat plate with a sharp leading edge was mounted in the center of a circular pipe of 25.4 cm diameter. The pipe was fitted with a bellmouth inlet with vacuum applied far downstream. Atmospheric air was then drawn into the pipe inlet and over the flat plate. A flat window in the side of the pipe wall permitted access of the laser beams. All measurements were made on the centerline of the plate at 12.5 cm downstream of the leading edge and 65.5 cm from the bellmouth inlet.

TABLE 10

LTA FREE JET TRAVERSE AT Z = 0.20 cm

LOCATION (cm)	VELOCITY (% OF CENTERLINE)	TURBULENCE LEVEL (% OF MEASURED VELOCITY)
-0.425	48.01	3.24
-0.420	66.20	2.27
-0.415	75.38	1.80
-0.410	86.46	1.05
-0.405	91.17	.95
-0.400	96.03	.80
-0.40	96.10	.80
-0.395	97.80	.78
-0.395	97.75	.77
-0.385	99.82	.76
-0.375	100.35	.78
-0.325	100.42	.75
-0.225	100.25	.74
-0.125	100.14	.77
-0.250	100.00	.76
0.075	100.00	.75
0.075	100.00	.79
0.175	100.04	.76
0.275	100.07	.79
0.375	99.89	.73
0.385	98.59	.75
0.390	96.73	.84
0.395	94.48	1.00
0.400	89.03	1.27
0.405	84.03	1.51
0.410	73.76	2.25
0.415	66.59	2.88
0.420	53.32	3.76

TABLE 11

LDA FREE JET TRAVERSE AT Z = 0.20 cm

LOCATION (cm)	VELOCITY (% OF CENTERLINE)	TURBULENCE LEVEL (% OF MEASURED VELOCITY)
-0.415	54.95	11.97
-0.410	73.68	15.92
-0.410	68.25	9.42
-0.405	78.45	7.54
-0.400	89.14	4.86
-0.395	93.60	2.94
-0.390	96.15	2.92
-0.380	99.67	1.51
-0.350	100.44	1.49
-0.300	100.24	1.39
-0.200	100.20	1.51
-0.100	100.17	1.50
0.000	100.00	1.30
0.000	99.66	1.39
0.100	99.83	1.36
0.300	100.07	1.31
0.230	99.93	1.33
0.380	99.16	1.64
0.390	96.55	3.03
0.395	94.07	4.00
0.400	90.18	5.11
0.400	90.78	6.17
0.405	84.18	6.67
0.405	85.69	6.97
0.410	72.75	16.07
0.415	61.62	18.45
0.420	52.63	19.40

TABLE 12

HOT WIRE FREE JET TRAVERSE AT Z = 0.20 cm

LOCATION (cm)	VELOCITY (% OF CENTERLINE)	TURBULENCE LEVEL (% OF MEASURED VELOCITY)
-0.425	33.60	4.1
-0.420	52.63	2.1
-0.415	64.20	1.3
-0.410	78.97	0.9
-0.405	85.85	0.6
-0.400	92.81	0.4
-0.395	95.73	0.3
-0.390	98.38	0.3
-0.385	99.35	0.2
-0.380	100.10	0.2
-0.375	100.72	0.2
-0.275	100.52	0.2
-0.175	100.20	0.2
-0.075	100.07	0.2
-0.075	100.00	0.2
0.025	100.60	0.2
0.125	99.97	0.2
0.225	100.14	0.2
0.325	100.52	0.2
0.370	100.80	0.2
0.375	100.60	0.2
0.380	100.28	0.2
0.385	99.76	0.2
0.390	98.11	0.3
0.395	96.39	0.3
0.400	91.91	0.4
0.405	87.19	0.6
0.410	76.59	0.9
0.415	67.44	1.3
0.420	51.50	1.7
0.425	40.34	2.6

TABLE 13

LTA FREE JET TRAVERSE AT Z = 1.00 cm

POSITION (cm)	VELOCITY (% OF CENTERLINE)	TURBULENCE LEVEL (% OF MEASURED VELOCITY)
-0.345	100.7	12.43
-0.340	105.9	9.82
-0.340	103.2	9.49
-0.340	103.0	11.09
-0.335	98.0	15.34
-0.330	98.6	14.72
-0.3298	96.4	15.83
-0.320	99.8	13.55
-0.310	101.8	11.12
-0.310	99.6	13.23
-0.300	101.6	9.74
-0.300	99.8	11.00
-0.250	99.8	6.16
-0.200	99.6	4.69
-0.100	99.7	3.19
0.00	100.0	2.37
0.000	100.0	2.57
0.000	99.7	2.46
0.100	100.2	2.37
0.200	100.2	3.28
0.250	100.2	4.55
0.275	100.3	5.92
0.300	100.0	7.07
0.305	100.4	7.15
0.310	100.0	7.52
0.315	100.3	7.55
0.320	99.4	8.03
0.325	98.8	8.11
0.330	99.3	8.32
0.340	98.2	8.61
0.350	98.7	8.04
0.360	97.5	7.16
0.370	96.4	6.91
0.380	97.1	6.53
0.390	91.5	10.29

TABLE 14

LDA FREE JET TRAVERSE AT Z = 1.00 cm

POSITION (cm)	VELOCITY (% OF CENTERLINE)	TURBULENCE LEVEL (% OF MEASURED VELOCITY)
-0.400	82.4	21.97
-0.400	83.6	21.87
-0.395	84.4	20.94
-0.390	86.8	20.06
-0.385	91.8	18.06
-0.380	92.4	16.86
-0.375	95.0	14.92
-0.370	95.7	14.59
-0.360	96.7	12.51
-0.350	97.9	11.60
-0.340	98.9	9.68
-0.330	100.1	8.77
-0.320	99.7	8.05
-0.310	99.7	7.55
-0.300	82.4	6.45
-0.250	100.1	4.41
-0.200	99.9	3.32
-0.100	99.8	2.36
0.000	100.0	2.12
0.000	99.8	2.15
0.100	100.2	2.23
0.200	100.3	3.09
0.250	100.5	4.71
0.275	100.8	5.79
0.300	100.3	7.33
0.305	99.7	8.06
0.310	99.2	8.48
0.320	99.3	10.16
0.325	96.5	10.86
0.330	94.7	12.42
0.340	92.2	14.04
0.350	87.6	18.06
0.360	81.6	21.50
0.370	76.2	23.90
0.404	55.4	-

TABLE 15

HOT WIRE FREE JET TRAVERSE AT Z = 1.00 cm

POSITION (cm)	VELOCITY (% OF CENTERLINE)	TURBULENCE LEVEL (% OF MEASURED VELOCITY)
-0.435	57.8	28.6
-0.425	65.6	24.8
-0.415	73.1	21.6
-0.405	79.6	18.8
-0.395	85.2	16.4
-0.385	89.8	14.7
-0.375	93.2	13.4
-0.355	97.4	11.7
-0.325	99.5	9.4
-0.275	99.6	6.2
-0.225	99.7	4.5
-0.175	99.6	3.3
0.075	100.0	2.4
0.075	100.2	2.2
0.125	100.3	2.4
0.175	100.4	2.8
0.225	100.5	3.8
0.275	100.4	5.8
0.295	100.1	6.6
0.325	97.9	7.9
0.335	96.5	8.5
0.345	94.8	9.2
0.355	92.1	9.9
0.365	89.3	11.1
0.375	85.2	12.3
0.385	81.1	14.4
0.395	75.5	16.4
0.405	69.8	18.7
0.415	63.2	20.6
0.425	55.8	25.8

The boundary layer was measured by both laser systems, and the measured profiles are shown in Figure 48. The data for Figure 48 are presented in Table 16. These profiles were obtained at a free stream velocity of 46 m/sec and a free stream turbulence level of 2.0%. Both systems appear to agree in the measurement of the boundary layer profile. As would be expected, because of its smaller focal volume height, the LTA could measure closer to the flat plate before the measurement signal was disrupted by flare reflections. An attempt to use both systems to measure the boundary layer with the optical axis perpendicular to the flat plate failed. The LTA system was able to measure velocity in this configuration to 0.75mm from the plate; however, it was still not close enough to begin to measure the profile of the boundary layer. Boundary layer measurements with the LTA system were also attempted near the window surface. In this configuration, the optical axis was within 4 degrees of being perpendicular to the window surface. The measured boundary layer profile is shown in Figure 49, and the data for this figure are presented in Table 17. This profile was obtained at a free stream velocity of 27 m/sec and a free stream turbulence level of 1.5 - 2%. This time, measurements were made to 0.3 mm of the window surface compared to 0.75 mm of the perpendicular flat plate, mentioned above.

8. Summary

The purpose of this appendix has been to describe the LTA system and to demonstrate its ability to measure the flows addressed in this

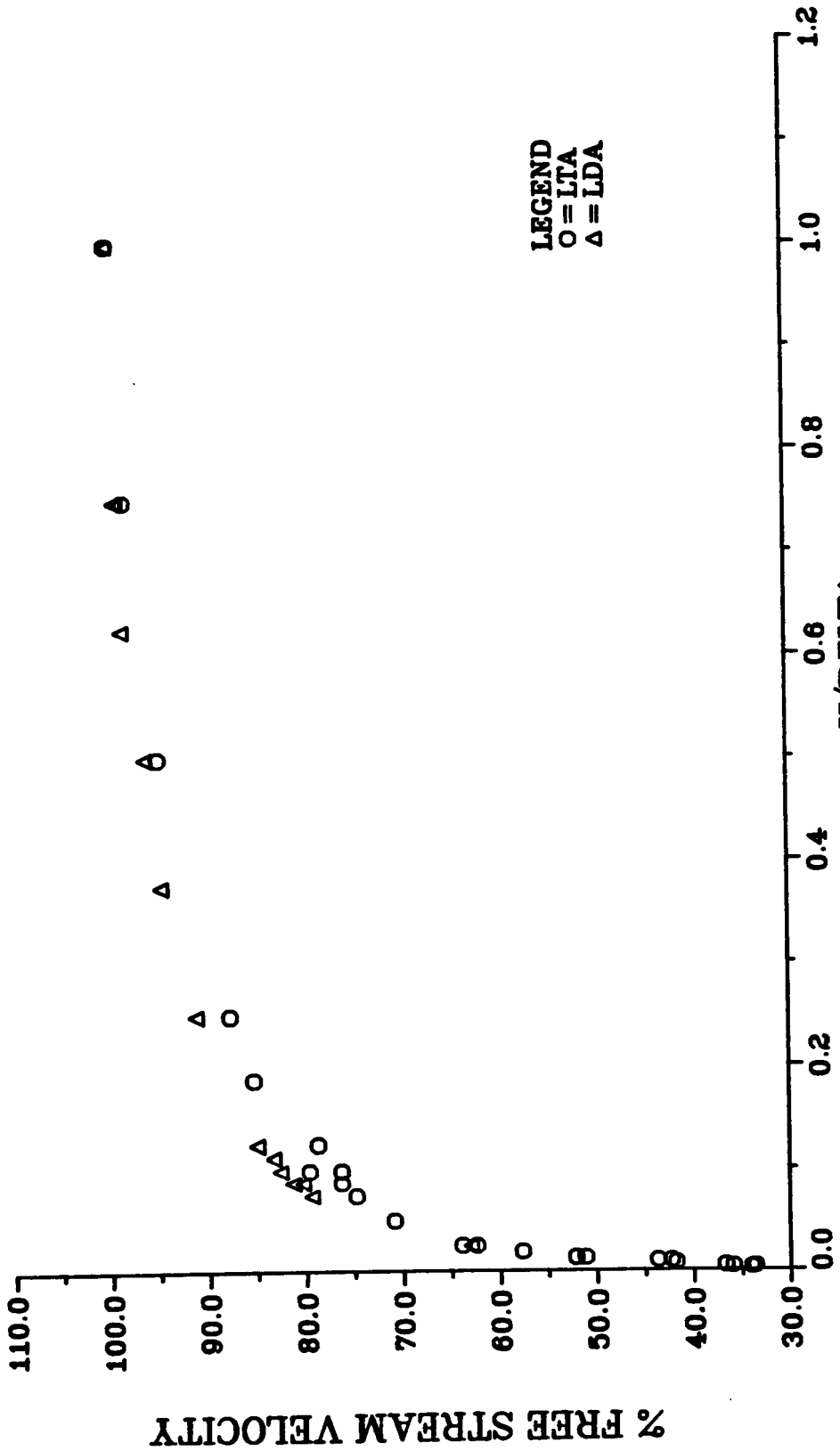

FIGURE 48 FLAT PLATE BOUNDARY LAYER TRAVERSE

TABLE 16

LTA AND LDA BOUNDARY LAYER TRAVERSE

Y (cm)	Y/DELTA	VELOCITY (m/sec)	% FREE STREAM VELOCITY	TURBULENCE LEVEL (% OF MEASURED VELOCITY)
LTA				
1.000	1.25	46.01	100.4	2.50
1.000	1.25	45.99	100.3	2.20
0.800	1.00	45.83	100.0	2.69
0.800	1.00	45.78	99.9	2.59
0.600	.75	45.09	98.4	3.98
0.400	.50	43.54	95.0	6.14
0.200	.25	40.17	87.7	8.68
0.150	.188	39.08	85.3	8.92
0.100	.125	36.07	78.7	11.10
0.080	.100	34.99	76.3	11.66
0.070	.088	34.95	76.3	10.19
0.060	.075	34.28	74.8	10.87
0.040	.050	32.51	70.9	10.98
0.020	.025	29.28	63.9	12.79
0.020	.025	28.59	62.4	15.63
0.015	.019	26.44	57.7	14.96
0.010	.013	23.46	51.2	13.05
0.010	.013	23.94	52.2	14.59
0.008	.010	19.37	42.3	17.85
0.008	.010	20.04	43.7	11.57
0.006	.008	19.14	41.8	11.57
0.004	.005	16.84	36.7	20.20
0.003	.004	16.47	35.9	11.65
0.003	.004	15.41	33.6	12.24
0.002	.003	15.57	34.0	4.08
0.080	.100	36.46	79.6	10.49

TABLE 16 (continued)

LTA AND LDA BOUNDARY LAYER TRAVERSE

Y (cm)	Y/DELTA	VELOCITY (m/sec)	% FREE STREAM VELOCITY	TURBULENCE LEVEL (% OF MEASURED VELOCITY)
LDA				
0.800	1.000	43.2	100.0	4.1
0.600	.750	42.8	99.1	4.5
0.600	.750	42.9	99.3	4.3
0.500	.625	42.6	98.6	4.3
0.400	.500	41.6	96.3	5.2
0.300	.375	40.9	94.7	6.3
0.200	.250	39.4	91.2	6.6
0.100	.125	36.7	85.0	8.4
0.090	.113	36.0	83.3	8.3
0.080	.100	35.7	82.6	8.0
0.070	.088	35.1	81.3	8.8
0.070	.088	34.7	80.3	10.3
0.060	.075	34.3	79.4	10.4
0.020	.025	27.2	63.0	17.0

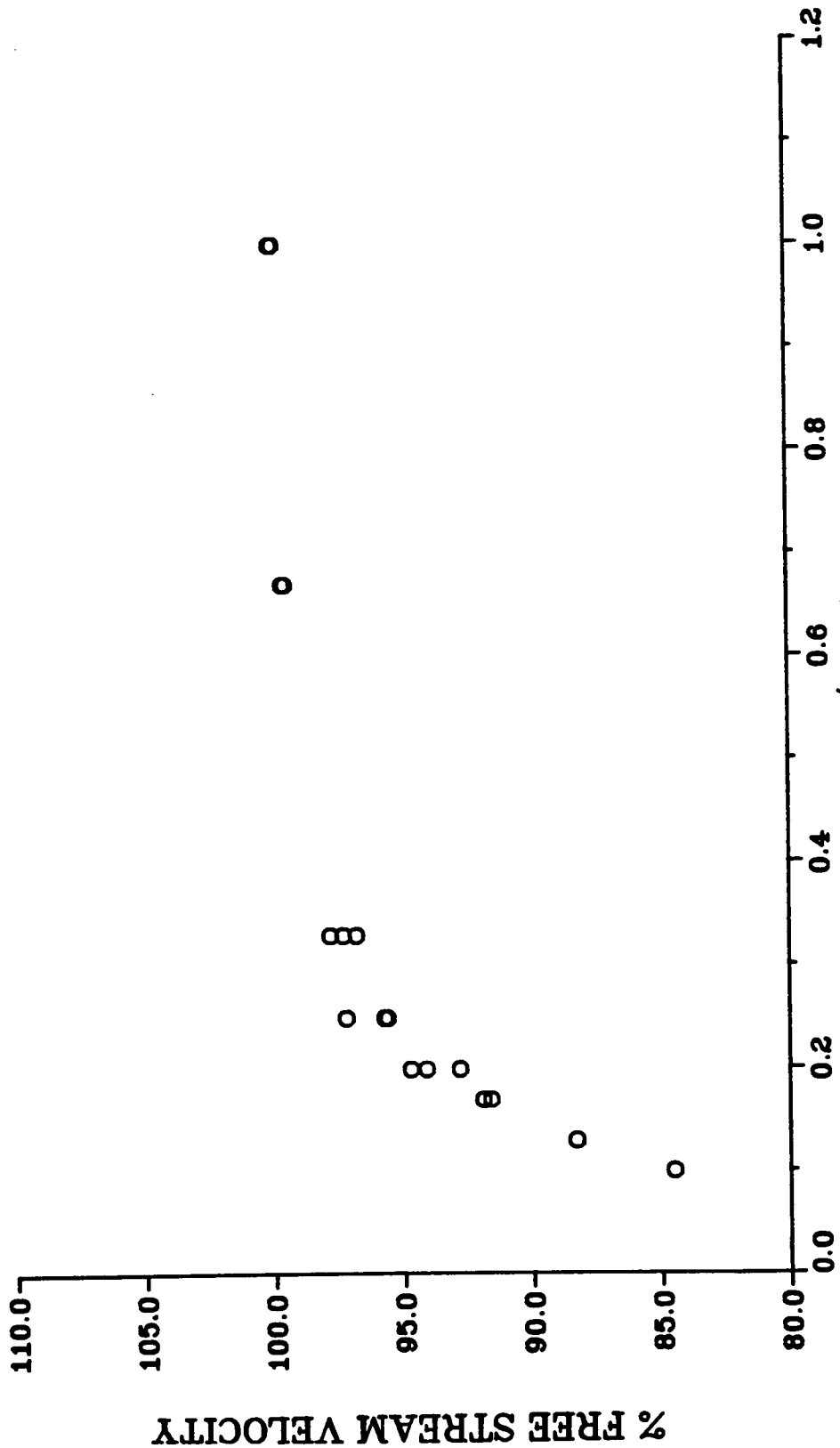

FIGURE 49 BOUNDARY LAYER TRAVERSE
ON THE WINDOW SURFACE

TABLE 17

BOUNDARY LAYER MEASUREMENTS ON

THE WINDOW SURFACE

Y (cm)	Y/DELTA	VELOCITY (m/sec)	% FREE STREAM VELOCITY	TURBULENCE LEVEL (% OF MEASURED VELOCITY)
3.0	1.0	27.01	100.0	2.18
3.0	1.0	26.98	99.9	1.81
2.0	.67	26.90	99.6	2.05
2.0	.67	26.85	99.5	1.98
1.0	.33	26.40	97.8	4.46
1.0	.33	26.14	96.8	5.31
1.0	.33	26.26	97.3	4.59
.75	.25	26.24	97.2	3.76
.75	.25	25.84	95.7	5.00
.75	.25	25.81	95.6	5.35
.60	.20	25.40	94.1	6.54
.60	.20	25.05	92.8	6.96
.60	.20	25.56	94.7	7.05
.50	.17	24.73	91.6	9.08
.50	.17	24.82	91.9	6.27
.40	.13	23.84	88.3	2.86
.30	.10	22.82	84.5	2.52

dissertation. Assuming that the 0.48 micron diameter PSL seed followed the flow in the calibration jet, the LTA system demonstrated the ability to measure the true velocity magnitude to within ± 1.0%. The temporal precision error of the system was measured to be less than ± 0.12%, while the variation from station to station was demonstrated to be within ± 0.2%. From the free jet experiments, however, it was found that the system could only measure the velocity of the flow if the turbulence level was below approximately 15%. The geometric measurement resolution of the system has also been quantified. The probe volume was measured to be 0.430 mm long with a spot separation of 0.279 mm. The spot diameter was measured to be approximately 0.016 mm. With this configuration, the system was found to be able to resolve the velocity vector angle to within ± 0.5 degrees. With the PAC timing in the Correlex, the system was able to resolve the circumferential position within the compressor to within ± 0.6% of the blade-to-blade distance. In the boundary layer experiments, velocity measurements could be made to within 0.0024 mm if the optical axis was essentially transverse to the flat plate. With the plate perpendicular to the optical axis, measurements could only be made to 0.75 mm of a metal surface. However, in essentially the same geometric configuration boundary layer measurements could be made to 0.3 mm of the far side of the window surface. The complete record of calibration and supporting experiments in this section has been presented to support the measurements and observations in this dissertation and to serve as a guide for future work. The measurement resolution and accuracy, as described in this appendix, essentially quantify the LTA system's ability to measure fluid flow.

APPENDIX B

LTA MECHANICAL CONFIGURATION FOR COMPRESSOR MEASUREMENTS

Many additional issues had to be considered in order to use the LTA system in measuring the flow field of the transonic compressor. A picture of the actual mechanical configuration of the setup is shown in Figure 50. In this section, the adaptation of the laser system to measure the compressor flow field will be described. Three major problems had to be resolved. First, the laser had to be translated to move the probe volume within the flow field. Secondly, the system with this traverse had to be mounted within the CRF which is essentially a cylindrical chamber 6.1 meters in diameter and 19.8 meters long. Finally, a window had to be installed in the compressor case to maintain the proper flow field while transmitting laser light into and out of the flow field.

1. Laser Traverse

The traverse used in the experiment is shown in Figure 50. It is a TSI model 9500 traverse system capable of 2.5 microns movement resolution in three orthoganol directions. Since the access to the compressor was located at 20 degrees to the horizon, the laser system had to be angled as shown in Figure 50. The table could not be tilted more than about 15 degrees on its own, so a 10 degree wedge was

FIGURE 50 LTA CONFIGURATION IN THE CRF

constructed and placed under the optical head. With this wedge and the table tilted at 10 degrees, a total angle of 20 degrees was obtained. One horizontal movement traversed the probe volume along the compressor axis. The vertical movement and the other horizontal movement were used together to move the laser in the radial direction. This combination of movement to position the probe volume in the radial direction required an accurate measurement of the 20 degrees of tilt which was performed with an inclinometer. The accuracy of this measurement was ± 0.1 degree.

The traverse table could be computer controlled; however, the data management system for the LTA system could not operate the traverse control simultaneously with the laser measurement software. Therefore, the traverse was operated manually using an extension cable with a remote controller. The position read-out from the traverse system was viewed with a closed circuit television. The read-out and television camera are visible to the left in Figure 50. The complete traverse system worked perfectly throughout the test.

2. Laser Table Mount

The laser system and traverse were mounted in close proximity to the compressor case using a specially designed laser table mount. The mount had to support the system weight of nearly 1100 Kg and suspend it almost four meters across the chamber. Constructed from two 15.24 cm steel I beams, the mount was supported at both ends and at two

locations near the center of the span. Most of the mount hardware is visible in Figure 50.

During the compressor testing, the relative motion between the traverse table and the case of the compressor was measured. Three accelerometers in the traverse table were used to measure the table movement in three orthogonal directions. Using these accelerometers in conjunction with three case mounted accelerometers, the relative motion between the two references could be measured. A Zonic 6088 four channel signal analyzer was used to cross-correlate the three sets of accelerometers. Relative motion between the traverse table and compressor case was measured to be less than 0.005 mm in the compressor's axial direction, 0.032 mm in the vertical direction and 0.005 mm in the horizontal radial direction. These relative motions are within the probe volume and circumferential measurement dimensions and should not effect the measurement accuracy or positioning.

The laser and optical head of the LTA system was protected from the environment of the CRF test chamber by the acoustical treatment shown in Figure 50. One side of the protective box has been removed in the figure. Except for an area in front of the output lens, the double lead/foam Soundcoat lining coated the complete inside of the wooden box and the underside of the 10 degree wedge. It was felt that this protection was necessary for the high noise environment within the CRF test chamber. The laser system remained in alignment and maintained sufficient power output so that no adjustments to the system were necessary through the 30 days of the installation.

3. Window Configuration

A window made of Corning VY COR 7913 fused silica was used in the compressor to maintain the flow field, transmit the laser light into the flow and permit the reflected light to enter the receiving optics. The window was designed to a 2 to 1 factor of safety of the recommended design load. This resulted in a 1000 to 1 factor of safety on fracture. This was necessary, since a failure of this window could result in catastrophic damage to the test compressor. The window and its mount are shown in Figure 51. Installation of the window is shown in Figures 52 and 53. A mechanical drawing, including specifications for the window and its mount, is presented in Figure 54. The window had to be flat for use with the LTA. With a curved window, any rotation of the beam would result in distortion of the probe geometry that would be dependent on the angle of rotation.

Using a 100 mm diameter 400 mm focal length lens in the LTA system, the window permitted measurements to be made to an immersion of 85.6% of the radius. The window extended from 16.9% of the axial chord ahead of the blade tip leading edge to 5% of the axial chord behind the blade tip trailing edge. As can be seen in Figure 53, the window blocked the circumferential groove tip treatment within the case. All of the measurements reported were made ahead of the first casing groove. However, during the experiment, there was evidence that flow at the upstream edge of the first groove shown in Figures 4 and 53, was affected by the window blockage.

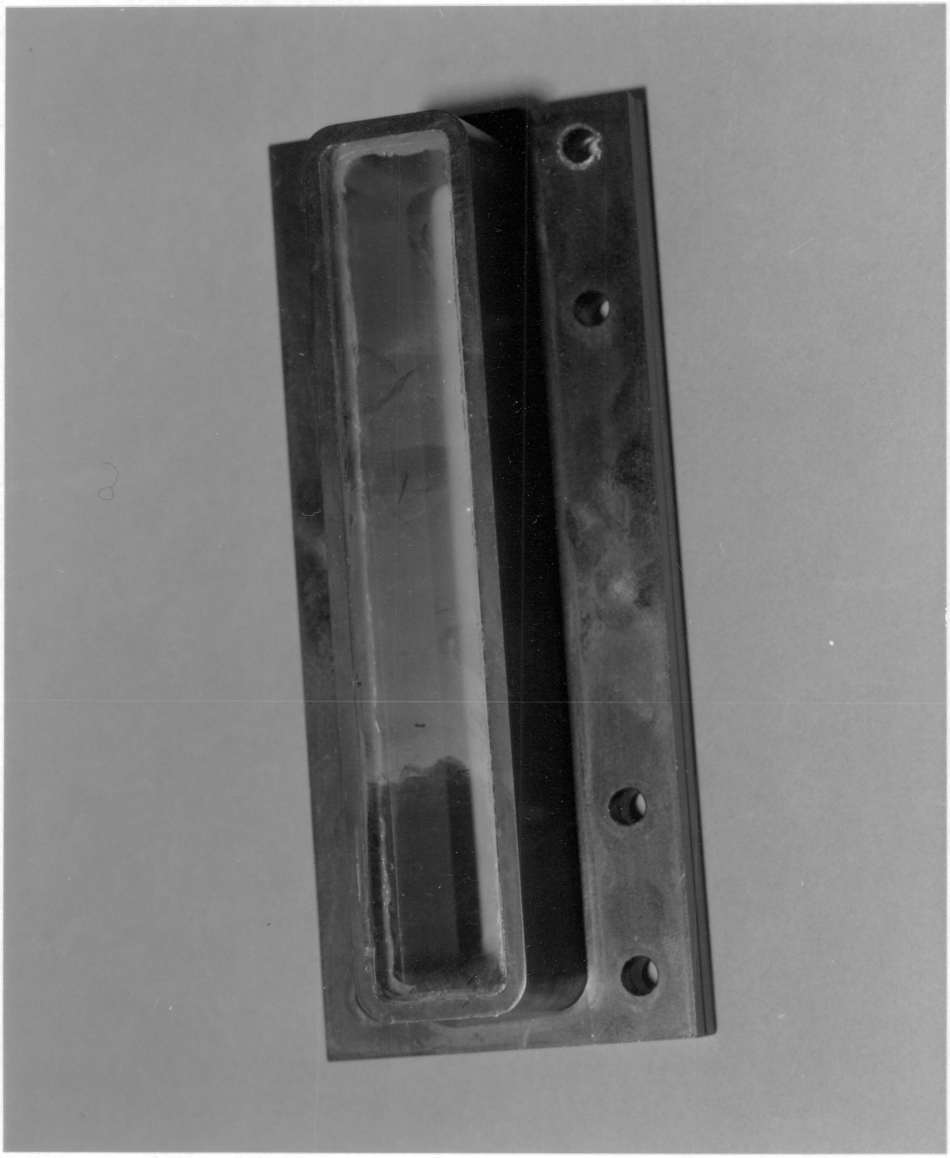

FIGURE 51 WINDOW AND WINDOW MOUNT

FIGURE 52 WINDOW INSTALLATION, EXTERNAL VIEW

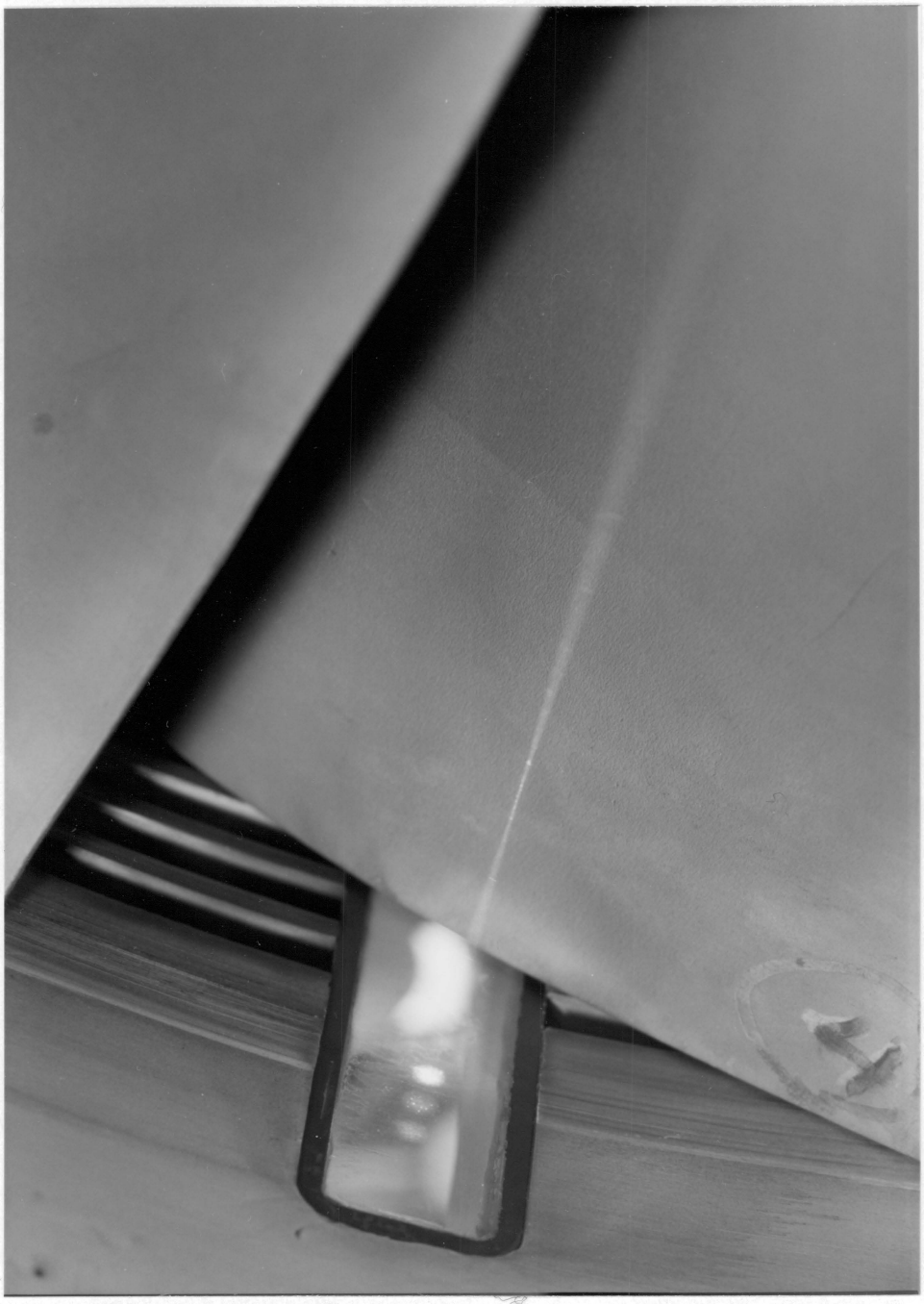

FIGURE 53 WINDOW INSTALLATION, INTERNAL VIEW

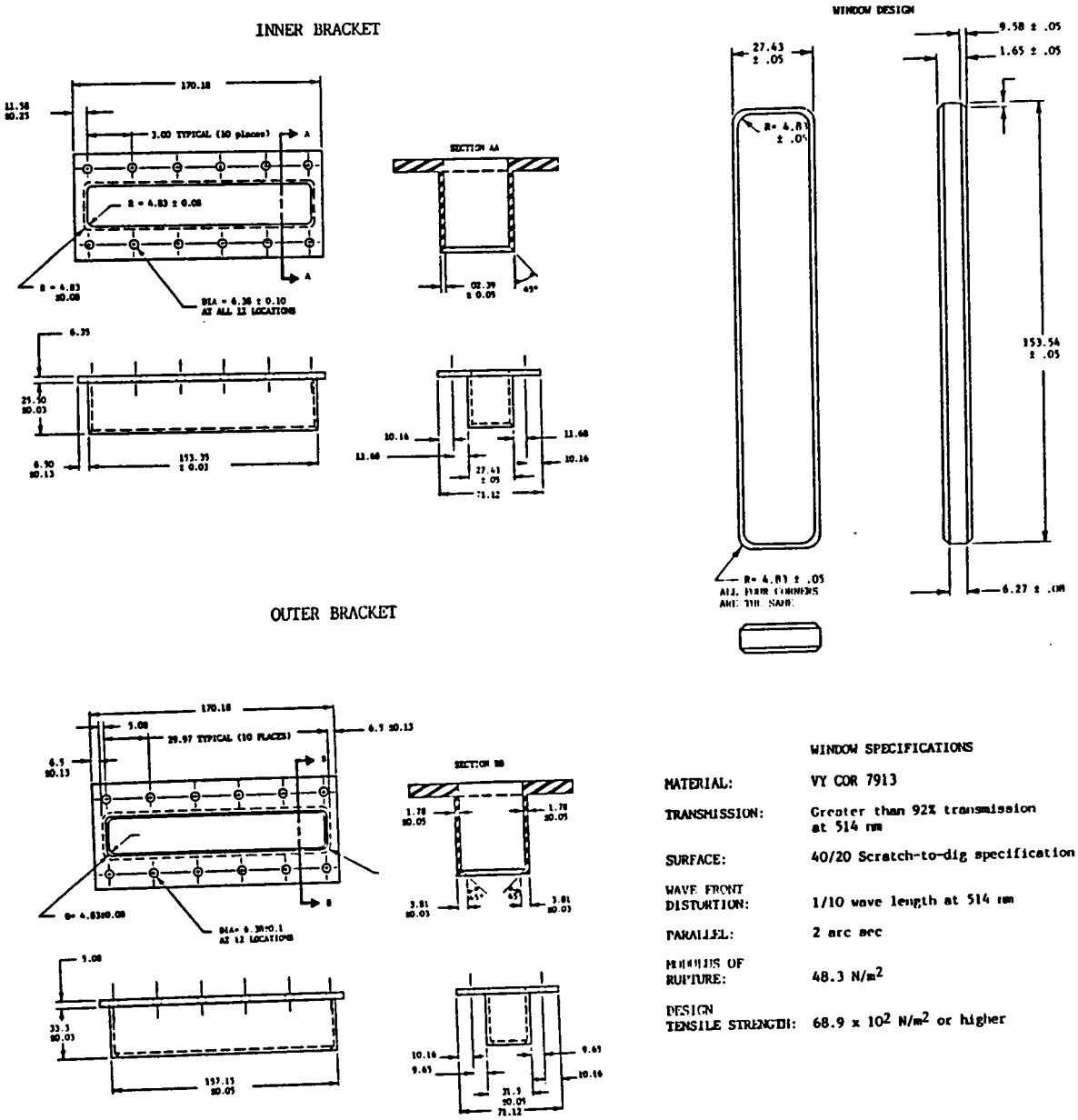

FIGURE 54 Compressor Case Window Design

During the experiment, the window needed to be cleaned periodically. After four to eight hours of running, a film would build up on the window as shown in Figure 51. A subsequent test showed that this film reduced the power transmission to approximately 70% of the incident power while the clean window would pass almost 90%.

4. Radial Positioning

The window did introduce a shift in the focal length of the laser beams. At the beginning of laser measurements, the blades and actual flow field region were inaccessible. Therefore, the laser system was positioned so that it appeared to be focused on the blade tip. This location was then used as the blade tip radius. All radial measurements were then referenced to this location. Following the test, the actual location of the probe volume was measured. With the inlet hardware removed, the focal length was measured at three different radial settings. A depth gage was used to measure the actual distance from the case to the focal point. The offset was measured at three different depths and was found to be 0.185 cm which was constant to within ± 0.013 cm. This offset was then used to correct the immersion set during the actual experiment, and the corrected immersion is contained in the data sets of Appendix C as a percent of the blade radius.

5. Angle Calibration

The spot rotation measured during the experiment was referenced internally to the LTA optical system. Before the laser system or compressor was removed, the spot angle was calibrated to the compressor center line. During the installation, the compressor was aligned to be exactly horizontal. This was checked by measuring the compressor face to be vertical within an inclinometer. The spot rotation was then calibrated to the horizontal axis determined with a precision level. The spot rotation was measured with an inclinometer accurate to 0.1 degree. The resulting calibration is shown in Figure 55 with the values tabulated in Table 18. Again, this calibration was taken into account in reducing the data presented in Appendix C. From this calibration, the LTA spot rotation could be referencd to the compressor reference frame to ±.5 degree.

6. Seed Injection

During the experiment, 0.48 micron diameter PSL seed was introduced in a tube located approximately two meters upstream of the compressor face. This is slightly further upstream than the view shown in Figure 50. The tube was in the shape of a pito tube, and it could be rotated and translated radially to adjust the location of seed injection. The probe was supplied with this seed from a TSI Model 9306 six jet atomizer. The seed was suspended in isopropanol as it had been in the free jet test described in Appendix A. During the test, there

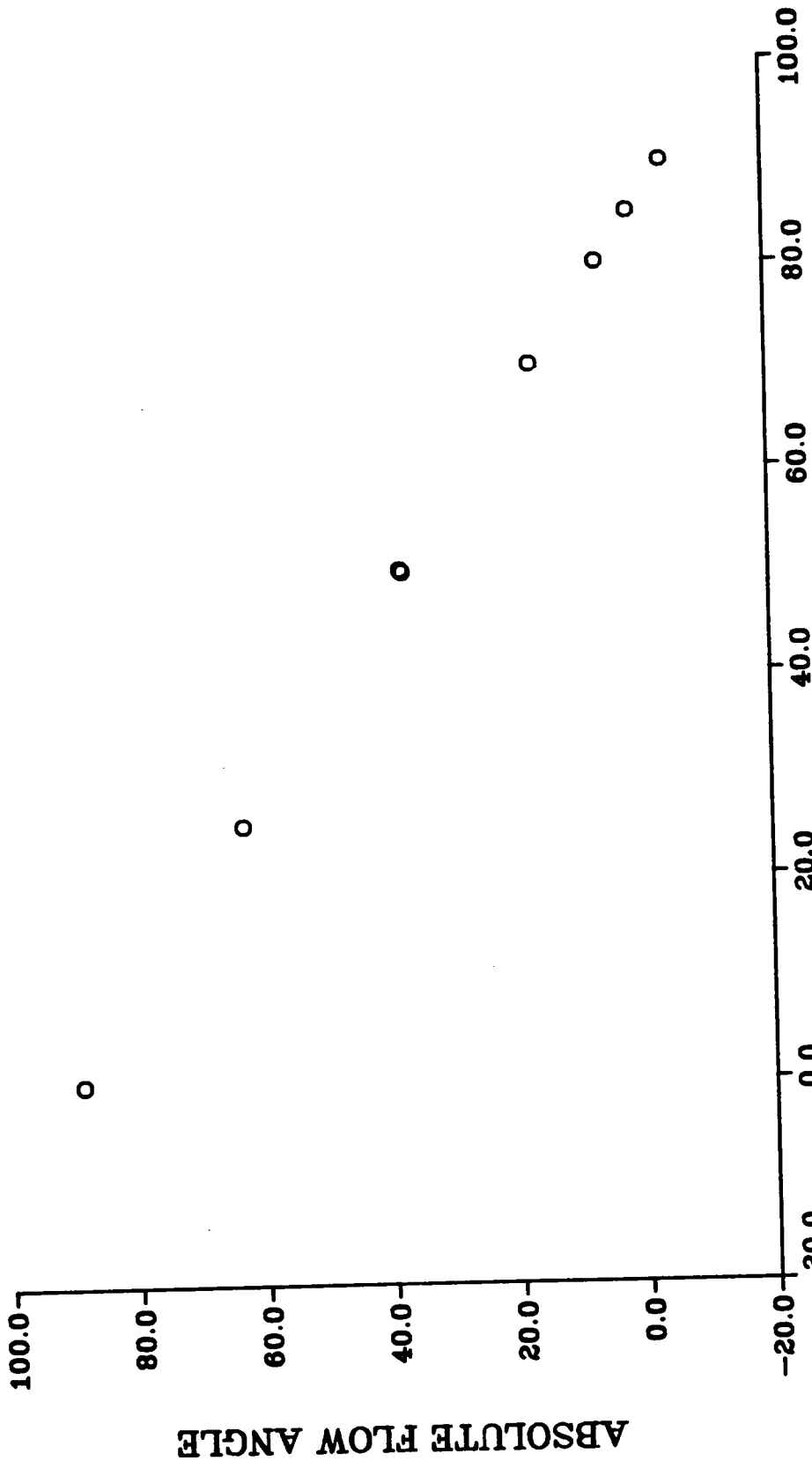

FIGURE 55 LTA SPOT ANGLE CALIBRATION

TABLE 18

LTA SPOT ANGLE CALIBRATION DATA

LTA SPOT ANGLE (degrees)	ANGLE REFERENCED TO COMPRESSOR CENTER LINE (degrees)
90.1	-4.1
85.1	1.3
80.1	6.4
70.1	17.0
50.1	37.9
50.0	37.8
49.9	37.5
25.1	63.2
0.0	88.8
175.2	-90.5

was no indication that any of this seed was measured by the LTA system. The data rate measured was independent of the probe's location and seed flow rate. Consequently, all of the measurements within the compressor flow field are considered to have been made using natural particles in the atmosphere.

7. Calibration Jet

The Dantec calibration jet is also shown in Figure 50. The calibration jet is mounted near the window just under the optical table. The jet was used during the experiment to verify the LTA system's operation. If any questions arose during the compressor test, the LTA system could be positioned by the traverse table to measure the jet flow. Then the system's operability would be verified. Originally, the jet flow was measured during the compressor start-up when it was thought the vibration and noise might cause measurement problems. No problems with the laser system were observed during the complete compressor test. After the initial testing, the calibration jet was only used during compressor down times to check out the laser system.

APPENDIX C

SUMMARY OF TRANSONIC COMPRESSOR DATA

This section contains all of the final laser measurement data from the transonic compressor. All of the locations measured are summarized in Table 19. This table contains the axial and radial locations, number of stations measured between the blades, and the angles of the two LTA spots used to search from the laser data. The first angle in each row of angles for a given location in Table 19 is the first angle measured in one data set. More than one row indicates that more than one series of angles was measured. The angle in a series of angles that has the highest contrast was automatically selected as the set of data for the corresponding station. In a few cases, data were obtained at two different angles from two or more sets of angles. These sets of data are reviewed manually, and the set with the maximum contrast is selected for the corresponding station.

The sets of laser data are tabulated in Table 20 separately for the two blade passages at each measurement location. As indicated in Table 19, some of the measurement locations were repeated. These repeat measurements are treated as a separate set of measurements. When the values for velocity and angles are zero in Table 20, no acceptable data were obtained for the corresponding station. This resulted when the number of events used in the velocity calculation was less than ten, independent of the total number of events recorded. The

TABLE 19

SUMMARY OF TRANSONIC COMPRESSOR
MEASUREMENT LOCATIONS

AXIAL LOCATION (% AXIAL CHORD)	RADIAL LOCATION (% RADIUS)	NUMBER OF STATIONS	SPOT ANGLES MEASURED (degrees)
-10.0	91.7	14	89.1,91.1,86.8,93.3,84.8 89.2,90.3,87.9 85.1,87.1,82.9,89.2,80.8
0.0	84.5	17	88.7,90.7,86.2
0.0	88.9	17	88.7,90.7,86.3 88.7,90.7,86.3
0.0	91.7	14 17	85.0,87.0,82.7,89.0,80.5 88.6,90.7,86.1
0.0	93.2	17	88.0,89.9,85.6
0.0	94.6	17	88.4,90.4,75.5 84.0,92.0,75.5
0.0	96.1	17	85.7,87.7,83.2,89.7
0.0	97.5	17	89.8,91.8,87.3,93.8,85.5, 84.0,85.9,81.7,88.0
12.0	88.9	17	83.9,85.9,81.4,87.9,79.4 90.0,92.1 45.0,48.1,41.5,51.0,38.7
12.0	91.7	17	86.1,88.1,83.7 81.7,89.7 50.0,53.1,46.7 44.0,46.2,41.5
12.0	93.8	17	86.0,88.0,83.7,90.0,81.8 78.0,80.1
12.0	94.6	17	83.9,85.9,81.7,87.9,79.7 45.0,47.9,41.8,51.1,38.7
12.0	96.1	17	84.1,86.2,81.6,88.1,79.7 45.1,48.3,41.9,51.1,38.8 54.3 84.1,86.1,81.9,88.1,79.8

TABLE 19 CONTINUED

SUMMARY OF TRANSONIC COMPRESSOR
MEASUREMENT LOCATIONS

AXIAL LOCATION (% AXIAL CHORD)	RADIAL LOCATION (% RADIUS)	NUMBER OF STATIONS	SPOT ANGLES MEASURED (degrees)
12.0	96.8	17	79.6,82.7,76.3 45.1,50.3,39.9,55.1,34.9, 60.2,29.9,65.3,24.9 70.2,19.7
12.0	97.5	17	82.0,83.9,79.8,86.2,77.7, 88.1 10.0,11.9,7.7 6.2,9.5,3.3,12.4,0.0
12.0	98.8	17	10.1,15.1,4.7,20.2,0.0 175.3 180.3 174.7,178.0,171.4,180.7, 169.0,55.0,60.1,49.8,65.1 44.7,70.1,39.7,75.1,34.7, 80.2,29.7,85.2,24.7,90.2 60.2,62.3,57.9,64.3,55.7
22.0	91.7	17	84.1,86.1,81.8,88.1,79.8 45.0,48.1,41.7,51.1,38.7, 54.1
22.0	94.6	17	82.0,84.1,79.7,86.1,77.5 45.0,48.1,41.7,51.1,38.7, 54.0
22.0	96.1	17	82.0,84.0,79.7,86.1,77.7 48.0,51.1,44.9,41.8,57.3 47.9,50.9,44.7,54.0,41.7, 57.0
22.0	96.8	17	75.6,79.7,71.4,83.7,67.3 20.1,25.3,14.9,30.3,9.8, 35.1,4.7 50.1,55.1,44.7,60.2,39.8 65.2,34.7
22.0	97.5	17	82.0,83.9,79.8,86.0,77.7 81.7,83.8,79.5 81.5,83.7,79.2,85.5,77.3

TABLE 19 CONTINUED

SUMMARY OF TRANSONIC COMPRESSOR
MEASUREMENT LOCATIONS

AXIAL LOCATION (% AXIAL CHORD)	RADIAL LOCATION (% RADIUS)	NUMBER OF STATIONS	SPOT ANGLES MEASURED (degrees)
25.0	88.9	17	84.1,86.0,81.8,88.2,79.8 73.6,75.7,71.4,77.6,69.3
25.0	91.7	29	80.7,82.8,78.3
		14	80.1,82.3,77.7
		14	48.0,52.2,43.6,56.1,39.7 60.3,35.7
		28	48.1,50.3,45.6
		28	82.1,84.3
		17	81.0,83.0,78.7,85.1,76.7
25.0	93.2	17	80.1,84.1,75.6,88.2,71.8
25.0	95.4	17	63.9,67.9,59.6,71.9,55.5 76.0,51.5,79.9,47.5 27.6,31.7,23.3,35.9,19.3 39.7,15.3,43.9
30.0	91.7		34.7,39.8,29.3,44.7,24.4, 49.7,19.4,54.8,14.3 15.1,17.2,12.7

values used to normalize the absolute and relative velocities are not the same. These selected values are not reported. Whether the data were acceptable or not, the total number of events observed during the data taking and the number actually used in the velocity calculation are reported in the tables for reference. Contrast is also reported in Table 20.

TABLE 20

TRANSONIC COMPRESSOR LTA DATA SUMMARY

BLADE PASSAGE NO. 6

% CHORD = -10.0
% RADIUS = 91.7
INLET TOTAL TEMPERATURE = 482.29

	ABSOLUTE		RELATIVE	EVENTS		
% Passage	% Vel	Angle	% Vel	Total	Used	Contrast
4.9	.0	.0	.0	11.	2.	.0
11.6	86.5	.4	126.3	43.	20.	12.3
18.2	93.4	.4	128.2	85.	43.	16.5
24.9	95.9	2.8	131.0	65.	40.	18.1
31.6	99.5	2.8	132.1	85.	62.	27.7
38.3	99.3	2.8	132.0	99.	77.	40.7
45.0	100.6	2.8	132.5	94.	63.	32.5
51.7	99.8	2.8	132.2	101.	64.	27.9
58.4	98.8	4.8	133.8	107.	87.	39.1
65.1	98.6	4.8	133.7	114.	87.	36.2
71.8	100.0	7.1	136.2	76.	50.	26.1
78.4	100.5	4.8	134.3	140.	102.	33.6
85.1	93.4	4.8	132.1	116.	90.	26.1
91.8	.0	.0	.0	20.	4.	.0

TABLE 20 (Continued)

TRANSONIC COMPRESSOR LTA DATA SUMMARY

BLADE PASSAGE NO. 8

% CHORD = -10.0
% RADIUS = 91.7
INLET TOTAL TEMPERATURE = 482.29

	ABSOLUTE		RELATIVE	EVENTS		
% Passage	% Vel	Angle	% Vel	Total	Used	Contrast
4.9	.0	.0	.0	26.	2.	.0
11.6	83.5	-1.7	123.8	106.	42.	12.7
18.2	91.6	.4	127.7	87.	51.	15.1
24.9	97.8	.4	129.4	74.	42.	20.6
31.6	100.5	2.8	132.4	72.	37.	21.6
38.3	100.3	2.8	132.4	100.	61.	20.5
45.0	100.0	4.8	134.1	62.	46.	33.8
51.7	99.2	2.8	132.0	94.	66.	25.0
58.4	99.9	2.8	132.2	91.	70.	34.7
65.1	99.7	4.8	134.1	145.	104.	33.1
71.8	98.4	4.8	133.7	141.	99.	29.5
78.4	98.8	4.8	133.8	155.	104.	32.9
85.1	96.4	4.8	133.0	75.	47.	16.0
91.8	.0	.0	.0	15.	2.	.0

TABLE 20 (Continued)

TRANSONIC COMPRESSOR LTA DATA SUMMARY

BLADE PASSAGE NO. 6

% CHORD = -10.0
% RADIUS = 91.7
INLET TOTAL TEMPERATURE = 481.30

	ABSOLUTE		RELATIVE	EVENTS		
% Passage	% Vel	Angle	% Vel	Total	Used	Contrast
4.9	.0	.0	.0	969.	13.	.0
11.6	103.2	1.5	132.1	475.	13.	2.7
18.2	108.7	1.5	133.8	526.	73.	5.8
24.9	113.6	1.5	135.4	534.	127.	12.7
31.6	117.3	1.5	136.6	486.	100.	9.8
38.3	115.7	1.5	136.1	454.	84.	7.8
45.0	115.1	1.5	135.9	541.	75.	8.1
51.7	118.0	4.0	139.4	711.	683.	5.9
58.4	114.4	4.0	138.2	668.	42.	5.8
65.1	114.0	4.0	138.1	713.	67.	6.9
71.8	115.4	4.0	138.5	715.	47.	5.6
78.4	113.3	4.0	137.8	787.	49.	6.9
85.1	105.1	2.9	134.0	31.	13.	6.3
91.8	.0	.0	.0	27.	2.	.0

TABLE 20 (Continued)

TRANSONIC COMPRESSOR LTA DATA SUMMARY

BLADE PASSAGE NO. 8

% CHORD = -10.0
% RADIUS = 91.7
INLET TOTAL TEMPERATURE = 481.30

	ABSOLUTE		RELATIVE	EVENTS		
% Passage	% Vel	Angle	% Vel	Total	Used	Contrast
4.9	.0	.0	.0	19.	2.	.0
11.6	.0	.0	.0	19.	3.	.0
18.2	105.4	1.5	132.8	553.	83.	7.1
24.9	114.0	1.5	135.5	537.	105.	12.1
31.6	114.9	1.5	135.8	571.	126.	10.9
38.3	116.4	1.5	136.3	504.	70.	9.2
45.0	115.4	1.5	136.0	607.	74.	6.2
51.7	115.5	1.5	136.0	677.	60.	5.6
58.4	116.4	1.5	136.3	621.	36.	4.8
65.1	114.0	1.5	135.5	639.	31.	5.4
71.8	.0	.0	.0	24.	3.	.0
78.4	111.8	1.5	134.8	736.	45.	3.8
85.1	.0	.0	.0	27.	6.	.0
91.8	.0	.0	.0	20.	2.	.0

TABLE 20 (Continued)

TRANSONIC COMPRESSOR LTA DATA SUMMARY

BLADE PASSAGE NO. 6

% CHORD = -10.0
% RADIUS = 91.7
INLET TOTAL TEMPERATURE = 482.20

	ABSOLUTE		RELATIVE	EVENTS		
% Passage	% Vel	Angle	% Vel	Total	Used	Contrast
4.9	84.2	-5.8	120.4	71.	23.	4.6
11.6	98.8	-1.4	128.0	95.	76.	27.9
18.2	107.3	.7	132.5	137.	114.	41.9
24.9	114.0	2.9	136.8	99.	83.	44.3
31.6	117.0	2.9	137.8	124.	107.	58.0
38.3	116.0	2.9	137.5	134.	119.	73.4
45.0	116.7	2.9	137.7	139.	124.	63.9
51.7	116.3	2.9	137.6	137.	113.	53.2
58.4	114.2	2.9	136.9	144.	120.	55.1
65.1	113.0	2.9	136.5	128.	103.	41.2
71.8	114.4	2.9	137.0	92.	75.	42.7
78.4	113.1	2.9	136.5	104.	93.	48.6
85.1	106.3	2.9	134.3	174.	136.	23.2
91.8	.0	.0	.0	15.	1.	.0

TABLE 20 (Continued)

TRANSONIC COMPRESSOR LTA DATA SUMMARY

BLADE PASSAGE NO. 8

% CHORD = -10.0
% RADIUS = 91.7
INLET TOTAL TEMPERATURE = 482.20

	ABSOLUTE		RELATIVE	EVENTS		
% Passage	% Vel	Angle	% Vel	Total	Used	Contrast
4.9	84.0	-5.8	120.4	218.	36.	5.5
11.6	97.6	-1.4	127.6	134.	82.	14.7
18.2	106.5	.7	132.2	119.	95.	35.6
24.9	112.9	.7	134.2	160.	124.	49.6
31.6	115.7	2.9	137.4	110.	82.	35.1
38.3	116.5	2.9	137.7	165.	141.	69.1
45.0	116.3	2.9	137.6	174.	153.	74.2
51.7	116.7	2.9	137.7	126.	107.	65.2
58.4	115.6	2.9	137.4	168.	130.	40.5
65.1	113.9	2.9	136.8	106.	91.	43.0
71.8	114.4	2.9	136.9	85.	59.	21.8
78.4	111.5	2.9	136.0	94.	71.	21.0
85.1	106.4	2.9	134.3	115.	67.	16.3
91.8	.0	.0	.0	21.	3.	.0

TABLE 20 (Continued)

TRANSONIC COMPRESSOR LTA DATA SUMMARY

BLADE PASSAGE NO. 5

% CHORD = .0
% RADIUS = 84.5
INLET TOTAL TEMPERATURE = 511.92

	ABSOLUTE		RELATIVE	EVENTS		
% Passage	% Vel	Angle	% Vel	Total	Used	Contrast
4.4	.0	.0	.0	75.	3.	.0
10.1	116.6	4.4	131.8	54.	53.	104.3
15.9	119.5	4.4	132.9	38.	38.	.2E+06
21.6	119.3	4.4	132.8	41.	39.	107.2
27.4	119.3	2.4	130.7	44.	43.	115.5
33.1	119.3	4.4	132.8	49.	49.	.3E+06
38.9	118.4	4.4	132.4	38.	38.	.2E+06
44.6	119.0	4.4	132.7	57.	55.	118.5
50.4	118.2	4.4	132.4	43.	42.	136.5
56.1	117.8	4.4	132.2	76.	73.	118.2
61.9	119.5	4.4	132.8	68.	66.	129.1
67.6	119.4	4.4	132.8	72.	70.	184.8
73.4	119.0	4.4	132.7	50.	48.	110.9
79.1	118.7	4.4	132.5	58.	56.	115.1
84.9	117.1	4.4	131.9	59.	56.	66.1
90.6	118.1	4.4	132.3	17.	13.	13.1
96.4	.0	.0	.0	1.	1.	.0

TABLE 20 (Continued)

TRANSONIC COMPRESSOR LTA DATA SUMMARY

BLADE PASSAGE NO. 7

% CHORD = .0
% RADIUS = 84.5
INLET TOTAL TEMPERATURE = 511.92

	ABSOLUTE		RELATIVE	EVENTS		
% Passage	% Vel	Angle	% Vel	Total	Used	Contrast
4.4	.0	.0	.0	685.	484.	.0
10.1	117.4	2.4	130.0	58.	57.	162.4
15.9	117.7	2.4	130.1	47.	44.	79.1
21.6	118.4	2.4	130.3	35.	33.	70.5
27.4	117.3	2.4	130.0	47.	46.	162.7
33.1	116.4	2.4	129.6	41.	40.	120.7
38.9	116.6	2.4	129.7	63.	61.	140.5
44.6	115.5	2.4	129.3	41.	39.	92.6
50.4	116.4	4.4	131.7	59.	59.	.3E+06
56.1	115.5	4.4	131.4	59.	59.	.4E+06
61.9	117.1	4.4	132.0	64.	62.	129.1
67.6	118.0	4.4	132.3	70.	68.	144.5
73.4	117.1	4.4	132.0	84.	82.	221.8
79.1	117.2	4.4	132.0	64.	63.	172.2
84.9	116.7	4.4	131.8	38.	34.	26.1
90.6	.0	.0	.0	1.	1.	.0
96.4	.0	.0	.0	0.	1.	.0

TABLE 20 (Continued)

TRANSONIC COMPRESSOR LTA DATA SUMMARY

BLADE PASSAGE NO. 6

% CHORD = .0
% RADIUS = 88.9
INLET TOTAL TEMPERATURE = 510.26

	ABSOLUTE		RELATIVE	EVENTS		
% Passage	% Vel	Angle	% Vel	Total	Used	Contrast
3.7	114.0	4.4	135.4	39.	18.	7.1
9.4	115.5	-.1	131.3	59.	56.	90.2
15.1	115.8	-.1	131.4	69.	66.	102.6
20.9	116.8	-.1	131.7	65.	63.	110.7
26.6	114.9	-.1	131.1	72.	68.	83.7
32.3	113.9	-.1	130.8	43.	41.	63.0
38.0	115.0	2.4	133.7	50.	50.	.2E+06
43.8	115.6	2.4	133.9	55.	53.	73.6
49.5	117.0	4.4	136.5	55.	54.	114.8
55.2	118.4	4.4	137.0	85.	79.	72.6
61.0	118.5	4.4	137.0	71.	69.	121.3
66.7	116.4	4.4	136.3	76.	71.	100.7
72.4	114.6	4.4	135.6	65.	62.	114.9
78.2	115.6	4.4	136.0	68.	65.	102.6
83.9	115.4	4.4	135.9	58.	56.	92.2
89.6	112.2	4.4	134.7	32.	22.	16.6
95.3	.0	.0	.0	0.	1.	.0

TABLE 20 (Continued)

TRANSONIC COMPRESSOR LTA DATA SUMMARY

BLADE PASSAGE NO. 8

% CHORD = .0
% RADIUS = 88.9
INLET TOTAL TEMPERATURE = 510.26

	ABSOLUTE		RELATIVE	EVENTS		
% Passage	% Vel	Angle	% Vel	Total	Used	Contrast
3.7	113.3	4.4	135.1	35.	14.	10.4
9.4	113.6	-.1	130.7	60.	57.	78.3
15.1	115.5	-.1	131.3	53.	53.	.3E+06
20.9	115.3	-.1	131.2	69.	65.	83.7
26.6	114.9	-.1	131.1	61.	51.	43.3
32.3	113.6	-.1	130.7	60.	56.	54.9
38.0	113.7	2.4	133.2	49.	48.	125.2
43.8	116.1	4.4	136.1	29.	28.	78.6
49.5	115.4	2.4	133.8	55.	53.	85.0
55.2	118.2	4.4	136.9	55.	54.	162.4
61.0	119.1	4.4	137.2	73.	68.	98.8
66.7	116.8	4.4	136.4	64.	64.	.2E+06
72.4	114.5	4.4	135.6	71.	68.	102.6
78.2	114.2	4.4	135.4	72.	71.	171.8
83.9	112.7	4.4	134.9	78.	75.	87.0
89.6	110.5	4.4	134.1	16.	13.	15.1
95.3	.0	.0	.0	0.	1.	.0

TABLE 20 (Continued)

TRANSONIC COMPRESSOR LTA DATA SUMMARY

BLADE PASSAGE NO. 5

% CHORD = .0
% RADIUS = 88.9
INLET TOTAL TEMPERATURE = 510.26

	ABSOLUTE		RELATIVE	EVENTS		
% Passage	% Vel	Angle	% Vel	Total	Used	Contrast
3.7	111.8	2.4	132.6	52.	33.	13.4
9.4	116.9	2.4	134.3	45.	44.	104.1
15.1	115.4	-.1	131.3	76.	75.	203.5
20.9	116.9	-.1	131.7	59.	58.	162.1
26.6	115.3	-.1	131.2	65.	64.	183.4
32.3	114.8	2.4	133.6	46.	45.	136.5
38.0	115.3	2.4	133.8	74.	72.	125.2
43.8	115.4	2.4	133.8	82.	81.	246.7
49.5	116.4	2.4	134.2	81.	81.	.4E+06
55.2	118.1	2.4	134.7	51.	51.	.3E+06
61.0	118.5	4.4	137.0	86.	82.	99.1
66.7	115.5	4.4	135.9	66.	65.	156.8
72.4	114.4	4.4	135.5	74.	74.	.4E+06
78.2	115.6	4.4	136.0	64.	59.	61.0
83.9	115.1	4.4	135.8	67.	66.	156.8
89.6	107.9	2.4	131.3	27.	12.	15.0
95.3	.0	.0	.0	0.	1.	.0

TABLE 20 (Continued)

TRANSONIC COMPRESSOR LTA DATA SUMMARY

BLADE PASSAGE NO. 7

% CHORD = .0
% RADIUS = 88.9
INLET TOTAL TEMPERATURE = 510.26

	ABSOLUTE		RELATIVE	EVENTS		
% Passage	% Vel	Angle	% Vel	Total	Used	Contrast
3.7	111.4	2.4	132.5	39.	22.	14.4
9.4	113.6	-.1	130.7	51.	45.	55.6
15.1	115.5	-.1	131.3	73.	71.	117.6
20.9	115.4	-.1	131.3	79.	78.	223.9
26.6	114.4	-.1	130.9	58.	58.	.3E+06
32.3	114.6	2.4	133.5	55.	54.	167.6
38.0	114.0	2.4	133.3	66.	66.	.4E+06
43.8	115.7	2.4	133.9	75.	73.	129.4
49.5	117.1	4.4	136.5	48.	46.	107.4
55.2	118.0	4.4	136.8	59.	58.	151.6
61.0	118.7	4.4	137.1	67.	64.	96.6
66.7	117.4	4.4	136.6	70.	69.	135.4
72.4	113.8	4.4	135.3	67.	59.	68.5
78.2	113.8	4.4	135.3	63.	61.	103.7
83.9	112.5	4.4	134.9	72.	71.	134.5
89.6	111.0	4.4	134.3	11.	10.	26.3
95.3	.0	.0	.0	0.	1.	.0

TABLE 20 (Continued)

TRANSONIC COMPRESSOR LTA DATA SUMMARY

BLADE PASSAGE NO. 5

% CHORD = .0
% RADIUS = 91.7
INLET TOTAL TEMPERATURE = 493.90

	ABSOLUTE		RELATIVE	EVENTS		
% Passage	% Vel	Angle	% Vel	Total	Used	Contrast
5.3	118.8	2.7	137.1	833.	97.	10.2
12.1	113.4	.6	133.1	224.	70.	14.2
18.9	111.2	.6	132.4	120.	66.	25.5
25.7	112.9	.6	133.0	66.	44.	19.4
32.5	109.0	2.7	133.8	39.	22.	13.1
39.3	109.2	2.7	133.8	52.	38.	30.9
46.1	110.0	2.7	134.1	51.	38.	24.8
53.0	109.1	2.7	133.8	41.	25.	16.2
59.8	105.2	2.7	132.5	55.	44.	21.2
66.6	104.1	2.7	132.2	52.	38.	15.9
73.4	101.6	.6	129.4	69.	15.	7.2
80.2	93.0	-1.5	125.1	102.	52.	15.9
87.0	.0	.0	.0	15.	3.	.0
93.8	.0	.0	.0	245.	9.	.0

TABLE 20 (Continued)

TRANSONIC COMPRESSOR LTA DATA SUMMARY

BLADE PASSAGE NO. 7

% CHORD = .0
% RADIUS = 91.7
INLET TOTAL TEMPERATURE = 493.90

	ABSOLUTE		RELATIVE	EVENTS		
% Passage	% Vel	Angle	% Vel	Total	Used	Contrast
5.3	.0	.0	.0	2095.	77.	.0
12.1	114.7	.6	133.6	236.	98.	16.8
18.9	114.1	.6	133.4	186.	91.	21.9
25.7	113.8	.6	133.3	133.	75.	18.3
32.5	110.5	.6	132.2	74.	41.	8.4
39.3	109.4	2.7	133.9	57.	47.	33.0
46.1	108.5	2.7	133.6	52.	44.	22.0
53.0	107.4	2.7	133.2	66.	50.	26.9
59.8	107.3	2.7	133.2	76.	61.	22.2
66.6	98.5	-1.5	126.6	48.	15.	8.4
73.4	92.1	-3.8	122.7	33.	12.	9.4
80.2	92.5	-1.5	124.9	79.	45.	12.8
87.0	.0	.0	.0	33.	3.	.0
93.8	.0	.0	.0	163.	13.	.0

TABLE 20 (Continued)

TRANSONIC COMPRESSOR LTA DATA SUMMARY

BLADE PASSAGE NO. 5

% CHORD = .0
% RADIUS = 91.7
INLET TOTAL TEMPERATURE = 508.82

% Passage	ABSOLUTE % Vel	ABSOLUTE Angle	RELATIVE % Vel	EVENTS Total	EVENTS Used	EVENTS Contrast
3.7	.0	.0	.0	229.	29.	.0
9.5	125.6	2.2	140.3	986.	108.	6.8
15.2	115.2	-.3	134.0	83.	65.	43.0
20.9	117.9	-.3	134.9	62.	60.	99.2
26.7	116.0	-.3	134.3	65.	59.	55.4
32.4	116.4	-.3	134.4	76.	58.	31.5
38.2	115.8	-.3	134.2	69.	43.	21.0
43.9	114.4	4.4	138.6	88.	74.	38.8
49.6	112.6	4.4	138.0	79.	70.	38.3
55.4	113.2	4.4	138.2	108.	96.	49.9
61.1	114.1	4.4	138.5	118.	98.	55.1
66.9	114.1	4.4	138.5	111.	105.	75.7
72.6	109.0	2.2	134.6	112.	111.	117.0
78.3	104.4	2.2	133.1	134.	125.	72.6
84.1	98.6	2.2	131.3	90.	85.	55.3
89.8	94.4	-.3	127.8	122.	117.	89.9
95.6	.0	.0	.0	3.	1.	.0

TABLE 20 (Continued)

TRANSONIC COMPRESSOR LTA DATA SUMMARY

BLADE PASSAGE NO. 7

% CHORD = .0
% RADIUS = 91.7
INLET TOTAL TEMPERATURE = 508.82

	ABSOLUTE		RELATIVE	EVENTS		
% Passage	% Vel	Angle	% Vel	Total	Used	Contrast
3.7	111.0	4.4	137.4	111.	46.	10.6
9.5	117.9	2.2	137.6	107.	96.	65.5
15.2	117.0	2.2	137.3	103.	98.	92.6
20.9	116.2	-.3	134.3	80.	72.	71.9
26.7	119.3	4.4	140.3	31.	29.	44.4
32.4	118.5	4.4	140.1	43.	37.	38.3
38.2	118.1	4.4	139.9	60.	50.	32.9
43.9	118.4	4.4	140.0	70.	65.	60.0
49.6	113.7	4.4	138.4	66.	51.	30.6
55.4	111.9	2.2	135.6	216.	154.	35.3
61.1	113.1	4.4	138.1	101.	94.	78.6
66.9	111.8	4.4	137.7	118.	114.	82.8
72.6	111.0	4.4	137.4	96.	89.	60.6
78.3	103.9	2.2	133.0	139.	127.	58.8
84.1	96.9	-.3	128.5	99.	91.	46.7
89.8	93.2	-.3	127.4	75.	67.	45.8
95.6	.0	.0	.0	3.	1.	.0

TABLE 20 (Continued)

TRANSONIC COMPRESSOR LTA DATA SUMMARY

BLADE PASSAGE NO. 5

% CHORD = .0
% RADIUS = 93.2
INLET TOTAL TEMPERATURE = 509.35

	ABSOLUTE		RELATIVE	EVENTS		
% Passage	% Vel	Angle	% Vel	Total	Used	Contrast
5.0	106.4	1.6	134.8	43.	16.	10.3
10.7	116.2	1.6	138.0	81.	51.	20.6
16.5	116.3	1.6	138.0	112.	91.	38.4
22.2	116.3	1.6	138.0	96.	71.	44.0
28.0	116.4	1.6	138.0	117.	95.	54.7
33.7	115.5	1.6	137.7	139.	113.	61.3
39.5	113.7	1.6	137.1	145.	106.	44.6
45.2	112.8	1.6	136.9	126.	96.	42.6
51.0	112.3	1.6	136.7	153.	94.	39.7
56.7	112.9	1.6	136.9	118.	71.	31.0
62.5	110.8	1.6	136.2	141.	105.	37.1
68.2	108.3	1.6	135.4	204.	136.	27.2
74.0	104.7	1.6	134.3	205.	123.	28.8
79.7	98.7	-.8	130.1	215.	84.	15.9
85.5	96.1	-.8	129.4	321.	181.	28.0
91.2	95.1	-.8	129.2	343.	178.	31.9
97.0	.0	.0	.0	77.	4.	.0

TABLE 20 (Continued)

TRANSONIC COMPRESSOR LTA DATA SUMMARY

BLADE PASSAGE NO. 7

% CHORD = .0
% RADIUS = 93.2
INLET TOTAL TEMPERATURE = 509.35

	ABSOLUTE		RELATIVE	EVENTS		
% Passage	% Vel	Angle	% Vel	Total	Used	Contrast
5.0	95.9	-.8	129.4	47.	17.	7.8
10.7	104.5	-.8	131.8	94.	40.	15.9
16.5	113.6	1.6	137.1	117.	85.	22.7
22.2	116.0	1.6	137.9	120.	90.	42.1
28.0	117.5	1.6	138.4	111.	89.	40.9
33.7	117.7	1.6	138.5	138.	117.	75.2
39.5	115.6	1.6	137.8	126.	96.	42.5
45.2	113.1	1.6	137.0	168.	132.	55.1
51.0	112.3	1.6	136.7	201.	127.	39.8
56.7	111.4	1.6	136.4	172.	115.	40.3
62.5	110.4	1.6	136.1	168.	118.	39.3
68.2	109.1	1.6	135.7	204.	141.	37.0
74.0	104.5	1.6	134.2	252.	142.	24.9
79.7	98.3	-.8	130.1	224.	111.	15.0
85.5	94.7	-.8	129.1	334.	181.	24.1
91.2	93.8	-.8	128.8	342.	179.	28.0
97.0	.0	.0	.0	103.	4.	.0

TABLE 20 (Continued)

TRANSONIC COMPRESSOR LTA DATA SUMMARY

BLADE PASSAGE NO. 5

% CHORD = .0
% RADIUS = 94.6
INLET TOTAL TEMPERATURE = 511.89

	ABSOLUTE		RELATIVE	EVENTS		
% Passage	% Vel	Angle	% Vel	Total	Used	Contrast
4.8	119.9	2.0	141.1	116.	19.	7.6
10.6	118.5	4.1	142.8	60.	43.	16.8
16.3	124.1	4.1	144.8	57.	48.	41.7
22.1	125.3	4.1	145.2	55.	48.	41.4
27.8	118.1	-.3	138.0	131.	34.	7.0
33.6	114.1	-.3	136.7	152.	41.	11.6
39.3	113.2	2.0	138.9	164.	47.	9.4
45.1	114.8	4.1	141.5	38.	25.	13.6
50.8	112.0	4.1	140.6	34.	27.	17.8
56.6	112.7	4.1	140.8	36.	19.	15.8
62.3	101.6	-.3	133.0	250.	66.	10.2
68.1	98.7	-.3	132.2	519.	91.	8.8
73.8	97.4	-.3	131.8	401.	106.	8.7
79.6	95.6	-.3	131.3	213.	70.	10.3
85.3	94.1	-.3	130.9	170.	62.	8.2
91.1	94.3	-.3	131.0	116.	68.	13.8
96.8	.0	.0	.0	49.	2.	.0

TABLE 20 (Continued)

TRANSONIC COMPRESSOR LTA DATA SUMMARY

BLADE PASSAGE NO. 7

% CHORD = .0
% RADIUS = 94.6
INLET TOTAL TEMPERATURE = 511.89

	ABSOLUTE		RELATIVE	EVENTS		
% Passage	% Vel	Angle	% Vel	Total	Used	Contrast
4.8	.0	.0	.0	163.	19.	.0
10.6	117.8	4.1	142.6	66.	42.	14.1
16.3	121.0	4.1	143.7	83.	63.	29.7
22.1	124.0	4.1	144.8	57.	47.	33.1
27.8	124.5	4.1	145.0	66.	55.	42.6
33.6	118.1	4.1	142.7	42.	34.	27.8
39.3	116.8	4.1	142.2	41.	36.	35.2
45.1	115.4	4.1	141.7	40.	28.	12.5
50.8	113.2	2.0	138.9	98.	37.	11.0
56.6	108.2	2.0	137.3	86.	31.	8.6
62.3	102.7	-.3	133.3	278.	57.	6.5
68.1	101.0	2.0	135.1	72.	24.	9.3
73.8	96.0	-.3	131.4	248.	93.	8.6
79.6	94.6	-.3	131.0	183.	70.	12.0
85.3	93.0	-.3	130.6	172.	79.	12.8
91.1	93.6	-.3	130.8	98.	50.	7.7
96.8	.0	.0	.0	35.	2.	.0

TABLE 20 (Continued)

TRANSONIC COMPRESSOR LTA DATA SUMMARY

BLADE PASSAGE NO. 5

% CHORD = .0
% RADIUS = 96.1
INLET TOTAL TEMPERATURE = 509.25

	ABSOLUTE		RELATIVE	EVENTS		
% Passage	% Vel	Angle	% Vel	Total	Used	Contrast
4.1	93.5	-3.3	129.7	142.	25.	5.4
9.8	104.9	-.7	135.2	157.	99.	21.6
15.5	111.7	1.3	139.3	173.	126.	34.3
21.3	114.7	3.4	142.4	208.	163.	41.4
27.0	116.0	3.4	142.9	220.	186.	84.9
32.8	114.8	3.4	142.4	232.	166.	35.5
38.5	114.3	3.4	142.3	191.	130.	42.2
44.3	110.8	1.3	139.0	235.	159.	40.4
50.0	109.2	1.3	138.5	287.	207.	44.0
55.7	104.1	-.7	134.9	270.	149.	27.1
61.5	100.6	-.7	134.0	403.	235.	30.0
67.2	97.9	-.7	133.2	436.	234.	22.5
72.9	96.4	-.7	132.8	531.	283.	28.4
78.7	93.9	-.7	132.2	523.	275.	22.3
84.4	92.4	-.7	131.8	491.	243.	20.6
90.2	93.3	-.7	132.0	553.	270.	24.4
95.9	94.1	-.7	132.2	318.	80.	9.0

TABLE 20 (Continued)

TRANSONIC COMPRESSOR LTA DATA SUMMARY

BLADE PASSAGE NO. 7

% CHORD = .0
% RADIUS = 96.1
INLET TOTAL TEMPERATURE = 509.25

	ABSOLUTE		RELATIVE	EVENTS		
% Passage	% Vel	Angle	% Vel	Total	Used	Contrast
4.1	88.8	-3.3	128.6	221.	41.	5.6
9.8	103.2	-.7	134.7	172.	91.	22.5
15.5	112.0	1.3	139.4	165.	116.	32.7
21.3	114.2	1.3	140.1	208.	141.	39.0
27.0	114.1	1.3	140.1	178.	127.	40.2
32.8	114.3	3.4	142.3	239.	180.	49.3
38.5	114.1	3.4	142.2	263.	190.	45.5
44.3	111.3	1.3	139.2	242.	164.	38.8
50.0	108.4	1.3	138.3	309.	201.	37.0
55.7	104.7	-.7	135.1	323.	167.	22.7
61.5	100.6	-.7	134.0	470.	262.	27.0
67.2	97.8	-.7	133.2	545.	270.	21.2
72.9	95.2	-.7	132.5	552.	302.	26.3
78.7	92.6	-.7	131.8	578.	248.	17.0
84.4	91.3	-.7	131.5	553.	268.	25.9
90.2	91.9	-.7	131.7	666.	332.	27.2
95.9	.0	.0	.0	353.	6.	.0

TABLE 20 (Continued)

TRANSONIC COMPRESSOR LTA DATA SUMMARY

BLADE PASSAGE NO. 5

% CHORD = .0
% RADIUS = 97.5
INLET TOTAL TEMPERATURE = 509.09

	ABSOLUTE		RELATIVE	EVENTS		
% Passage	% Vel	Angle	% Vel	Total	Used	Contrast
4.2	.0	.0	.0	933.	910.	.0
9.9	67.9	-.5	128.1	118.	78.	9.3
15.6	71.1	1.6	130.3	150.	90.	11.0
21.3	74.2	1.6	131.0	85.	23.	7.4
27.0	.0	.0	.0	12.	2.	.0
32.7	.0	.0	.0	9.	2.	.0
38.5	73.1	1.6	130.7	84.	39.	8.0
44.2	68.4	1.6	129.7	98.	66.	10.4
49.9	67.3	-.5	128.0	161.	95.	12.4
55.6	65.4	-2.5	126.3	156.	105.	14.2
61.3	64.0	-2.5	126.0	192.	110.	14.7
67.0	61.1	-.5	126.8	120.	76.	12.8
72.7	61.9	-2.5	125.7	182.	123.	16.7
78.4	64.5	-2.5	126.1	178.	87.	12.3
84.1	61.7	-.5	126.9	167.	117.	13.6
89.8	62.9	-.5	127.1	163.	91.	13.2
95.6	.0	.0	.0	30.	3.	.0

TABLE 20 (Continued)

TRANSONIC COMPRESSOR LTA DATA SUMMARY

BLADE PASSAGE NO. 7

% CHORD = .0
% RADIUS = 97.5
INLET TOTAL TEMPERATURE = 509.09

	ABSOLUTE		RELATIVE	EVENTS		
% Passage	% Vel	Angle	% Vel	Total	Used	Contrast
4.2	63.0	-.5	127.2	547.	470.	35.8
9.9	72.3	-.5	129.0	94.	40.	10.2
15.6	75.1	1.6	131.2	91.	36.	7.2
21.3	66.2	1.6	129.2	109.	71.	6.9
27.0	.0	.0	.0	13.	2.	.0
32.7	76.7	1.6	131.6	60.	22.	5.2
38.5	76.4	1.6	131.5	76.	14.	6.8
44.2	69.8	1.6	130.0	104.	75.	11.9
49.9	71.4	-.5	128.8	131.	51.	6.6
55.6	65.8	-2.5	126.4	165.	107.	16.1
61.3	65.3	-2.5	126.3	177.	87.	12.9
67.0	61.1	-2.5	125.6	172.	128.	12.8
72.7	60.4	-2.5	125.5	156.	115.	14.1
78.4	62.6	-2.5	125.8	159.	93.	14.4
84.1	62.7	-.5	127.1	134.	61.	12.5
89.8	61.8	-.5	126.9	111.	64.	10.8
95.6	.0	.0	.0	37.	2.	.0

TABLE 20 (Continued)

TRANSONIC COMPRESSOR LTA DATA SUMMARY

BLADE PASSAGE NO. 5

% CHORD = .0
% RADIUS = 97.5
INLET TOTAL TEMPERATURE = 509.19

	ABSOLUTE		RELATIVE	EVENTS		
% Passage	% Vel	Angle	% Vel	Total	Used	Contrast
4.7	.0	.0	.0	1047.	1020.	.0
10.4	73.4	-.9	128.9	49.	20.	6.9
16.1	.0	.0	.0	26.	4.	.0
21.8	69.4	3.5	131.2	54.	10.	7.3
27.5	.0	.0	.0	37.	4.	.0
33.3	.0	.0	.0	51.	7.	.0
39.0	.0	.0	.0	41.	7.	.0
44.7	71.1	.9	129.7	49.	18.	7.6
50.4	.0	.0	.0	12.	3.	.0
56.1	.0	.0	.0	7.	1.	.0
61.8	.0	.0	.0	16.	4.	.0
67.6	.0	.0	.0	17.	4.	.0
73.3	61.9	-.9	126.7	71.	17.	5.1
79.0	62.8	-.9	126.8	79.	43.	9.8
84.7	.0	.0	.0	16.	2.	.0
90.4	67.4	-.9	127.7	66.	18.	6.2
96.2	.0	.0	.0	9.	3.	.0

TABLE 20 (Continued)

TRANSONIC COMPRESSOR LTA DATA SUMMARY

BLADE PASSAGE NO. 7

% CHORD = .0
% RADIUS = 97.5
INLET TOTAL TEMPERATURE = 509.19

	ABSOLUTE		RELATIVE	EVENTS		
% Passage	% Vel	Angle	% Vel	Total	Used	Contrast
4.7	.0	.0	.0	1263.	768.	.0
10.4	73.0	.9	130.1	39.	14.	8.6
16.1	74.0	.9	130.4	67.	14.	8.1
21.8	75.9	3.5	132.7	48.	11.	5.3
27.5	69.1	3.5	131.1	41.	10.	5.8
33.3	.0	.0	.0	49.	8.	.0
39.0	.0	.0	.0	57.	5.	.0
44.7	.0	.0	.0	30.	3.	.0
50.4	71.4	.9	129.8	48.	15.	6.5
56.1	67.8	-.9	127.8	74.	22.	7.4
61.8	64.8	-.9	127.2	63.	11.	5.9
67.6	.0	.0	.0	14.	1.	.0
73.3	.0	.0	.0	12.	1.	.0
79.0	65.6	-.9	127.3	68.	24.	5.6
84.7	58.8	-.9	126.1	74.	31.	6.5
90.4	67.8	-.9	127.8	59.	13.	5.5
96.2	.0	.0	.0	31.	4.	.0

TABLE 20 (Continued)

TRANSONIC COMPRESSOR LTA DATA SUMMARY

BLADE PASSAGE NO. 5

% CHORD = 12.0
% RADIUS = 88.9
INLET TOTAL TEMPERATURE = 499.53

	ABSOLUTE		RELATIVE	EVENTS		
% Passage	% Vel	Angle	% Vel	Total	Used	Contrast
3.9	107.6	1.5	130.4	11683.	3963.	106.3
9.6	107.4	1.5	130.4	1568.	983.	97.3
15.2	106.5	1.5	130.0	1589.	1114.	140.8
20.9	108.8	3.7	132.9	4368.	2206.	153.6
26.6	108.9	3.7	133.0	5230.	2855.	186.1
32.3	107.7	3.7	132.5	5562.	2792.	162.2
38.0	106.9	3.7	132.3	5964.	2216.	103.8
43.7	92.7	-5.2	119.8	1184.	685.	60.9
49.4	94.8	-2.6	122.7	512.	409.	97.6
55.1	91.5	-5.2	119.5	1321.	909.	92.7
60.8	92.2	-5.2	119.7	757.	111.	13.9
66.4	102.5	-36.5	89.0	163.	50.	8.0
72.1	106.2	-39.5	85.6	1031.	608.	82.2
77.8	107.5	-36.5	89.0	646.	404.	76.1
83.5	99.7	-46.3	78.8	271.	124.	30.8
89.2	.0	.0	.0	0.	1.	.0
94.9	.0	.0	.0	6093.	6078.	.0

TABLE 20 (Continued)

TRANSONIC COMPRESSOR LTA DATA SUMMARY

BLADE PASSAGE NO. 7

% CHORD = 12.0
% RADIUS = 88.9
INLET TOTAL TEMPERATURE = 499.53

	ABSOLUTE		RELATIVE	EVENTS		
% Passage	% Vel	Angle	% Vel	Total	Used	Contrast
3.9	107.9	1.5	130.5	5530.	1872.	87.5
9.6	107.9	1.5	130.5	1230.	964.	159.7
15.2	105.3	1.5	129.7	1031.	808.	157.3
20.9	107.3	1.5	130.3	1186.	924.	163.3
26.6	106.9	1.5	130.2	1243.	884.	113.1
32.3	105.6	1.5	129.7	1430.	1016.	141.5
38.0	105.6	1.5	129.8	1624.	1190.	150.1
43.7	92.7	-5.2	119.8	773.	488.	64.7
49.4	92.8	-5.2	119.8	1151.	882.	108.9
55.1	90.2	-7.2	117.4	3492.	1634.	87.7
60.8	.0	.0	.0	2478.	43.	.0
66.4	102.4	-39.5	85.8	280.	114.	22.3
72.1	105.6	-39.5	85.6	1061.	593.	74.2
77.8	107.1	-39.5	85.6	536.	318.	65.4
83.5	108.3	-36.5	89.0	369.	270.	92.0
89.2	.0	.0	.0	3.	2.	.0
94.9	.0	.0	.0	3567.	3563.	.0

TABLE 20 (Continued)

TRANSONIC COMPRESSOR LTA DATA SUMMARY

BLADE PASSAGE NO. 5

% CHORD = 12.0
% RADIUS = 91.7
INLET TOTAL TEMPERATURE = 499.21

	ABSOLUTE		RELATIVE	EVENTS		
% Passage	% Vel	Angle	% Vel	Total	Used	Contrast
4.8	108.0	1.7	133.9	9570.	3269.	100.0
10.5	108.7	1.7	134.1	1240.	878.	149.3
16.2	108.1	1.7	133.9	1019.	787.	159.6
21.9	107.2	1.7	133.6	1116.	805.	137.5
27.6	107.2	1.7	133.6	1262.	868.	137.0
33.3	105.1	-.3	130.9	828.	467.	60.9
39.0	92.9	-4.9	123.3	128.	94.	35.4
44.7	94.8	-4.9	123.8	218.	187.	74.0
50.4	96.5	-2.8	126.1	774.	556.	112.3
56.1	97.8	-2.8	126.5	664.	473.	90.3
61.8	99.2	-.3	129.2	833.	443.	54.0
67.5	103.5	-43.7	84.0	86.	84.	113.2
73.2	107.3	-40.9	86.8	122.	107.	82.3
78.9	109.1	-37.5	90.7	42.	42.	.2E+06
84.6	109.4	-43.7	83.5	152.	143.	163.5
90.3	.0	.0	.0	13.	1.	.0
96.0	.0	.0	.0	30095.	30081.	.0

TABLE 20 (Continued)

TRANSONIC COMPRESSOR LTA DATA SUMMARY

BLADE PASSAGE NO. 7

% CHORD = 12.0
% RADIUS = 91.7
INLET TOTAL TEMPERATURE = 499.21

	ABSOLUTE		RELATIVE	EVENTS		
% Passage	% Vel	Angle	% Vel	Total	Used	Contrast
4.8	108.4	1.7	134.0	3334.	2014.	133.6
10.5	109.7	1.7	134.4	1170.	956.	192.8
16.2	108.1	1.7	133.9	914.	818.	260.4
21.9	106.8	1.7	133.5	960.	813.	202.2
27.6	105.8	-.3	131.2	816.	680.	180.2
33.3	104.6	-.3	130.8	789.	660.	180.7
39.0	93.4	-4.9	123.4	50.	29.	11.7
44.7	94.5	-4.9	123.7	214.	200.	145.3
50.4	95.5	-4.9	124.0	200.	181.	101.2
56.1	97.7	-2.8	126.5	662.	550.	136.1
61.8	98.5	-40.9	87.5	76.	59.	36.6
67.5	102.7	-43.7	84.1	97.	91.	97.6
73.2	106.1	-43.7	83.8	97.	93.	123.1
78.9	108.3	-40.9	86.8	130.	124.	149.7
84.6	108.6	-34.3	94.4	38.	36.	70.7
90.3	106.0	-34.3	94.4	25.	21.	23.7
96.0	.0	.0	.0	14821.	14815.	.0

TABLE 20 (Continued)

TRANSONIC COMPRESSOR LTA DATA SUMMARY

BLADE PASSAGE NO. 5

% CHORD = 12.0
% RADIUS = 93.2
INLET TOTAL TEMPERATURE = 498.00

	ABSOLUTE		RELATIVE	EVENTS		
% Passage	% Vel	Angle	% Vel	Total	Used	Contrast
3.2	109.9	1.6	135.9	87.	68.	66.7
8.7	110.0	1.6	135.9	81.	48.	24.1
14.1	108.8	1.6	135.5	76.	53.	40.5
19.5	107.1	-.4	132.9	75.	51.	33.8
25.0	107.0	-.4	132.9	92.	62.	40.9
30.4	102.2	-2.8	129.2	83.	38.	14.3
35.8	.0	.0	.0	85.	4.	.0
41.3	.0	.0	.0	63.	3.	.0
46.7	96.0	-2.8	127.6	110.	49.	17.8
52.1	96.8	-2.8	127.7	192.	146.	63.0
57.5	97.5	-2.8	127.9	137.	87.	31.8
63.0	97.1	-.4	130.0	105.	47.	11.9
68.4	.0	.0	.0	24.	3.	.0
73.8	.0	.0	.0	45.	3.	.0
79.3	.0	.0	.0	20.	2.	.0
84.7	.0	.0	.0	14.	2.	.0
90.1	.0	.0	.0	2.	1.	.0

TABLE 20 (Continued)

TRANSONIC COMPRESSOR LTA DATA SUMMARY

BLADE PASSAGE NO. 7

% CHORD = 12.0
% RADIUS = 93.2
INLET TOTAL TEMPERATURE = 498.00

	ABSOLUTE		RELATIVE	EVENTS		
% Passage	% Vel	Angle	% Vel	Total	Used	Contrast
3.2	105.3	-4.8	128.0	56.	53.	121.5
8.7	109.4	1.6	135.7	83.	47.	26.6
14.1	108.4	1.6	135.4	99.	74.	51.3
19.5	108.2	-.4	133.3	59.	38.	32.2
25.0	106.5	-.4	132.8	98.	57.	21.8
30.4	103.1	-2.8	129.4	82.	52.	24.3
35.8	.0	.0	.0	60.	4.	.0
41.3	.0	.0	.0	71.	4.	.0
46.7	95.6	-2.8	127.4	54.	11.	6.5
52.1	97.1	-2.8	127.8	139.	97.	37.9
57.5	97.3	-2.8	127.9	189.	137.	40.0
63.0	96.6	-2.8	127.7	92.	38.	12.4
68.4	.0	.0	.0	51.	4.	.0
73.8	.0	.0	.0	29.	2.	.0
79.3	.0	.0	.0	20.	3.	.0
84.7	.0	.0	.0	19.	5.	.0
90.1	.0	.0	.0	6.	1.	.0

TABLE 20 (Continued)

TRANSONIC COMPRESSOR LTA DATA SUMMARY

BLADE PASSAGE NO. 5

% CHORD = 12.0
% RADIUS = 94.6
INLET TOTAL TEMPERATURE = 493.65

	ABSOLUTE		RELATIVE	EVENTS		
% Passage	% Vel	Angle	% Vel	Total	Used	Contrast
3.7	109.8	1.5	137.4	156.	120.	49.0
9.1	109.6	1.5	137.3	101.	85.	62.0
14.6	110.4	1.5	137.6	66.	52.	47.8
20.0	110.0	-.5	135.4	127.	86.	42.2
25.4	106.0	-2.6	132.1	82.	59.	18.8
30.8	94.0	-6.9	124.9	104.	69.	17.2
36.2	94.4	-6.9	125.0	154.	117.	49.2
41.7	95.1	-4.9	127.1	108.	88.	39.3
47.1	96.9	-2.6	129.7	97.	69.	31.1
52.5	96.7	-2.6	129.6	131.	116.	66.5
57.9	95.3	-2.6	129.3	94.	76.	36.4
63.3	94.8	-.5	131.0	135.	100.	38.9
68.8	104.5	-46.0	84.5	142.	88.	32.6
74.2	106.7	-46.0	84.2	76.	52.	25.0
79.6	107.0	-39.7	91.3	23.	17.	23.6
85.0	105.5	-36.4	95.1	82.	68.	49.2
90.4	108.2	-36.4	95.0	66.	62.	57.0

TABLE 20 (Continued)

TRANSONIC COMPRESSOR LTA DATA SUMMARY

BLADE PASSAGE NO. 7

% CHORD = 12.0
% RADIUS = 94.6
INLET TOTAL TEMPERATURE = 493.65

	ABSOLUTE		RELATIVE	EVENTS		
% Passage	% Vel	Angle	% Vel	Total	Used	Contrast
3.7	109.9	1.5	137.4	123.	94.	42.6
9.1	110.1	1.5	137.5	103.	86.	68.0
14.6	110.2	1.5	137.5	49.	32.	26.8
20.0	109.0	-2.6	133.0	109.	83.	44.6
25.4	107.3	-2.6	132.5	110.	79.	29.9
30.8	95.4	-6.9	125.2	107.	77.	30.3
36.2	94.5	-6.9	125.0	158.	118.	34.4
41.7	95.2	-6.9	125.2	137.	105.	39.7
47.1	95.6	-4.9	127.2	110.	91.	40.1
52.5	95.8	-2.6	129.4	124.	112.	41.9
57.9	95.3	-2.6	129.3	122.	109.	66.9
63.3	96.6	-46.0	85.8	54.	14.	8.4
68.8	103.6	-46.0	84.7	119.	64.	16.5
74.2	105.2	-46.0	84.4	104.	82.	42.0
79.6	107.1	-42.7	87.9	43.	32.	20.5
85.0	105.0	-36.4	95.1	56.	42.	30.4
90.4	103.9	-36.4	95.1	78.	63.	43.1

TABLE 20 (Continued)

TRANSONIC COMPRESSOR LTA DATA SUMMARY

BLADE PASSAGE NO. 5

% CHORD = 12.0
% RADIUS = 96.1
INLET TOTAL TEMPERATURE = 494.15

	ABSOLUTE		RELATIVE	EVENTS		
% Passage	% Vel	Angle	% Vel	Total	Used	Contrast
3.4	110.8	1.7	139.5	110.	81.	32.7
8.8	112.3	1.7	140.0	36.	26.	23.2
14.2	112.9	-2.4	135.9	26.	23.	30.3
19.6	105.5	-4.7	131.4	23.	11.	13.7
25.0	101.0	-6.8	128.1	45.	33.	21.2
30.4	95.6	-6.8	126.9	52.	47.	34.8
35.8	93.7	-6.8	126.6	34.	30.	26.0
41.2	93.0	-4.7	128.4	26.	23.	33.3
46.6	93.5	-4.7	128.5	34.	17.	14.1
52.0	91.8	-2.4	130.2	63.	47.	22.9
57.4	91.4	-.3	132.0	58.	43.	23.5
62.8	91.1	-.3	131.9	37.	25.	11.0
68.2	103.4	-45.9	86.4	371.	76.	9.6
73.6	104.0	-45.9	86.2	279.	112.	17.3
79.0	104.7	-42.6	89.8	153.	78.	16.6
84.4	103.0	-39.3	93.5	95.	77.	35.4
89.8	109.6	-39.3	93.1	58.	48.	42.9

TABLE 20 (Continued)

TRANSONIC COMPRESSOR LTA DATA SUMMARY

BLADE PASSAGE NO. 7

% CHORD = 12.0
% RADIUS = 96.1
INLET TOTAL TEMPERATURE = 494.15

	ABSOLUTE		RELATIVE	EVENTS		
% Passage	% Vel	Angle	% Vel	Total	Used	Contrast
3.4	111.3	1.7	139.7	256.	58.	13.3
8.8	112.5	-.3	137.9	39.	33.	25.6
14.2	114.1	-2.4	136.2	23.	17.	23.7
19.6	110.2	-4.7	132.7	16.	14.	22.2
25.0	106.5	-6.8	129.4	29.	16.	10.2
30.4	97.4	-6.8	127.4	29.	22.	19.8
35.8	95.2	-6.8	126.9	35.	21.	24.0
41.2	94.0	-6.8	126.6	42.	38.	36.4
46.6	93.0	-4.7	128.4	35.	26.	27.9
52.0	92.1	-2.4	130.3	51.	34.	15.6
57.4	90.6	-2.4	129.9	72.	62.	34.3
62.8	91.7	-.3	132.0	32.	17.	13.6
68.2	100.2	-49.0	83.6	225.	84.	13.9
73.6	102.5	-45.9	86.5	326.	111.	15.6
79.0	103.0	-42.6	90.0	142.	74.	18.7
84.4	103.0	-39.3	93.5	92.	75.	54.8
89.8	106.7	-39.3	93.3	82.	71.	37.6

TABLE 20 (Continued)

TRANSONIC COMPRESSOR LTA DATA SUMMARY

BLADE PASSAGE NO. 5

% CHORD = 12.0
% RADIUS = 96.1
INLET TOTAL TEMPERATURE = 493.89

	ABSOLUTE		RELATIVE	EVENTS		
% Passage	% Vel	Angle	% Vel	Total	Used	Contrast
3.4	107.2	-.2	136.3	464.	69.	10.7
8.8	112.2	-.2	137.8	55.	27.	13.1
14.2	113.3	-2.4	135.9	41.	30.	25.2
19.6	108.3	-5.0	131.8	88.	36.	10.3
25.0	102.2	-5.0	130.2	119.	17.	4.8
30.4	95.2	-6.9	126.7	166.	29.	5.0
35.8	94.3	-6.9	126.5	114.	30.	5.8
41.2	92.9	-5.0	128.0	149.	66.	10.6
46.6	91.7	-2.4	130.1	94.	36.	8.4
52.0	91.6	-2.4	130.1	87.	39.	13.9
57.4	91.1	-.2	131.9	95.	62.	17.5
62.8	90.7	-.2	131.8	77.	48.	13.9
68.2	.0	.0	.0	29.	2.	.0
73.6	.0	.0	.0	3.	1.	.0
79.0	.0	.0	.0	6.	1.	.0
84.4	.0	.0	.0	7.	1.	.0
89.8	.0	.0	.0	8.	1.	.0

TABLE 20 (Continued)

TRANSONIC COMPRESSOR LTA DATA SUMMARY

BLADE PASSAGE NO. 7

% CHORD = 12.0
% RADIUS = 96.1
INLET TOTAL TEMPERATURE = 493.89

	ABSOLUTE		RELATIVE	EVENTS		
% Passage	% Vel	Angle	% Vel	Total	Used	Contrast
3.4	.0	.0	.0	7065.	2009.	.0
8.8	111.1	-.2	137.5	74.	37.	14.1
14.2	.0	.0	.0	56.	7.	.0
19.6	107.7	-5.0	131.6	146.	43.	7.3
25.0	105.7	-5.0	131.1	150.	37.	9.0
30.4	95.4	-6.9	126.7	235.	17.	2.9
35.8	94.8	-5.0	128.5	93.	13.	6.0
41.2	94.5	-5.0	128.4	135.	51.	12.3
46.6	94.3	-5.0	128.3	128.	28.	5.9
52.0	91.0	-2.4	129.9	111.	71.	16.0
57.4	91.2	-2.4	130.0	89.	55.	16.4
62.8	91.6	-.2	132.0	60.	19.	7.4
68.2	.0	.0	.0	37.	4.	.0
73.6	.0	.0	.0	9.	1.	.0
79.0	.0	.0	.0	9.	1.	.0
84.4	.0	.0	.0	11.	1.	.0
89.8	.0	.0	.0	9.	1.	.0

TABLE 20 (Continued)

TRANSONIC COMPRESSOR LTA DATA SUMMARY

BLADE PASSAGE NO. 5

% CHORD = 12.0
% RADIUS = 97.5
INLET TOTAL TEMPERATURE = 495.30

	ABSOLUTE		RELATIVE	EVENTS		
% Passage	% Vel	Angle	% Vel	Total	Used	Contrast
3.7	.0	.0	.0	446.	11.	.0
9.1	.0	.0	.0	67.	3.	.0
14.5	.0	.0	.0	28.	2.	.0
19.9	.0	.0	.0	97.	4.	.0
25.3	123.1	1.7	145.1	199.	23.	6.4
30.7	107.8	1.7	140.2	397.	14.	3.5
36.1	.0	.0	.0	101.	3.	.0
41.6	.0	.0	.0	51.	2.	.0
47.0	.0	.0	.0	72.	3.	.0
52.4	.0	.0	.0	48.	2.	.0
57.8	.0	.0	.0	82.	3.	.0
63.2	.0	.0	.0	62.	2.	.0
68.6	.0	.0	.0	80.	3.	.0
74.0	.0	.0	.0	103.	2.	.0
79.4	.0	.0	.0	30.	3.	.0
84.8	.0	.0	.0	24.	2.	.0
90.3	.0	.0	.0	45.	2.	.0

TABLE 20 (Continued)

TRANSONIC COMPRESSOR LTA DATA SUMMARY

BLADE PASSAGE NO. 7

% CHORD = 12.0
% RADIUS = 97.5
INLET TOTAL TEMPERATURE = 495.30

% Passage	ABSOLUTE % Vel	ABSOLUTE Angle	RELATIVE % Vel	EVENTS Total	EVENTS Used	EVENTS Contrast
3.7	.0	.0	.0	1541.	1305.	.0
9.1	.0	.0	.0	75.	2.	.0
14.5	.0	.0	.0	51.	2.	.0
19.9	.0	.0	.0	62.	2.	.0
25.3	130.3	1.7	147.6	31.	17.	18.4
30.7	111.4	1.7	141.3	386.	18.	6.1
36.1	.0	.0	.0	36.	4.	.0
41.6	.0	.0	.0	70.	3.	.0
47.0	.0	.0	.0	60.	2.	.0
52.4	.0	.0	.0	109.	3.	.0
57.8	.0	.0	.0	70.	3.	.0
63.2	.0	.0	.0	132.	2.	.0
68.6	.0	.0	.0	66.	3.	.0
74.0	.0	.0	.0	63.	3.	.0
79.4	.0	.0	.0	55.	1.	.0
84.8	.0	.0	.0	56.	2.	.0
90.3	.0	.0	.0	81.	3.	.0

TABLE 20 (Continued)

TRANSONIC COMPRESSOR LTA DATA SUMMARY

BLADE PASSAGE NO. 5

% CHORD = 12.0
% RADIUS = 97.5
INLET TOTAL TEMPERATURE = 496.36

	ABSOLUTE		RELATIVE	EVENTS		
% Passage	% Vel	Angle	% Vel	Total	Used	Contrast
3.7	.0	.0	.0	263.	11.	.0
9.1	.0	.0	.0	15.	2.	.0
14.5	.0	.0	.0	0.	1.	.0
19.9	.0	.0	.0	5.	1.	.0
25.3	152.6	-76.8	37.1	126.	13.	6.5
30.7	159.0	-81.1	29.2	4629.	386.	29.1
36.1	.0	.0	.0	7.	2.	.0
41.6	.0	.0	.0	16.	1.	.0
47.0	.0	.0	.0	15.	1.	.0
52.4	.0	.0	.0	10.	2.	.0
57.8	.0	.0	.0	38.	2.	.0
63.2	.0	.0	.0	41.	2.	.0
68.6	.0	.0	.0	64.	3.	.0
74.0	.0	.0	.0	50.	3.	.0
79.4	163.3	-81.1	27.2	202.	169.	154.0
84.8	156.0	-81.1	30.6	4165.	204.	19.5
90.3	.0	.0	.0	7.	1.	.0

TABLE 20 (Continued)

TRANSONIC COMPRESSOR LTA DATA SUMMARY

BLADE PASSAGE NO. 7

% CHORD = 12.0
% RADIUS = 97.5
INLET TOTAL TEMPERATURE = 496.36

	ABSOLUTE		RELATIVE	EVENTS		
% Passage	% Vel	Angle	% Vel	Total	Used	Contrast
3.7	.0	.0	.0	1344.	980.	.0
9.1	.0	.0	.0	3.	1.	.0
14.5	.0	.0	.0	3.	1.	.0
19.9	.0	.0	.0	2.	1.	.0
25.3	162.8	-81.1	27.5	76.	26.	15.1
30.7	159.4	-81.1	29.0	2650.	388.	37.2
36.1	.0	.0	.0	16.	1.	.0
41.6	.0	.0	.0	44.	2.	.0
47.0	.0	.0	.0	25.	2.	.0
52.4	.0	.0	.0	3.	1.	.0
57.8	.0	.0	.0	3.	1.	.0
63.2	.0	.0	.0	13.	2.	.0
68.6	.0	.0	.0	7.	1.	.0
74.0	.0	.0	.0	13.	1.	.0
79.4	.0	.0	.0	7.	1.	.0
84.8	158.2	-81.1	29.6	541.	199.	54.2
90.3	.0	.0	.0	0.	1.	.0

TABLE 20 (Continued)

TRANSONIC COMPRESSOR LTA DATA SUMMARY

BLADE PASSAGE NO. 5

% CHORD = 12.0
% RADIUS = 97.5
INLET TOTAL TEMPERATURE = 497.37

	ABSOLUTE		RELATIVE	EVENTS		
% Passage	% Vel	Angle	% Vel	Total	Used	Contrast
3.7	.0	.0	.0	8.	2.	.0
9.1	.0	.0	.0	0.	1.	.0
14.5	.0	.0	.0	0.	1.	.0
19.9	.0	.0	.0	0.	1.	.0
25.3	184.6	-85.6	12.0	89.	11.	6.1
30.7	163.0	-82.6	25.5	66.	12.	7.2
36.1	.0	.0	.0	0.	1.	.0
41.6	.0	.0	.0	0.	1.	.0
47.0	.0	.0	.0	0.	1.	.0
52.4	.0	.0	.0	0.	1.	.0
57.8	.0	.0	.0	0.	1.	.0
63.2	.0	.0	.0	0.	1.	.0
68.6	.0	.0	.0	0.	1.	.0
74.0	.0	.0	.0	0.	1.	.0
79.4	.0	.0	.0	0.	1.	.0
84.8	.0	.0	.0	3.	1.	.0
90.3	.0	.0	.0	0.	1.	.0

TABLE 20 (Continued)

TRANSONIC COMPRESSOR LTA DATA SUMMARY

BLADE PASSAGE NO. 7

% CHORD = 12.0
% RADIUS = 97.5
INLET TOTAL TEMPERATURE = 497.37

	ABSOLUTE		RELATIVE	EVENTS		
% Passage	% Vel	Angle	% Vel	Total	Used	Contrast
3.7	.0	.0	.0	31.	2.	.0
9.1	.0	.0	.0	0.	1.	.0
14.5	.0	.0	.0	0.	1.	.0
19.9	.0	.0	.0	1.	1.	.0
25.3	168.6	-82.6	22.9	26.	15.	19.1
30.7	176.0	-85.6	15.9	169.	17.	6.1
36.1	.0	.0	.0	1.	1.	.0
41.6	.0	.0	.0	0.	1.	.0
47.0	.0	.0	.0	0.	1.	.0
52.4	.0	.0	.0	0.	1.	.0
57.8	.0	.0	.0	0.	1.	.0
63.2	.0	.0	.0	1.	1.	.0
68.6	.0	.0	.0	0.	1.	.0
74.0	.0	.0	.0	2.	1.	.0
79.4	.0	.0	.0	0.	1.	.0
84.8	.0	.0	.0	0.	1.	.0
90.3	.0	.0	.0	3.	1.	.0

TABLE 20 (Continued)

TRANSONIC COMPRESSOR LTA DATA SUMMARY

BLADE PASSAGE NO. 5

% CHORD = 12.0
% RADIUS = 98.8
INLET TOTAL TEMPERATURE = 484.49

	ABSOLUTE		RELATIVE	EVENTS		
% Passage	% Vel	Angle	% Vel	Total	Used	Contrast
4.3	.0	.0	.0	62.	2.	.0
9.8	.0	.0	.0	245.	8.	.0
15.2	.0	.0	.0	163.	4.	.0
20.6	.0	.0	.0	79.	4.	.0
26.1	.0	.0	.0	38.	2.	.0
31.5	102.7	-27.1	109.8	91.	26.	13.2
37.0	.0	.0	.0	52.	3.	.0
42.4	.0	.0	.0	43.	3.	.0
47.8	.0	.0	.0	44.	3.	.0
53.3	.0	.0	.0	46.	3.	.0
58.7	.0	.0	.0	33.	3.	.0
64.2	.0	.0	.0	46.	4.	.0
69.6	.0	.0	.0	34.	2.	.0
75.1	.0	.0	.0	36.	2.	.0
80.5	.0	.0	.0	33.	3.	.0
85.9	101.3	-27.1	109.7	79.	14.	3.3
91.4	.0	.0	.0	36.	3.	.0

TABLE 20 (Continued)

TRANSONIC COMPRESSOR LTA DATA SUMMARY

BLADE PASSAGE NO. 7

% CHORD = 12.0
% RADIUS = 98.8
INLET TOTAL TEMPERATURE = 484.49

	ABSOLUTE		RELATIVE	EVENTS		
% Passage	% Vel	Angle	% Vel	Total	Used	Contrast
4.3	.0	.0	.0	76.	1.	.0
9.8	.0	.0	.0	258.	8.	.0
15.2	.0	.0	.0	177.	5.	.0
20.6	.0	.0	.0	105.	4.	.0
26.1	.0	.0	.0	73.	3.	.0
31.5	151.0	-78.6	37.0	89.	19.	10.2
37.0	168.1	-27.1	119.3	49.	16.	8.4
42.4	.0	.0	.0	61.	4.	.0
47.8	.0	.0	.0	70.	3.	.0
53.3	.0	.0	.0	56.	5.	.0
58.7	.0	.0	.0	40.	2.	.0
64.2	.0	.0	.0	37.	3.	.0
69.6	.0	.0	.0	42.	2.	.0
75.1	.0	.0	.0	36.	5.	.0
80.5	.0	.0	.0	41.	3.	.0
85.9	.0	.0	.0	69.	10.	.0
91.4	.0	.0	.0	73.	5.	.0

TABLE 20 (Continued)

TRANSONIC COMPRESSOR LTA DATA SUMMARY

BLADE PASSAGE NO. 5

% CHORD = 22.0
% RADIUS = 91.7
INLET TOTAL TEMPERATURE = 488.70

	ABSOLUTE		RELATIVE	EVENTS		
% Passage	% Vel	Angle	% Vel	Total	Used	Contrast
3.1	.0	.0	.0	25920.	18622.	.0
8.3	93.2	-6.8	122.7	28.	23.	40.0
13.5	95.0	-6.8	123.1	64.	60.	70.7
18.7	98.1	-6.8	123.8	67.	65.	118.3
23.9	100.6	-4.8	126.5	79.	75.	102.2
29.0	101.8	-4.8	126.8	87.	85.	169.4
34.2	103.9	-2.4	129.7	77.	75.	155.3
39.4	102.7	-2.4	129.3	38.	37.	104.8
44.6	102.8	-39.5	89.8	74.	71.	98.6
49.8	106.6	-39.5	89.6	116.	110.	78.7
55.0	110.8	-36.4	93.0	118.	117.	329.4
60.2	112.5	-36.4	93.0	114.	113.	291.6
65.4	112.8	-36.4	93.0	31.	28.	42.4
70.6	.0	.0	.0	2.	2.	.0
75.8	101.6	-39.5	89.9	20.	14.	21.5
80.9	110.1	-36.4	93.1	43.	39.	41.7
86.1	107.8	-36.4	93.1	42.	40.	62.8

TABLE 20 (Continued)

TRANSONIC COMPRESSOR LTA DATA SUMMARY

BLADE PASSAGE NO. 7

% CHORD = 22.0
% RADIUS = 91.7
INLET TOTAL TEMPERATURE = 488.70

	ABSOLUTE		RELATIVE	EVENTS		
% Passage	% Vel	Angle	% Vel	Total	Used	Contrast
3.1	.0	.0	.0	20900.	16194.	.0
8.3	94.5	-6.8	123.0	31.	28.	36.2
13.5	95.4	-6.8	123.2	59.	58.	177.8
18.7	97.8	-6.8	123.8	55.	53.	133.4
23.9	100.2	-4.8	126.4	59.	57.	96.1
29.0	101.5	-4.8	126.7	65.	61.	81.2
34.2	103.5	-2.4	129.6	34.	34.	.1E+06
39.4	98.8	-6.8	124.0	41.	40.	93.5
44.6	102.2	-39.5	89.9	115.	113.	184.1
49.8	106.1	-36.4	93.1	101.	99.	162.0
55.0	110.1	-36.4	93.1	115.	114.	281.2
60.2	112.1	-36.4	93.0	105.	94.	74.2
65.4	111.3	-36.4	93.0	61.	60.	151.0
70.6	.0	.0	.0	0.	1.	.0
75.8	102.3	-36.4	93.2	31.	29.	55.6
80.9	109.8	-36.4	93.1	66.	66.	.2E+06
86.1	109.8	-36.4	93.1	30.	24.	38.7

TABLE 20 (Continued)

TRANSONIC COMPRESSOR LTA DATA SUMMARY

BLADE PASSAGE NO. 5

% CHORD = 22.0
% RADIUS = 94.6
INLET TOTAL TEMPERATURE = 493.00

	ABSOLUTE		RELATIVE	EVENTS		
% Passage	% Vel	Angle	% Vel	Total	Used	Contrast
4.4	94.0	-6.9	124.8	837.	665.	83.7
9.6	98.2	-6.9	125.8	248.	226.	108.4
14.8	101.8	-4.5	129.0	72.	70.	117.8
19.9	103.1	-4.5	129.3	109.	102.	124.0
25.1	103.8	-4.5	129.5	112.	109.	156.3
30.3	103.5	-4.5	129.4	97.	94.	126.5
35.4	100.0	-4.5	128.5	116.	111.	95.3
40.6	99.1	-2.4	130.4	167.	156.	109.6
45.7	99.9	-.3	132.5	90.	78.	42.2
50.9	106.9	-39.5	91.4	242.	215.	103.5
56.0	109.8	-39.5	91.3	201.	179.	96.0
61.2	109.7	-36.4	94.9	238.	219.	122.2
66.4	109.6	-33.4	98.4	138.	129.	111.1
71.5	106.0	-33.4	98.4	150.	136.	87.6
76.7	112.4	-33.4	98.5	65.	56.	25.2
81.8	111.6	-39.5	91.2	78.	71.	45.1
87.0	106.4	-39.5	91.5	52.	50.	66.4

TABLE 20 (Continued)

TRANSONIC COMPRESSOR LTA DATA SUMMARY

BLADE PASSAGE NO. 7

% CHORD = 22.0
% RADIUS = 94.6
INLET TOTAL TEMPERATURE = 493.00

	ABSOLUTE		RELATIVE	EVENTS		
% Passage	% Vel	Angle	% Vel	Total	Used	Contrast
4.4	93.8	-6.9	124.8	470.	417.	113.1
9.6	97.6	-9.2	123.4	212.	198.	122.0
14.8	101.2	-6.9	126.4	260.	249.	193.9
19.9	103.1	-6.9	126.9	232.	217.	173.6
25.1	105.4	-4.5	129.9	114.	107.	98.6
30.3	105.9	-2.4	132.2	149.	143.	112.0
35.4	101.2	-2.4	130.9	136.	129.	113.2
40.6	99.2	-2.4	130.4	154.	149.	154.7
45.7	104.3	-42.7	88.1	108.	86.	45.2
50.9	106.6	-39.5	91.5	313.	277.	102.7
56.0	109.2	-39.5	91.3	249.	220.	84.3
61.2	110.0	-36.4	94.9	228.	213.	155.2
66.4	107.9	-36.4	94.9	144.	119.	54.1
71.5	105.4	-36.4	95.0	117.	103.	83.9
76.7	105.6	-33.4	98.4	82.	68.	40.6
81.8	116.3	-42.7	87.1	73.	69.	77.6
87.0	107.9	-39.5	91.4	51.	49.	88.7

TABLE 20 (Continued)

TRANSONIC COMPRESSOR LTA DATA SUMMARY

BLADE PASSAGE NO. 5

% CHORD = 22.0
% RADIUS = 96.1
INLET TOTAL TEMPERATURE = 496.60

	ABSOLUTE		RELATIVE	EVENTS		
% Passage	% Vel	Angle	% Vel	Total	Used	Contrast
5.1	.0	.0	.0	45130.	3188.	.0
10.3	101.3	-6.9	128.0	64.	59.	60.5
15.4	103.9	-6.9	128.6	47.	42.	32.5
20.6	107.3	-4.5	131.9	47.	45.	77.3
25.8	108.5	-2.5	134.4	58.	54.	46.6
31.0	108.4	-2.5	134.4	56.	46.	19.8
36.2	101.7	-2.5	132.6	60.	55.	37.1
41.3	99.5	-2.5	132.0	25.	25.	.6E+05
46.5	.0	.0	.0	4.	1.	.0
51.7	99.1	-39.7	93.4	13.	13.	.8E+05
56.9	105.6	-39.5	93.0	19.	11.	9.3
62.1	.0	.0	.0	15.	6.	.0
67.3	108.6	-39.7	92.6	19.	15.	23.7
72.4	106.8	-36.4	96.5	29.	18.	11.1
77.6	119.7	-43.0	87.9	14.	13.	37.0
82.8	115.0	-43.0	88.2	16.	13.	30.5
88.0	112.2	-42.8	88.7	29.	19.	14.9

TABLE 20 (Continued)

TRANSONIC COMPRESSOR LTA DATA SUMMARY

BLADE PASSAGE NO. 7

% CHORD = 22.0
% RADIUS = 96.1
INLET TOTAL TEMPERATURE = 496.60

	ABSOLUTE		RELATIVE	EVENTS		
% Passage	% Vel	Angle	% Vel	Total	Used	Contrast
5.1	.0	.0	.0	56499.	939.	.0
10.3	100.8	-6.9	127.9	76.	70.	51.0
15.4	104.7	-6.9	128.8	41.	38.	42.1
20.6	108.8	-4.5	132.3	54.	41.	19.6
25.8	109.9	-4.5	132.6	70.	54.	33.3
31.0	107.0	-4.5	131.9	50.	45.	39.4
36.2	104.2	-2.5	133.2	60.	41.	17.2
41.3	100.3	-2.5	132.2	29.	22.	19.8
46.5	100.4	-39.5	93.5	13.	12.	36.8
51.7	98.7	-39.7	93.4	16.	15.	47.4
56.9	106.6	-39.5	93.0	17.	14.	12.1
62.1	.0	.0	.0	13.	5.	.0
67.3	108.6	-39.5	92.8	17.	14.	24.3
72.4	108.7	-39.7	92.6	13.	13.	.9E+05
77.6	.0	.0	.0	3.	1.	.0
82.8	112.1	-43.0	88.5	12.	12.	.9E+05
88.0	112.3	-42.8	88.7	29.	14.	5.6

TABLE 20 (Continued)

TRANSONIC COMPRESSOR LTA DATA SUMMARY

BLADE PASSAGE NO. 5

% CHORD = 22.0
% RADIUS = 96.8
INLET TOTAL TEMPERATURE = 499.83

	ABSOLUTE		RELATIVE	EVENTS		
% Passage	% Vel	Angle	% Vel	Total	Used	Contrast
5.1	.0	.0	.0	25783.	65.	.0
10.3	.0	.0	.0	472.	9.	.0
15.5	.0	.0	.0	31.	12.	.0
20.7	108.9	-53.3	78.0	1831.	112.	15.1
25.9	96.6	-53.3	81.2	3570.	34.	5.4
31.0	.0	.0	.0	187.	3.	.0
36.2	.0	.0	.0	196.	7.	.0
41.4	.0	.0	.0	265.	4.	.0
46.6	.0	.0	.0	518.	12.	.0
51.8	.0	.0	.0	824.	9.	.0
57.0	.0	.0	.0	632.	7.	.0
62.2	.0	.0	.0	603.	6.	.0
67.4	.0	.0	.0	380.	6.	.0
72.6	91.3	-52.9	83.1	402.	11.	3.5
77.8	107.3	-53.3	78.4	999.	74.	14.2
82.9	86.3	-53.3	84.3	529.	72.	4.5
88.1	.0	.0	.0	144.	4.	.0

TABLE 20 (Continued)

TRANSONIC COMPRESSOR LTA DATA SUMMARY

BLADE PASSAGE NO. 7

% CHORD = 22.0
% RADIUS = 96.8
INLET TOTAL TEMPERATURE = 499.83

	ABSOLUTE		RELATIVE	EVENTS		
% Passage	% Vel	Angle	% Vel	Total	Used	Contrast
5.1	.0	.0	.0	11027.	105.	.0
10.3	.0	.0	.0	464.	4.	.0
15.5	.0	.0	.0	114.	6.	.0
20.7	109.5	-53.3	77.8	1078.	68.	12.4
25.9	28.3	-53.3	107.2	1866.	11.	3.2
31.0	.0	.0	.0	223.	6.	.0
36.2	.0	.0	.0	221.	6.	.0
41.4	87.0	-21.9	112.2	978.	11.	3.6
46.6	.0	.0	.0	530.	5.	.0
51.8	.0	.0	.0	645.	11.	.0
57.0	.0	.0	.0	634.	8.	.0
62.2	31.9	-52.9	105.6	414.	10.	4.0
67.4	.0	.0	.0	223.	6.	.0
72.6	.0	.0	.0	112.	4.	.0
77.8	107.7	-53.3	78.3	1476.	120.	19.5
82.9	.0	.0	.0	77.	3.	.0
88.1	.0	.0	.0	112.	4.	.0

TABLE 20 (Continued)

TRANSONIC COMPRESSOR LTA DATA SUMMARY

BLADE PASSAGE NO. 5

% CHORD = 22.0
% RADIUS = 97.5
INLET TOTAL TEMPERATURE = 497.37

	ABSOLUTE		RELATIVE	EVENTS		
% Passage	% Vel	Angle	% Vel	Total	Used	Contrast
4.2	.0	.0	.0	966.	11.	.0
9.3	.0	.0	.0	35.	2.	.0
14.5	.0	.0	.0	17.	1.	.0
19.7	110.0	-9.0	129.5	709.	181.	19.5
24.9	96.7	-9.0	126.6	91.	13.	6.1
30.1	.0	.0	.0	31.	2.	.0
35.2	.0	.0	.0	26.	1.	.0
40.4	.0	.0	.0	36.	2.	.0
45.6	.0	.0	.0	49.	3.	.0
50.8	.0	.0	.0	40.	2.	.0
56.0	.0	.0	.0	21.	2.	.0
61.1	.0	.0	.0	25.	3.	.0
66.3	.0	.0	.0	50.	2.	.0
71.5	.0	.0	.0	34.	2.	.0
76.7	108.5	-9.0	129.1	396.	127.	29.6
81.9	.0	.0	.0	21.	2.	.0
87.0	.0	.0	.0	15.	1.	.0

TABLE 20 (Continued)

TRANSONIC COMPRESSOR LTA DATA SUMMARY

BLADE PASSAGE NO. 7

% CHORD = 22.0
% RADIUS = 97.5
INLET TOTAL TEMPERATURE = 497.37

	ABSOLUTE		RELATIVE	EVENTS		
% Passage	% Vel	Angle	% Vel	Total	Used	Contrast
4.2	.0	.0	.0	4555.	20.	.0
9.3	.0	.0	.0	32.	2.	.0
14.5	.0	.0	.0	9.	2.	.0
19.7	107.4	-9.0	128.9	282.	25.	4.7
24.9	185.1	-9.0	152.8	113.	51.	10.1
30.1	.0	.0	.0	20.	2.	.0
35.2	.0	.0	.0	28.	2.	.0
40.4	.0	.0	.0	27.	3.	.0
45.6	.0	.0	.0	13.	2.	.0
50.8	.0	.0	.0	31.	2.	.0
56.0	.0	.0	.0	8.	1.	.0
61.1	.0	.0	.0	14.	1.	.0
66.3	.0	.0	.0	39.	3.	.0
71.5	.0	.0	.0	39.	2.	.0
76.7	103.6	-9.0	128.0	215.	178.	86.8
81.9	.0	.0	.0	51.	3.	.0
87.0	.0	.0	.0	55.	3.	.0

TABLE 20 (Continued)

TRANSONIC COMPRESSOR LTA DATA SUMMARY

BLADE PASSAGE NO. 5

% CHORD = 25.0
% RADIUS = 88.9
INLET TOTAL TEMPERATURE = 498.79

	ABSOLUTE		RELATIVE	EVENTS		
% Passage	% Vel	Angle	% Vel	Total	Used	Contrast
4.0	99.3	-.4	126.0	188.	16.	4.1
9.2	96.4	-2.4	123.3	40.	12.	7.1
14.3	101.0	-15.5	111.5	94.	62.	30.0
19.5	.0	.0	.0	17.	6.	.0
24.7	99.0	-4.8	121.8	45.	26.	17.3
29.8	100.2	-2.4	124.4	20.	11.	8.8
35.0	.0	.0	.0	9.	2.	.0
40.2	.0	.0	.0	8.	2.	.0
45.4	.0	.0	.0	7.	1.	.0
50.5	.0	.0	.0	20.	2.	.0
55.7	.0	.0	.0	8.	2.	.0
60.9	.0	.0	.0	7.	1.	.0
66.0	.0	.0	.0	14.	3.	.0
71.2	101.0	-15.5	111.6	300.	88.	11.0
76.4	.0	.0	.0	13.	2.	.0
81.5	.0	.0	.0	7.	2.	.0
86.7	.0	.0	.0	20.	2.	.0

TABLE 20 (Continued)

TRANSONIC COMPRESSOR LTA DATA SUMMARY

BLADE PASSAGE NO. 7

% CHORD = 25.0
% RADIUS = 88.9
INLET TOTAL TEMPERATURE = 498.79

% Passage	ABSOLUTE % Vel	ABSOLUTE Angle	RELATIVE % Vel	EVENTS Total	EVENTS Used	EVENTS Contrast
4.0	.0	.0	.0	1955.	24.	.0
9.2	93.3	-6.8	118.5	34.	18.	9.2
14.3	99.3	-15.5	111.2	98.	55.	16.3
19.5	94.7	-6.8	118.8	35.	22.	21.8
24.7	94.9	-9.1	116.7	42.	17.	8.4
29.8	.0	.0	.0	5.	1.	.0
35.0	.0	.0	.0	13.	2.	.0
40.2	.0	.0	.0	14.	1.	.0
45.4	.0	.0	.0	16.	3.	.0
50.5	.0	.0	.0	8.	1.	.0
55.7	.0	.0	.0	10.	2.	.0
60.9	.0	.0	.0	6.	1.	.0
66.0	.0	.0	.0	12.	1.	.0
71.2	.0	.0	.0	13.	1.	.0
76.4	.0	.0	.0	5.	2.	.0
81.5	.0	.0	.0	7.	1.	.0
86.7	.0	.0	.0	19.	2.	.0

TABLE 20 (Continued)

TRANSONIC COMPRESSOR LTA DATA SUMMARY

BLADE PASSAGE NO. 5

% CHORD = 25.0
% RADIUS = 91.7
INLET TOTAL TEMPERATURE = 487.53

	ABSOLUTE		RELATIVE	EVENTS		
% Passage	% Vel	Angle	% Vel	Total	Used	Contrast
9.1	96.5	-6.5	122.2	638.	116.	12.6
14.6	99.2	-4.2	125.0	115.	57.	18.2
20.1	101.1	-4.2	125.5	103.	66.	18.4
25.6	102.8	-4.2	126.0	72.	47.	14.9
31.1	.0	.0	.0	59.	4.	.0
36.6	99.3	-39.6	88.5	45.	38.	31.7
42.1	104.1	-39.6	88.1	177.	68.	14.8
47.6	107.4	-39.6	88.0	266.	113.	19.4
53.1	109.8	-39.6	87.9	400.	138.	19.4
58.6	109.4	-39.6	87.9	442.	127.	17.7
64.0	110.4	-39.6	87.8	434.	116.	14.1
69.5	101.0	-35.2	93.0	793.	250.	22.2
75.0	108.5	-39.6	87.9	392.	87.	10.1
80.5	107.7	-39.6	87.9	367.	102.	14.1

TABLE 20 (Continued)

TRANSONIC COMPRESSOR LTA DATA SUMMARY

BLADE PASSAGE NO. 7

% CHORD = 25.0
% RADIUS = 91.7
INLET TOTAL TEMPERATURE = 487.53

	ABSOLUTE		RELATIVE	EVENTS		
% Passage	% Vel	Angle	% Vel	Total	Used	Contrast
9.1	95.2	-6.5	121.9	632.	140.	13.7
14.6	98.4	-4.2	124.8	135.	64.	10.8
20.1	99.8	-4.2	125.2	155.	88.	21.5
25.6	98.2	-6.5	122.6	181.	76.	13.6
31.1	96.3	-39.6	88.7	140.	46.	12.1
36.6	98.3	-39.6	88.5	120.	56.	17.3
42.1	102.8	-39.6	88.2	79.	37.	18.1
47.6	106.4	-39.6	88.0	132.	55.	13.4
53.1	109.0	-39.6	87.9	253.	92.	18.5
58.6	109.1	-39.6	87.9	525.	127.	14.7
64.0	107.2	-39.6	88.0	445.	140.	18.3
69.5	102.5	-35.2	93.0	467.	156.	17.3
75.0	108.3	-39.6	87.9	420.	105.	8.7
80.5	108.1	-39.6	87.9	307.	87.	11.9

TABLE 20 (Continued)

TRANSONIC COMPRESSOR LTA DATA SUMMARY

BLADE PASSAGE NO. 5

% CHORD = 25.0
% RADIUS = 91.7
INLET TOTAL TEMPERATURE = 485.17

	ABSOLUTE		RELATIVE	EVENTS		
% Passage	% Vel	Angle	% Vel	Total	Used	Contrast
11.3	95.9	-5.9	122.6	78.	25.	11.0
13.4	99.3	-5.9	123.4	51.	23.	14.2
15.6	100.5	-3.7	125.8	23.	19.	23.7
17.8	98.9	-3.7	125.4	39.	16.	14.6
20.0	101.3	-3.7	126.0	24.	19.	18.8
22.1	.0	.0	.0	14.	2.	.0
24.3	102.3	-3.7	126.3	25.	12.	11.7
26.5	102.3	-3.7	126.3	23.	16.	15.9
28.7	.0	.0	.0	7.	4.	.0
32.4	98.3	-42.0	85.6	20.	12.	9.3
35.2	97.5	-39.5	88.4	26.	19.	21.9
37.9	99.5	-37.2	90.6	22.	14.	9.3
40.6	102.5	-39.5	88.0	28.	14.	12.7
43.4	103.3	-37.2	90.5	67.	23.	8.8
46.1	109.2	-39.5	87.7	55.	19.	9.7
48.8	109.0	-39.5	87.7	103.	48.	14.4
51.6	111.1	-39.5	87.6	93.	40.	15.3
54.3	111.1	-37.2	90.3	77.	21.	11.4
57.1	111.8	-39.5	87.6	69.	33.	9.8
59.8	109.5	-37.2	90.3	89.	41.	10.7
62.5	109.4	-39.5	87.7	49.	30.	13.5
65.3	111.2	-42.0	84.6	42.	12.	9.8
68.0	106.6	-37.2	90.4	97.	39.	14.7
70.8	104.1	-37.2	90.4	52.	27.	14.9
73.5	106.8	-37.2	90.4	71.	25.	6.3
76.3	111.5	-39.5	87.6	96.	39.	12.0
79.0	107.7	-39.5	87.7	62.	27.	12.6
81.7	105.7	-39.5	87.8	59.	29.	13.6

TABLE 20 (Continued)

TRANSONIC COMPRESSOR LTA DATA SUMMARY

BLADE PASSAGE NO. 7

% CHORD = 25.0
% RADIUS = 91.7
INLET TOTAL TEMPERATURE = 485.17

	ABSOLUTE		RELATIVE	EVENTS		
% Passage	% Vel	Angle	% Vel	Total	Used	Contrast
11.3	99.9	-3.7	125.7	41.	12.	9.8
13.4	97.3	-5.9	122.9	52.	35.	13.0
15.6	98.5	-5.9	123.2	34.	17.	13.1
17.8	99.9	-3.7	125.7	61.	30.	8.6
20.0	98.0	-5.9	123.1	46.	16.	12.8
22.1	99.5	-5.9	123.5	39.	20.	13.6
24.3	98.9	-3.7	125.4	35.	12.	8.8
26.5	.0	.0	.0	18.	2.	.0
29.7	96.4	-42.0	85.8	40.	11.	5.0
32.4	95.6	-39.5	88.5	59.	27.	10.3
35.2	97.9	-37.2	90.7	55.	32.	12.2
37.9	100.2	-37.2	90.6	35.	20.	11.2
40.6	101.6	-39.5	88.1	35.	18.	10.5
43.4	102.1	-37.2	90.5	38.	11.	8.2
46.1	105.9	-39.5	87.8	49.	25.	17.6
48.8	108.5	-37.2	90.3	22.	15.	19.9
51.6	110.0	-39.5	87.7	23.	20.	27.2
54.3	110.3	-39.5	87.6	42.	35.	29.6
57.1	109.3	-39.5	87.7	64.	29.	11.7
59.8	108.0	-37.2	90.3	59.	29.	12.7
62.5	107.8	-37.2	90.3	67.	38.	16.9
65.3	108.1	-39.5	87.7	70.	37.	18.5
68.0	106.3	-39.5	87.8	103.	46.	12.0
70.8	104.2	-37.2	90.4	90.	46.	12.8
73.5	104.6	-37.2	90.4	75.	25.	7.6
76.3	111.0	-37.2	90.3	78.	39.	11.1
79.0	108.2	-42.0	84.7	83.	27.	10.7
81.7	106.7	-37.2	90.4	21.	13.	13.0

TABLE 20 (Continued)

TRANSONIC COMPRESSOR LTA DATA SUMMARY

BLADE PASSAGE NO. 5

% CHORD = 25.0
% RADIUS = 91.7
INLET TOTAL TEMPERATURE = 497.97

	ABSOLUTE		RELATIVE	EVENTS		
% Passage	% Vel	Angle	% Vel	Total	Used	Contrast
4.0	.0	.0	.0	1924.	19.	.0
9.2	95.8	-7.9	121.0	48.	22.	9.4
14.3	99.1	-5.6	124.0	43.	23.	16.8
19.5	100.7	-3.5	126.4	30.	24.	27.8
24.7	102.3	-3.5	126.9	36.	28.	20.4
29.8	102.4	-3.5	126.9	38.	24.	12.6
35.0	.0	.0	.0	44.	9.	.0
40.2	.0	.0	.0	22.	1.	.0
45.4	.0	.0	.0	37.	3.	.0
50.5	.0	.0	.0	54.	3.	.0
55.7	.0	.0	.0	30.	2.	.0
60.9	.0	.0	.0	22.	2.	.0
66.0	.0	.0	.0	15.	1.	.0
71.2	.0	.0	.0	31.	1.	.0
76.4	.0	.0	.0	27.	2.	.0
81.5	.0	.0	.0	9.	1.	.0
86.7	.0	.0	.0	20.	2.	.0

TABLE 20 (Continued)

TRANSONIC COMPRESSOR LTA DATA SUMMARY

BLADE PASSAGE NO. 7

% CHORD = 25.0
% RADIUS = 91.7
INLET TOTAL TEMPERATURE = 497.97

	ABSOLUTE		RELATIVE	EVENTS		
% Passage	% Vel	Angle	% Vel	Total	Used	Contrast
4.0	.0	.0	.0	3061.	42.	.0
9.2	95.8	-7.9	121.0	39.	24.	14.9
14.3	99.1	-5.6	124.0	49.	28.	21.2
19.5	99.6	-5.6	124.2	63.	34.	11.9
24.7	102.1	-3.5	126.8	49.	35.	20.3
29.8	100.9	-5.6	124.5	56.	21.	9.0
35.0	.0	.0	.0	33.	5.	.0
40.2	.0	.0	.0	22.	2.	.0
45.4	.0	.0	.0	32.	2.	.0
50.5	.0	.0	.0	35.	3.	.0
55.7	.0	.0	.0	27.	2.	.0
60.9	.0	.0	.0	28.	2.	.0
66.0	.0	.0	.0	43.	3.	.0
71.2	.0	.0	.0	26.	3.	.0
76.4	.0	.0	.0	14.	1.	.0
81.5	.0	.0	.0	12.	1.	.0
86.7	.0	.0	.0	35.	2.	.0

TABLE 20 (Continued)

TRANSONIC COMPRESSOR LTA DATA SUMMARY

BLADE PASSAGE NO. 5

% CHORD = 30.0
% RADIUS = 91.7
INLET TOTAL TEMPERATURE = 481.18

	ABSOLUTE		RELATIVE	EVENTS		
% Passage	% Vel	Angle	% Vel	Total	Used	Contrast
6.1	.0	.0	.0	296.	6.	.0
13.1	36.2	-73.5	93.1	973.	560.	17.1
20.1	35.9	-73.5	93.3	279.	100.	4.8
27.1	39.5	-73.5	91.2	240.	9.	2.8
34.1	38.9	-73.5	91.5	296.	28.	3.9
41.1	35.5	-73.5	93.5	361.	67.	6.8
48.1	35.4	-73.5	93.5	386.	113.	5.5
55.1	35.7	-73.5	93.4	242.	77.	7.9
62.1	34.0	-73.5	94.3	264.	67.	6.1
69.1	36.1	-73.5	93.1	204.	60.	5.3

TABLE 20 (Continued)

TRANSONIC COMPRESSOR LTA DATA SUMMARY

BLADE PASSAGE NO. 7

% CHORD = 30.0
% RADIUS = 91.7
INLET TOTAL TEMPERATURE = 481.18

	ABSOLUTE		RELATIVE	EVENTS		
% Passage	% Vel	Angle	% Vel	Total	Used	Contrast
6.1	36.0	-73.5	93.2	494.	131.	7.0
13.1	36.3	-73.5	93.0	2636.	1429.	30.1
20.1	34.6	-73.5	94.0	313.	78.	5.9
27.1	33.8	-73.5	94.5	245.	36.	5.2
34.1	36.9	-73.5	92.7	335.	111.	5.3
41.1	35.7	-73.5	93.4	307.	83.	6.4
48.1	36.3	-73.5	93.0	317.	90.	5.7
55.1	35.2	-73.5	93.7	205.	56.	8.8
62.1	35.0	-73.5	93.8	239.	82.	4.3
69.1	38.7	-75.9	91.3	938.	21.	3.3

The two page vita has been removed from the scanned document. Page 1 of 2

The two page vita has been removed from the scanned document. Page 2 of 2